NEURAL CREST SPECIFICATION BY MAX'S GIANT ASSOCIATED PROTEIN AND REGULATION OF MICROTUBULE'S FUNCTION BY ALPHA-TUBULIN ACETYLTRANSFERASE 1 IN ZEBRAFISH

by

WEI-CHIA TSENG

(Under the Direction of SCOTT T. DOUGAN)

ABSTRACT

During the embryonic development of vertebrates, progenitor cells receive guidance and start to proliferate, differentiate, and migrate to form various tissues and organs. This process requires the coordination of cell signaling, transcriptional regulation, and cytoskeleton reorganization. In this study, we focus on understanding the roles of two different proteins, Max's giant associate protein (Mga) and α-tubulin acetyltranferase 1(ATAT1), in zebrafish development. It has been suggested that Mga is a Myc antagonist and participates in activating the expression of *bmp2b* in the yolk syncytial layer (YSL) of zebrafish. Here we show that Mga plays a novel role in regulating neural crest development in zebrafish. Suppressing the expression of Mga by antisense morpholino oligonucleotides leads to various developmental defects in zebrafish embryos. Most cell lineages that derive from neural crest are affected in *mga* morphants, suggesting that Mga might play a role in maintaining the normal formation of neural crest cell population. Mga might control neural crest formation by positively regulating BMP signaling, or alternatively, by antagonizing the activity of Myc. To understand more about the

mechanism, we further targeted *mga* with RGN system and identified five different potentially null alleles. Further characterization of *mga* mutants is required to understand the function of Mga. ATAT1 is the major α-tubulin acetyltransferase responsible for tubulin acetylation, a conserved tubulin post-translational modification (PTM) associated with stable microtubules, in ciliates, worms, and mice. Here we employed TALENs to target zebrafish *atat1* and successfully generated two *atat1* null mutants. *atat1* mutants deplete acetylated α-tubulin completely in microtubules, suggesting that ATAT1 is also the major α-tubulin acetyltranferase in zebrafish. *atat1* mutants are viable, fertile, and exhibiting no overt developmental defect. However, *atat1* mutant embryos are more sensitive to Paclitaxel treatment. Furthermore, several tubulin PTMs are altered in *atat1* mutants. Tubulin monoglycylation is elevated in *atat1* mutants. Severe cilia-related defects are observed in zebrafish embryos void of both ATAT1 and tubulin monoglycylase TTLL3. This result suggests a possible interaction among different tubulin PTMs.

INDEX WORDS: Transcription factor, Neural crest, Cell signaling, Gene targeting, Microtubule, Acetylation, Tubulin Post-translational modification, Embryonic development, Zebrafish.

NEURAL CREST SPECIFICATION BY MAX'S GIANT ASSOCIATED PROTEIN AND REGULATION OF MICROTUBULE'S FUNCTION BY ALPHA-TUBULIN ACETYLTRANSFERASE 1 IN ZEBRAFISH

by

WEI-CHIA TSENG

BS, NATIONAL TAIWAN UNIVERSITY, TAIWAN, JUNE 2003

MS, NATIONAL TAIWAN UNIVERSITY, TAIWAN, JUNE 2005

A Dissertation Submitted to the Graduate Faculty of The University of Georgia in Partial Fulfillment of the Requirements for the Degree

DOCTOR OF PHILOSOPHY

ATHENS, GEORGIA

2015

NEURAL CREST SPECIFICATION BY MAX'S GIANT ASSOCIATED PROTEIN AND REGULATION OF MICROTUBULE'S FUNCTION BY ALPHA-TUBULIN ACETYLTRANSFERASE 1 IN ZEBRAFISH

by

WEI-CHIA TSENG

Major Professor:	Scott T. Dougan
Committee:	Jacek Gaertig
	Marcus Fechheimer
	James D. Lauderdale

Electronic Version Approved:

Julie Coffield
Interim Dean of the Graduate School
The University of Georgia
May 2015

DEDICATION

I dedicate this dissertation to my beloved parents, wife, and the Tseng family.

ACKNOWLEDGEMENTS

I would like to express my greatest appreciation to my major advisor Scott Dougan. Although I've been changing my research topic many times during the past few years, he always encourages me and is very supportive. He also gives me a lot of free space for me to develop my own experimental design and to try out new techniques. I'll always remember the discussion we had regarding what to do and not to do in my research. I would not be who I am today without his support.

I would like to thank Yuhua Sun. He taught me many experimental techniques, especially the most important one, microinjection, when I first joined Dougan Lab. He also provided me a lot of technical support and suggestions while we worked on the same project. I would also like to thank Rebecca Ball. I learned how to do most of the fish room work from her. It's my pleasure to work with her in the fish room to ensure my fish receive good care. I am deeply indebted to my committee members, Jacek Gaertig, Marcus Fechheimer, and Jim Lauderdale. They always give me insightful advices and steer me in the right direction. Special thanks to Jacek Gaertig. He is the person who brings me into the world of microtubules. I can't express how much I appreciate his help for me to keep working on my favorite cytoskeletons.

I would like to thank my parents and wife for being so supportive over the past few years. Although we are quite far away from each other, the love makes us all

connected. My parents always support me to do whatever I want to pursue. They also teach me how to become an independent person. Thank them for taking care of my pet fish back in Taiwan while I am away from home. I would like to delicate my special appreciation to my wife, Yen-Ling. We met here in UGA and made a lot of memories together. Although it has been several years since you graduated and moved up to Maryland for the job, she is always independent and encourages me to take on challenges. Words are not enough to express my appreciation for all the things that she has done for me. Finally, I would like to thank my grandparents I lost in past fifteen years. Their attitude toward life had always been the inspiration to me to become a good person.

Lastly, I would like to thank those who have helped me here in UGA. No matter what happens, they are always there to help me. I may not remember all of their names, but I certainly appreciate what they have done for me.

TABLE OF CONTENTS

LIST OF FIGURES

Page

CHAPTER 1

INTRODUCTION AND LITERITURE REVIEW

Embryonic morphogenesis and patterning in vertebrates

From a single fertilized oocyte to a fully functional multicellular organism, progenitor cells receive guidance and undergo proliferation, differentiation, and migration to form a variety of tissues and organs. Every step in embryonic development has to be tightly controlled, and every embryonic cell has to coordinate and communicate with each other properly in order to contribute to a fully developed organism. Therefore, it is essential to understand underlying mechanisms that regulate the embryonic morphogenesis and patterning. Initially, embryos develop from a group of identical cells shortly after fertilization. These cells are called stem cells because they have potential to form almost any structure in the organism. Later in early embryonic development, embryonic cells receive directional instructions from groups of specialized cells called signaling centers and are further turned into a multi-layered structure. This process is called the gastrulation when three germ layers including endoderm, mesoderm and ectoderm form depending on the signals that each cell receives. The endoderm will form the lining of guts; the mesoderm will form connective tissues, muscles and blood; the ectoderm will form neural and skin cells. The polarity of embryo, including anterior-posterior and dorsal-ventral, is also established during the process. Once germ layers form, embryonic

stem cells are turned from pluripotent cells into groups of cells with different cell fates. Each group of cells will keep proliferating and eventually develop into particular types of tissues and organs according to their cell fate that they acquire during the gastrulation.

Gastrulation and signaling centers

The gastrulation in vertebrates begins when embryonic cells receive extracellular signaling molecules secreted from signaling centers. The first signaling centers form in vertebrates when cells with extraembryonic identity physically separate from the rest of the embryos [1]. These extraembryonic tissues such as visceral endoderm (VE) in mammals, hypoblast in avian and yolk syncytial layer (YSL) in teleost fish serve as signaling centers to instruct germ layer formation in embryonic tissues. Extraembryonic tissues were first discovered in mammals and avian at the end of the 19th century[2, 3]. In chick, the extraembryonic hypoblast forms from the merging of yolky cell 'islands' underlying primitive ectoderm/epiblast [4]. In mouse, VE segregates from primitive endoderm of the implanting blastocyst during embryonic day E4.5-5.5 [4]. In teleost fish, YSL formation occurs when cells at the margin of blastomeres collapse and release their cell contents into nearby yolk cell to form a multinuclear cell syncytium [5]. Though extraembryonic tissues will not become parts of the embryo, the transcription remains active since signaling molecules are largely required from blastomeres for patterning the embryo at this stage. Therefore, extraembryonic signaling centers produce and secrete morphogens, diffusible molecules that form concentration gradients in the embryo, to communicate with blastomeres. Each cell receives different level of morphogens according to their positions in the blastomeres. The difference in signaling strength

received by each blastomere determines what cell type they will become in the future. Overall, extraembryonic tissues serve as the important source of signaling molecules that could be utilized to initiate the formation of germ layers.

Polarity and axes formation

In vertebrates, axes formation starts as early as oogenesis when maternal factors are deposited into oocytes. Animal-vegetal axis is established during oogenesis. These factors are localized to the vegetal pole during oogenesis and later asymmetrically distributed in the egg via microtubule-mediated transport to initiate the formation of dorsoventral axis shortly after fertilization. These maternal factors soon mediate the primary axes formation through regulating Wnt, BMP, Nodal, and FGF signaling pathways. This process provides the foundation for the establishment of body plan [6]. While signaling centers signal embryonic cells to adapt their cell fate during the gastrulation, another group of cells called organizer also actively provides directional instructions for axis formation. The organizer was first discovered by Spemann and Mangold in early 20^{th} century using salamander as a model. In their experiment, the dorsal lip of the blastopore where the gastrulation starts was grafted into the ventral side of the host, from a lightly pigmented donor to a more pigmented host. Surprisingly, the transplanted dorsal tissue not only maintained its original dorsal cell fate gave rise to mostly the notochord but also induced neighboring host cells to form a Siamese twin containing dorsal tissues [7]. Since the dorsal lip of the blastopore had the ability to induce a Siamese twin formed in the host, Spemann named this structure as the

'organizer'. This dorsal signaling center is now known as Spemann organizer in Xenopus and the shield in zebrafish. The formation of the organizer requires Nodal and possibly some other signals from ventral signaling center in both Xenopus and zebrafish. A variety of signal antagonists such as Chordin and Noggin as BMP antagonists, Dkk-1 as Wnt antagonists, and a multi-signal antagonist Cerberus, are secreted from the organizer to define the functional signaling domain during the gastrulation [8-10]. At the same time, a ventral signaling center at the opposite end of the mesoderm from Spemann organizer secretes BMPs to signal embryonic cells [11]. Thus, dorsal and ventral signaling centers appear to battle each other to ensure the accurate delivery of instructional signals to each cell. The presence of organizer highlights the requirement of the complex signaling regulation during the gastrulation other than just the existence of morphogen concentration gradient.

TGF β signaling in embryonic patterning

Signaling mechanism of TGFβ signaling

The transforming growth factor β (TGFβ) superfamily includes numbers of secreted proteins acting as extracellular ligands for signal transduction, such as TGFβ/Activin/Nodal and BMPs. These ligands bind to transmembrane receptors on the cell surface and turn on the signaling cascade through activating serine/threonine kinase activity of receptors. There are two types of TGFβ receptors: Type I receptor and Type II receptor. When TGFβ ligand binds to the type II receptor, the ligand-bound type II receptor has higher affinity to the type I receptor and a complex is formed in which the

type II receptor phosphorylates the type I receptor for activation. Unlike TGFβ, BMPs form homodimers or heterodimers first and bind to type I and type II receptors together. Once the complex is formed, the type I receptor phosphorylates receptor regulated Smad proteins (R-Smad) including Smad2/3 (activating TGFβ/Activin/Nodal pathway) and Smad1/5 (activating BMP pathway) for intracellular signal transduction. Common Smad (Co-Smad), Smad4, binds to phosphorylated R-Smad proteins and form a heterodimer. This heterodimer translocates to the cell nucleus and binds to regulatory regions of the target genes together with some other binding partners for regulating gene transcription [12, 13].

1. Nodal

Nodal signaling is a well known signaling pathway essential for the formation of germ layers in vertebrates. At the beginning of the gastrulation, Nodal induces mesendoderm formation and later different levels of Nodal signaling together with other signaling are required for further patterning of germ layers. Mouse has a single *nodal* gene, whereas Xenopus has at least six and zebrafish has three [14-16]. In mouse embryos, *nodal* is initially expressed in the proximal epiblast before and during early gastrulation then its expression is restricted to the node [17-19]. Nodal signaling is required for the establishment of proximal-distal axis polarity, which later is converted into anterior-posterior axis when anterior VE moves [18, 20, 21]. Loss of Nodal signaling in mice leads to the absence of mesoderm, excessive formation of ectoderm, and eventually the embryonic death during the early gastrulation [17, 18]. Similar effects of Nodal proteins are also found in other species during the gastrulation, such as Xenopus and zebrafish.

Five out of the six known Nodal proteins have the ability to induce mesoderm formation in animal caps in Xenopus [22-25]. In zebrafish, embryos develop abnormally with the absence of mesoderm in head and trunk, and all endoderm when two *nodal* genes, *cyclops* and *squint*, are not functional [15]. Nodal signals to patterns the gastrulation through TGFβ signaling pathway and requires an additional co-receptor for ligand-receptor activation. Mutation in *cripto* shows a phenotype similar to *nodal* mutant mice [26]. A similar phenotype is also observed in a zebrafish losing both maternal and zygotic expression of *one-eyed pinhead* (MZ*oep*). Overexpression of *cyclops* and *squint* fails to rescue the MZ*oep* phenotype, whereas overexpression of a constitutively active type I receptor or activated Smad2 rescues the mutant phenotype [27]. This suggests the possible role of *oep* in Nodal signaling as a player in ligand-receptor binding/activation. Through analyses, *oep* is identified encoding a *cripto* homologue. Cripto and Oep are named EGF-CFC because they both contain EGF homology domain and Cripto-Frl-Criptic (CFC) homology domain [28, 29]. EGF-CFC is identified as a co-receptor of Nodal receptors ALK4 and ALK7 [30, 31]. During the gastrulation, Nodal signaling from extraembryonic tissues also plays an essential role to pattern germ layers. Mouse *nodal* mutant chimeras show that Nodal signaling is required in VE for the formation of prechordal plate and anterior neural tissue [19]. Targeted depletion of *nodal* genes in zebrafish demonstrates that Nodal proteins are required in the YSL for endoderm and head mesoderm formation [32]. In order to shape up the adequate level of Nodal signaling in different parts of embryos during the gastrulation, Nodal signaling can be controlled at the level of *nodal* gene expression and the regulation of other Nodal signaling components. *nodal* genes are expressed both maternally and zygotically, and

their expression is regulated by various mechanisms. In zebrafish, *squint* positively regulates the expression of bozozok in the dorsal organizer in conjunction with Wnt/β-catenin and is essential for the early steps of dorsoventral axis formation [15]. Expression of *nodal* genes in both embryonic and extraembryonic tissues depends on reciprocal Nodal signaling interaction between two tissues [32]. Recent studies in microRNAs (miRNAs) have shown that miRNAs play important roles in regulating the expression of a variety of genes, including essential genes required for embryonic development in Xenopus and zebrafish [33]. miRNAs are originally transcribed as primary RNAs and later being processed by RNase III Dorsha and Dicer into small non-coding RNA fragments about 22 bases each piece. These miRNAs are complementary to sequences within the 3' untranslated region (UTR) of their target genes. Once they bind to target sequences, the miRNA/mRNA binding will promote mRNA cleavage or deadenylation and further inhibit the expression of target genes. It has been shown in zebrafish that a miRNA, *miR-430*, targets a *nodal* gene *squint* and a Nodal inhibitor *lefty2* [34]. *miR-430* plays an important role in maintaining the adequate level of Nodal signaling by balancing the expression of *squint* and *lefty2* in early developing embryos. In Xenopus embryos, *miR-15* and *miR-16* target the mRNA of Nodal type II receptor, suggesting their role in regulating Nodal signaling [35]. Additionally, binding of proteins on mRNAs could also affect their stability. It has been reported that Y box-binding protein 1 (Ybx1) binds to 3' UTR of maternal *squint* transcripts and prevents pre-mature translation and Nodal signaling [36]. However, Nodal signaling can also be inhibited even when Nodal proteins exist. Cerl binds to Nodal, and Lefty1/2 bind to Nodal and FGF-CFC to antagonize Nodal signaling [37]. Depletion of *lefty1/2* by injecting antisense morpholino oligonucleotides

into zebrafish embryos causes unchecked Nodal signaling, expansion of mesendoderm, and loss of ectoderm [38]. In Xenopus, the expression of Nodal responsive organizer genes expands away from the dorsal blastopore lip and affects organizer patterning and the gastrulation when *Xlefty* is depleted [39].

2. BMP

Bone morphogenetic proteins (BMPs) participate in a variety of biological processes from embryonic development through the entire life. They are especially known for their role in dorsoventral and anterior-posterior (A-P) axis formation during embryogenesis [40, 41]. In zebrafish, the expression of *bmp2b* and *bmp7a* begins rapidly throughout the blastoderm following the mid-blastula transition. *bmp4* is expressed slightly later in a ventrally restricted domain, and its expression depends on *bmp2b* and *bmp7a*. The ventral to dorsal BMP signaling gradient begins to form in late blastula stages, and BMP signaling is cleared from the dorsal side of the embryo by the onset of gastrulation [6]. This ventral to dorsal BMP gradient is essential for the establishment of dorsoventral axis in developing embryos. Zebrafish with mutations in different BMP signaling components including *swirl/bmp2b*, *snailhouse/bmp7a*, *somitabun/smad5*, *lost-a-fin/alk8, mini fin/tolloid, chordin/chordino,* and *ogon/sizzled* all show dorsoventral patterning defects [6]. In Xenopus, organizer-specific transcription from the midblastula transition onwards is repressed by BMP2 while BMP4 has no significant effect on preventing the early activation of organizer-specific genes. However, BMP4 takes place to pattern mesodermal structures once the gastrulation begins. [42]. Therefore, different BMPs might play different roles before and during the gastrulation to pattern developing

embryos. Meanwhile, BMP signaling also plays a role in negatively regulating adhesion and migration of mesodermal cells during the gastrulation. This function is independent of its role of dorsoventral patterning. In zebrafish, BMP acts through Alk8 and Smad5 to negatively regulate Ca^{2+}/Cadherin-dependent cell-cell adhesiveness. This effect results in defining different migratory zones and directing lamelli-podia-driven cell migration during the dorsal convergence in lateral regions of zebrafish gastrula [43]. Moreover, BMPs act as important players in patterning extraembryonic tissues and guiding germ layer development during the gastrulation. The proximal-distal (P-D) polarity in the mouse embryo is established around embryonic day 3.5 (E3.5) [44]. At this stage, the embryo consists of both embryonic tissues and extraembryonic tissues. Shortly before the gastrulation (E5.5-E6.0), an extraembryonic signaling center called anterior visceral endoderm (AVE) forms when a group of cells from the distal tip of the visceral endoderm moves toward the opposite direction [45, 46]. When the gastrulation starts at E6.5, mesodermal cells in the posterior epiblast start to form the primitive streak at the junction between the epiblast and the extraembryonic endoderm. This process is called axis rotation that converts the initial P-D polarity to A-P polarity and is essential for the gastrulation [47]. The mechanism that regulates this process is still not well understood. However, several studies have shown that BMP signaling is required for embryonic patterning at this stage. BMP4 is expressed in both primitive streak and extraembryonic ectoderm before and during the gastrulation [48]. Loss of *bmp4* leads to the formation of a ventrally projected bulge in the posterior region of the primitive streak in mice. This phenotype can be rescued by generating tetraploid chimeras that combine both *bmp4* mutant embryonic stem (ES) cells and wildtype embryos [49]. In this experiment, all

cells in the embryonic region are derived from *bmp4* mutant ES cells and extraembryonic cells are derived from wild type. This result suggests that BMP4 in the extraembryonic ectoderm is essential for the formation of primitive streak through a non-autonomous mechanism. Loss of *bmp2* in mice leads to the abnormal development of the extraembryonic tissues while the gastrulation can still proceed, and later the embryos die by E8.5 [50]. The maintenance of adequate BMP gradient during the gastrulation is achieved by the combination of the regulation of BMP expression and the effect of BMP antagonists. In the dorsal part of the embryo, the secreted BMP antagonist Chordin and Noggin are known to block the BMP signaling by binding to secreted BMP molecules and preventing their binding to receptors [51-53]. Through this mechanism, the strength of BMP signaling can be regulated at the post-translational level. A recent study also shows that the ventral to dorsal BMP gradient in the zebrafish early embryos is determined by graded expression of BMP ligands [54]. This result suggests that BMP gradient can also be maintained at the transcriptional level. The maintenance of *bmp* expression is controlled by an auto-regulatory loop via Smad5. In zebrafish *smad5* mutants, the expression of both *swirl/bmp2b* and *snailhouse/bmp7a* fails to be maintained because of the disrupted auto-regulatory loop [55, 56]. Sequential ChIP experiment using chromatin from zebrafish gastrulating embryos shows that Mga, Max and Smad4 form a complex and bind to a region 3.3kb upstream of the *bmp2b* transcription start site containing both E-box and T-box sites, suggesting a possible transcriptional regulatory mechanism of *bmp2b* expression during the gastrulation [57]. To sum up, maintaining adequate BMP signaling strength is essential and required for the normal embryonic patterning.

Cilia in embryonic development

Cilia and their biological functions

Cilia are projection-like organelles found in eukaryotic cells. They can serve as either sensory or motile organelles and are involved in a variety of biological events [58]. The backbone inside a cilium is a microtubule-based cytoskeleton called axoneme. Cilia can be found throughout different tissues and organs in vertebrates, such as the lining of the trachea, brain ventricles, fallopian tubes in female reproduction system, photoreceptor cells, olfactory neurons, kidney cells, and embryonic nodal cells. This broad distribution of cilia in the body suggests that cilia participate in many different important biological functions from embryos to adults. The external body plan of vertebrates is bilaterally symmetrical, but several internal organs, including heart, blood vessels, digestive organs, and parts of the brain, are highly left-right asymmetrical. This internal left-right asymmetry is essential for the functions of these organs. In vertebrate embryos, motile cilia are required to establish the left-right (LR) axis at the end of gastrulation [59]. A model has been proposed from studies of mouse embryos that monocilia protruding from cells in the late gastrula node direct an asymmetric flow of extracellular fluid that results in the establishment of asymmetric gene expression [60]. The first cilia form in an embryonic tissue of zebrafish called Kupffer's vesicle (KV), which is analogous to the mouse node [61]. Disruptions of the KV cilia result in a complete reversal of the LR axis, known as situs inversus, or in a randomized LR axis, called heterotaxia [59]. Taken together, KV motile cilia can regulate the formation of left-right asymmetry of zebrafish in early developmental stages. Besides, ependymal cilia form the lining of brain

ventricles, and direct the cerebrospinal fluid (CSF) flow in ventricles [62, 63]. Disruption of ependymal cilia-directed CSF flow in brain ventricles results in the abnormal accumulation of CSF and further causes hydrocephalus [64]. Furthermore, cilia are also required for the maintenance of kidney's function. Cystic kidney, a severe disorder results in kidney dysfunction, could be a result of disrupting the expression of a variety of cilia-related genes [65]. In brief, the cilium is an important organelle in regulating functions of many organs.

Cilia as the signaling center

Cilia have been considered as either motile or sensory organelles to maintain functions of a variety of organs. This also implies the importance of how cilia communicate with signaling pathways to achieve these functions. Indeed, it has been revealed that several signaling pathways show high correlation with the presence of cilia. In renal tubules, cilia can act as mechanosensors to detect fluid flow. This mechanism requires the participation of two ciliary membrane proteins polycystin-1 (PC1) and polycystin-2 (PC2) to turn on downstream calcium-dependent signaling pathways. Mutations of PC1, PC2, or some other cilia-related genes will lead to the formation of cystic kidney, suggesting cilia are important organelles to transmit extracellular signals into cells [66]. However, there are some other signaling pathways might be involved in the maintenance of kidney's function through cilia, including Wnt/PCP and mTOR [67-69]. Meanwhile, cilia of olfactory neurons can initiate olfaction through cAMP-dependent depolarization upon the binding of odorant ligands to G-protein coupled receptors [70]. Primary cilia also play critical roles in cell-cell communication during the

developmental process. Components of Hedgehog (Hh) signaling have been shown to localize dynamically within cilia [71]. Dampened Hh signaling is found in zebrafish without cilia [72], suggesting the possible role that cilia play in the regulation of normal Hh signaling pattern. Cilia might act as not only cellular antennae but also compartments to concentrate a variety of signaling components in order to respond rapidly when receiving signals from extracellular environment.

Gastrulation and cell movement

Before and during the gastrulation, embryonic cells adapt their cell fates according to the instructional signals that they receive. Embryonic cells also undergo massive cell migration and rearrangement in order to organize the embryo into a multi-layered structure. Three major types of cell movement, epiboly, internalization, and convergent extension are involved in the gastrulation [73]. Epiboly is the process involving the spreading and thinning of cell layers; internalization moves the mesodermal and endodermal precursors from the blastula surface beneath the prospective ectodermal layer through a gateway known as the blastopore; finally, convergent extension narrows embryonic tissues mediolaterally and extends them anteroposteriorly [73, 74]. In zebrafish, gastrulation cell movements start at sphere stage (4 hours post-fertilization) when cells in the blastoderm sitting atop of YSL begin to migrate [75]. Epiboly, the first event of gastrulation cell movements, begins when the yolk cell domes into the blastoderm. At the same time, the blastoderm becomes thinner and extends toward the vegetal pole [76]. The coordination of the EVL, deep cells and YSL is required for proper

vegetal cell migration. Removal of blastoderm from killifish *Fundulus heteroclitus* embryos shows that YSL can still undergo epiboly movement, suggesting the importance of YSL movement during the epiboly [77]. It has been implicated that the yolk cytoskeleton plays important roles in the epiboly [74]. Two types of cytoskeleton, microtubule and actin, cooperate to move YSL, EVL and deep cells toward vegetal pole during the epiboly. The yolk cell contains two different arrays of microtubules. When blastoderm and YSL move halfway towards the vegetal pole during the early gastrulation, the EVL leads the vegetal movement of deep cells. A dense network of microtubules in the yolk cell surrounds the yolk syncytial nuclei beneath and vegetal to the blastoderm. Another set of long microtubules oriented along the animal-vegetal axis emerges from YSL into the yolk cytoplasmic layer [74, 78]. Dense actin filaments also cover the vegetal cortical region of the yolk cell. The yolk syncytial nuclei lead in the epibolic movement while the EVL in front of the deep cells continues to move towards the vegetal pole at the late gastrulation. In the cortex of the yolk cell, the dense network and the animal–vegetal oriented sets of microtubules are also present. A structure containing the dense organization of actin filaments continues to form in the vegetal cortical region of the yolk cell [74]. One study using drugs affecting microtubule stabilization and destabilization suggests that changing the organization of microtubules has significant impact on the epiboly in zebrafish. Treating embryos with microtubule stabilizing reagent Paclitaxel delays all epibolic movements toward the vegetal pole, whereas the disruption of microtubules with microtubule destabilizing reagent Nocodazole blocks vegetal movement of the YSL completely, but only partially prevents epiboly of the EVL and deep cells [78]. One explanation to this phenomenon is a microtubule-independent

endocytosis that drives epiboly of the EVL that occurs in the external YSL just vegetal to the EVL attachment. The removal of the external YSL membrane by endocytosis together with the expansion of the internal YSL membrane underlying the blastoderm, could lead to the epiboly of YSL membrane, towing the EVL with it [78]. Proper organization of actin filaments is also essential for the epiboly. Treating zebrafish embryos with cytochalasin B or the calcium chelator dibromo-BAPTA results in the disruption of all actin-based structures found in the yolk, leading to the slowing or immediate arrest of epiboly, respectively, followed by a failure of yolk cell occlusion and the eventual lysis of the embryo through the vegetal pole region [79]. Nevertheless, little is known regarding the cytoskeletal regulation during the epiboly. It has been shown that pregnenolone, a lipid produced from cholesterol in the yolk cell, is required to maintain a level of polymerized microtubules to ensure normal epiboly movement. Pregnenolone is produced by an enzyme Cyp11a1 expressed in YSL during the epiboly. Suppressing *cyp11a1* expression in zebrafish embryos using antisense morpholino oligonucleotides did not perturb cell fates, but caused epibolic delay. This epibolic defect was partially rescued by either the injection of *cyp11a1* mRNA or the supplementation of pregnenolone [80]. Other than cytoskeletal components, several transcription factors have also been shown to be essential for normal epiboly progression. A T-box transcription factor Eomesodermin A (Eomesa) has been implicated as playing a role during the epiboly through promoting the expression of *mtx2* [81]. Maternal Eomesa has been reported to play a role in the initiation of epiboly, which involves doming of the yolk cell up into the overlying blastoderm. However, the epiboly progression is normal, suggesting that the epiboly initiation is genetically separable from the progression. The microtubules

in the yolk cell are also defective in maternal-zygotic *eomesa* mutant embryos [82]. Moreover, Zebrafish transcription factor *pou5f1* deficient maternal and zygotic *spiel ohne grenzen* (MZ*spg*) mutant embryos develop severe epiboly defects. An altered array of cortical microtubules and F-Actin, with large patches of microtubule-free area are found in the yolk cell of MZ*spg* mutants during the epiboly [83]. The transcription regulation might require the participation of some post-translational modifications on transcription factors. For example, the monosaccharide O-linked β-N-acetylglucosamine (O-GlcNAc) is added onto a variety of proteins to regulate their activities. Two different enzymes, O-GlcNAc Transferase (Ogt) and O-GlcNAcase (Oga), catalyze the attachment and removal of O-GlcNAc to target proteins respectively. Overexpression of *ogt* and *oga* mRNAs in zebrafish embryos delays the epiboly and cause a severe disorganization of microtubules and actin filaments in the YSL. These cytoskeletal defects are similar to the phenotypes found in mutants lacking Pou5f1. Since O-GlcNAc modified Pou5f1/Oct4 is identified in mouse stem cells, it is also possible that zebrafish Pou5f1 also undergoes the same modification in order to perform its activity in regulating the epiboly progression [84]. Besides, the gastrulation is a stage particularly sensitive to environmental teratogen exposure. Ethanol exposure disrupts both the cell adhesion and the yolk microtubule organization and further causes the cell movement defects in the epiboly. E-cadherin expression is not affected, but the distribution is changed when exposing zebrafish embryos to ethanol [85]. E-cadherin has been implicated to play a critical role in the epiboly. Moderate reduction of E-cadherin protein level by injecting antisense morpholino oligonucleotides leads to epibolic defects, whereas lacking functional E-cadherin completely in the *half baked* mutant results in severe defects in the early cell

division and halts the embryonic development [86, 87]. Taken together, a successful epiboly requires both the cytoskeletal reorganization and the proper regulation of cell adhesion.

Neural crest development

Neural crest (NC) cells are a unique multipotent cell population only found in embryos of vertebrates. NC cells are derived from the dorsal neural tube in developing embryos and undergo the migration to many different locations in the body to give rise to a variety of derivatives, including neurons and glia of the peripheral nervous system, sympathoadrenal cells, cardiac cells, melanocytes, and most of the bones and cartilages of the face and skull as well as tendons, muscles and connective tissues of the ear, eye, teeth and blood vessels [88, 89]. NC cells originate from the neural plate border (NPB), which is a region of ectoderm sitting in between the neural plate (NP) and the non-neural ectoderm (NNE). Presumptive NC cells occupy the dorsal tips of the neural plate (the neural folds) when the NP starts to fold inwardly to form the neural tube, and are laterally flanked by prospective placodal ectoderm in cranial regions and by prospective epidermis in the trunk and tail [89]. After NC cells adapt their fate, they undergo an epithelial-mesenchymal transition (EMT) from rostral to caudal and eventually migrate to form various cell types in different regions. NC cells start migrating soon after the neural tube completely fuses in the mouse, Xenopus, and zebrafish. However, chick NC cells begin to migrate before the neural tube is closed [89]. The establishment of NC cell population is influenced by many different signaling pathways, such as BMP, Wnt, fibroblast growth

factor (FGF), Notch/Delta, retinoic acid (RA), Hedgehog (Hh), and endothelin signaling [89, 90]. A recent study showed that NC induction starts as early as in the gastrulation when the ventral BMP and dorsal Wnt signaling form gradients in the gastrula to maintain the prospective NC cell population in zebrafish. Two transcription factors, Tfap2a and Foxd3, are responsible for regulating BMP and Wnt signaling during this process respectively [91]. Similar event is also observed in other species. Chick NC cells are thought to originate from the neural plate border where the transcription factor Pax7 is also expressed in the mid-gastrula as early as stage HH4+. When tissue explants from this Pax7-expressing domain of the gastrula were cultured in the absence of exogenous inductive signals, they were able to generate NC cells despite the lack of added factors or other tissue interactions [92]. In fact, it is known that NC is induced as early as at stage HH2 [89]. Several signaling pathways, such as BMP, Wnt, FGF, and Notch/Delta signaling, are proposed to be involved in the early NC induction. These signaling pathways further affect the expression of a set of transcription factors, including Msx1, Pax3, Zic1, Hairy2, Gbx2, Pax7, Ap2a, and Meis3, which act as crucial regulators of NPB specification [89]. These transcription factors together with the same signaling pathways further trigger the expression of another set of transcription factors for NC specification. NC specifiers include Snail1b, Ap2a, Foxd3, Sox9/10, Twist, and cMyc, which are proposed to regulate and control NC behavior, from EMT and delamination to migration and differentiation [89, 90]. Together, NC development is tightly controlled by the spatiotemporal expression patterns of these transcription factors, and their combinational effect with signaling pathways may also be required to ensure the normal NC formation.

REFERENCES

1. Alexander W Bruce, M.Z.-G. (2010). Developmental control of the early mammalian embryo: competition among heterogeneous cells that biases cell fate. Current Opinion in Genetics & Development *20*, 485-491.
2. Duval, M. (1891). The rodent placenta. Third part. The placenta of the mouse andof the rat. J. Anat. Physiol. Normales et Pathol. de l'Homme et des Animaux *27*, 24-73; 344-395; 515-612.
3. Sobotta, J. (1911). Die Entwicklung des Eies der Maus vom ersten Auftreten des Mesoderms an bis zur Ausbildung der Embryonalanlage und dem Auftreten der Allantois. I. Teil: Die Keimblase. Archiv. fur mikroskopische Anatomie *78*, 271-352.
4. Claudio D. Stern, K.M.D. (2012). The hypoblast (visceral endoderm): an evo-devo perspective. Development *139*, 1059-1069.
5. Charles. B. Kimmel, R.D.L. (1985). Cell lineage of zebrafish blastomeres. II. Formation of the yolk syncytial layer. Developmental Biology *108*, 86-93.
6. Yvette G Landon, M.C.M. (2011). Maternal and zygotic control of zebrafish dorsoventral axial patterning. Annual Review of Genetics *45*, 357-377.
7. H. Spemann, H.M. (1924). Induction of embryonic primordial by implantation of organizers from a different species. Roux's Arch Entw Mech *100*.
8. Tewis Bouwmeester, S.-H.K., Yoshiki Sasai, Bin Lu, Eddy M. De Robertis (1996). Cerberus is a head-inducing secreted factor expressed in the anterior endoderm of Spemann's organizer. Nature *382*, 595-601.

9. Stefano Piccolo, E.A., Luc Leyns, Subha Bhattacharyya, Horst Grunz, Tewis Bouwmeester, E. M. De Robertis (1999). The head inducer Cerberus is a multifunctional antagonist of Nodal, BMP and Wnt signals. Nature *397*, 707-710.

10. Hiroki Kuroda, O.W., E. M. De Robertis (2004). Neural Induction in Xenopus: Requirement for Ectodermal and Endomesodermal Signals via Chordin, Noggin, β-Catenin, and Cerberus. PLoS Biology *2*, E92.

11. Robertis, E.M.D. (2009). Spemann's organizer and the self-regulation of embryonic fields. Mechanism of Development *126*, 925-941.

12. Mary Y. Wu, C.S.H. (2009). TGF-β Superfamily Signaling in Embryonic Development and Homeostasis. Developmental Cell *16*, 329-343.

13. Alexander Weiss, L.A. (2013). The TGFbeta Superfamily Signaling Pathway. WIRESs Developmental Biology *2*, 47-63.

14. Kohei Hatta, C.B.K., Robert K. Ho, Charline Walker (1991). The cyclops mutation blocks specification of the floor plate of the zebrafish central nervous system. Nature *350*, 339-341.

15. Benjamin Feldman, M.A.G., Elizabeth S. Egan, Scott T. Dougan, Gabriela Rennebeck, Howard I. Sirotkin, Alexander F. Schier, William S. Talbot (1998). Zebrafish organizer development and germ-layer formation require nodal-related signals. Nature *395*, 181-185.

16. Sarah Long, N.A., Michael Rebagliati (2003). The zebrafish nodal-related gene southpaw is required for visceral and diencephalic left-right asymmetry Development *130*, 2303-2316.

17. Xunlei Zhou, H.S., Linda Lowe, Brigid L. M. Hogan, Michael R. Kuehn (1993). Nodal is a novel TGF-β-like gene expressed in the mouse node during gastrulation. Nature *361*, 543-547.

18. Frank L Conlon, K.M.L., Norma Takaesu, Katrin S Barth, Andreas Kispert, Bernhard Herrmann, Elizabeth J Robertson (1994). A primary requirement for nodal in the formation and maintenance of the primitive streak in the mouse. Development *120*, 1919-1928.

19. Isabelle Varlet, J.C., Elizabeth J. Robertson (1997). *nodal* expression in the primitive endoderm is required for specification of the anterior axis during mouse gastrulation Development *124*, 1033-1044.

20. Dominic P. Norris, E.J.R. (1999). Asymmetric and node-specific nodal expression patterns are controlled by two distinct cis-acting regulatory elements Genes & Development *13*, 1575-1588.

21. Jane Brennan, C.C.L., Dominic P. Norris, Tristan A. Rodriguez, Rosa S. P. Beddington, Elizabeth J. Robertson (2001). Nodal signalling in the epiblast patterns the early mouse embryo. Nature *411*, 965-969.

22. C. Michael Jones, M.R.K., Brigid L. M. Hogan, James C. Smith, Christopher V. E. Wright (1995). Nodal-related signals induce axial mesoderm and dorsalize mesoderm during gastrulation. Development *121*, 3651-3662.

23. K. D. Lustig, K.K., E. Sun, R. Ramos, H. Elmendorf, M. W. Kirschner (1996). A Xenopus nodal-related gene that acts in synergy with noggin to induce complete secondary axis and notochord formation. Development *122*, 3275-3282.

24. Elaine M. Joseph, D.A.M. (1997). Xnr4: A Xenopus Nodal-Related Gene Expressed in the Spemann Organizer. Developmental Biology *184*, 367-372.

25. Shuji Takahashi, C.Y., Kazuhiro Takano, Kousuke Tanegashima, Yasuko Onuma, Jun-Ichi Goto, Makoto Asashima (2000). Two novel nodal-related genes initiate early inductive events in Xenopus Nieuwkoop center. Development *127*, 5319-5329.

26. Jixiang Ding, L.Y., Yu-Ting Yan, Amy Chen, Nishita Desai, Anthony Wynshaw-Boris, Michael M. Shen (1998). Cripto is required for correct orientation of the anterior–posterior axis in the mouse embryo. Nature *395*, 702-707.

27. Kira Gritsman, J.Z., Simon Cheng, Elizabeth Heckscher, William S Talbot, Alexander F Schier (1999). The EGF-CFC Protein One-Eyed Pinhead Is Essential for Nodal Signaling. Cell *97*, 121-132.

28. Fortunato Ciardiello, R.D., Nancy Kim, Maria Graziella Persico, David S. Salomon (1991). Expression of cripto, a novel gene of the epidermal growth factor gene family, leads to in vitro transformation of a normal mouse mammary epithelial cell line. Cancer Research *51*, 1051-1054.

29. Wei Weng, D.L.S. (2003). Nodal Signaling and Vertebrate Germ Layer Formation. Birth Defects Research (Part C) *69*, 325-332.

30. Chang-Yeol Yeo, M.W. (2001). Nodal Signals to Smads through Cripto-Dependent and Cripto-Independent Mechanisms. Molecular Cell *7*, 949-957.

31. Rui Sakuma, Y.-i.O., Chikara Meno, Hideta Fujii, Hou Juan, Jun Takeuchi, Toshihiko Ogura, En Li, Kohei Miyazono, Hiroshi Hamada (2002). Inhibition

of Nodal signalling by Lefty mediated through interaction with common receptors and efficient diffusion. Genes to Cells *7*, 401-412.

32. Xiang Fan, E.G.H., , Bo Xu, Christina Sias, Koichi Kawakami, Rebecca D. Burdine, Scott T. Dougan (2007). Nodal signals mediate interactions between the extra-embryonic and embryonic tissues in zebrafish. Developmental Biology *310*, 363-378.

33. Benjamin L. Martin, D.K. (2007). Developmental Biology: Micro(RNA)-Managing Nodal. Current Biology *17*, R975-R977.

34. Wen-Yee Choi, A.J.G., Alexander F. Schier (2007). Target Protectors Reveal Dampening and Balancing of Nodal Agonist and Antagonist by miR-430. Science *318*, 271-274.

35. Graziano Martello, L.Z., Masafumi Inui, Marco Montagner, Maddalena Adorno, Anant Mamidi, Leonardo Morsut, Sandra Soligo, Uyen Tran, Sirio Dupont, Michelangelo Cordenonsi, Oliver Wessely, Stefano Piccolo (2007). MicroRNA control of Nodal signalling. Nature *449*, 183-188.

36. Pooja Kumari, P.C.G., Shimin Lim, Long Duc Tran, Sylke Winkler, Robin Philp, Karuna Sampath (2013). An essential role for maternal control of Nodal signaling. eLIFE *2*, e00683.

37. Satoshi Kishigami, Y.M. (2005). BMP signaling and early embryonic patterning. Cytokine & Growth Factor Reviews *16*, 265-278.

38. Benjamin. Feldman, M.L.C., L. Saúde, M. J. Parsons, R. J. Adams, S. W. Wilson, D. L. Stemple. (2002). Lefty antagonism of Squint is essential for normal gastrulation. Current Biology *12*, 2129-2135.

39. W. W. Branford, H.J.Y. (2002). Lefty-dependent inhibition of Nodal- and Wnt-responsive organizer gene expression is essential for normal gastrulation. Current Biology *12*, 2136-2141.

40. Hogan, B.L. (1996). Bone morphogenetic proteins in development. Current Opinion in Genetics & Development *6*, 432-438.

41. Whitman, M. (1998). Smads and early developmental signaling by the TGFβ superfamily. Genes & Development *12*, 2445-2462.

42. Karen Marom, V.L., Graciela Pillemer, Abraham Fainsod (2005). Temporal analysis of the early BMP functions identifies distinct anti-organizer and mesoderm patterning phases. Developmental Biology *282*, 442-454.

43. Sophia von der Hardt, J.B., Adi Inbal, Lara Carvalho, Lilianna Solnica-Krezel, Carl-Philipp Heisenberg, Matthias Hammerschmidt (2007). The Bmp Gradient of the Zebrafish Gastrula Guides Migrating Lateral Cells by Regulating Cell-Cell Adhesion. Current Biology *17*, 475-487.

44. Rosa S.P Beddington, E.J.R. (1999). Axis Development and Early Asymmetry in Mammals. Cell *96*, 195-209.

45. J. A. Rivera-Pérez, J.M., T. Magnuson (2003). Dynamic morphogenetic events characterize the mouse visceral endoderm. Developmental Biology *261*, 470-487.

46. Shankar Srinivas, T.R., Melanie Clements, James C. Smith, Rosa S. P. Beddington (2004). Active cell migration drives the unilateral movements of the anterior visceral endoderm Development *131*, 1157-1164.

47. Cindy C Lu , J.B., Elizabeth J Robertson (2001). From fertilization to gastrulation: axis formation in the mouse embryo. Current Opinion in Genetics & Development *11*, 384-392.

48. Glenn Winnier, M.B., Patricia A. Labosky, Brigid L.M. Hogan (1995). Bone morphogenetic protein-4 is required for mesoderm formation and patterning in the mouse. Genes & Development *9*, 2105-2116.

49. Takeshi Fujiwara, D.B.D., Kathleen K. Sulik, Brigid L. M. Hogan (2002). Distinct requirements for extra-embryonic and embryonic bone morphogenetic protein 4 in the formation of the node and primitive streak and coordination of left-right asymmetry in the mouse Development *129*, 4685-4696.

50. Hongbing Zhang, A.B. (1996). Mice deficient for BMP2 are nonviable and have defects in amnion/chorion and cardiac development. Development *122*, 2977-2986.

51. Stefano Piccolo, Y.S., Bin Lu, Eddy M. De Robertis (1996). Dorsoventral Patterning in Xenopus: Inhibition of Ventral Signals by Direct Binding of Chordin to BMP-4. Cell *86*, 589-598.

52. Stefan Schulte-Merker, K.J.L., Andrew P. McMahon, Matthias Hammerschmidt (1997). The zebrafish organizer requires chordino. Nature *387*, 862-863.

53. Sasai, Y. (2001). Regulation of neural determination by evolutionarily conserved signals: anti-BMP factors and what next? current opinion in Neurobiology *11*, 22-26.

54. Marie-Christine Ramel, C.S.H. (2013). The ventral to dorsal BMP activity gradient in the early zebrafish embryo is determined by graded expression of BMP ligands. Developmental Biology *378*, 170-182.

55. Bettina Schmid, M.F., Stephanie A. Connors, Jamie Trout, Bernard Thisse, Christine Thisse, Mary C. Mullins (2000). Equivalent genetic roles for bmp7/snailhouse and bmp2b/swirl in dorsoventral pattern formation. Development *127*, 957-967.

56. Marc Hild, A.D., Gerd-Jörg Rauch, Andrea Meier, Tewis Bouwmeester, Pascal Haffter, Matthias Hammerschmid (1999). The smad5 mutation somitabun blocks Bmp2b signaling during early dorsoventral patterning of the zebrafish embryo. Development *126*, 2149-2159.

57. Yuhua Sun, W.-C.T., Xiang Fan, Rebecca Ball, Scott T. Dougan (2014). Extraembryonic Signals under the Control of MGA, Max, and Smad4 Are Required for Dorsoventral Patterning. Developmental Cell *28*, 322-334.

58. Gregory J Pazour, George B Witman (2003). The vertebrate primary cilium is a sensory organelle. Current Topics in Cell Biology *15*, 105-110.

59. Rebecca D. Burdine, A.F.S. (2000). Conserved and divergent mechanisms in left–right axis formation. Genes & Development *14*, 763-776.

60. Shigenori Nonaka, Y.T., Yasushi Okada, Sen Takeda, Akihiro Harada, Yoshimitsu Kanai, Mizuho Kido, Nobutaka Hirokawa (1998). Randomization of Left–Right Asymmetry due to Loss of Nodal Cilia Generating Leftward Flow of Extraembryonic Fluid in Mice Lacking KIF3B Motor Protein. Cell *95*, 829-837.

61. Jeffrey J. Essner, J.D.A., Molly K. Nyholm, Erin B. Harris, H. Joseph Yost (2005). Kupffer's vesicle is a ciliated organ of asymmetry in the zebrafish embryo that initiates left-right development of the brain, heart and gut. Development *132*, 1247-1260.

62. Bigio, M.R.D. (2010). Ependymal cells: biology and pathology. Acta Neuropathologica *119*, 55-73.

63. Bruni, J.E. (1998). Ependymal development, proliferation, and functions: A review. Microscopy Research and Technique *41*, 2-13.

64. Inés Ibañez-Tallon1, A.P., Manfred Fliegauf3, Heike Olbrich3, Andreas Kispert4, Uwe-Peter Ketelsen3, Alison North5, Nathaniel Heintz1 and Heymut Omran (2004). Dysfunction of axonemal dynein heavy chain Mdnah5 inhibits ependymal flow and reveals a novel mechanism for hydrocephalus formation Human Molecular Genetics *13*, 2133-2141.

65. Drummond, I.A. (2005). Kidney Development and Disease in the Zebrafish. Journal of the American Society of Nephrology *16*, 299-304.

66. Nicolas F. Berbari, A.K.O.C., Courtney J. Haycraft, Bradley K. Yoder (2010). The Primary Cilium as a Complex Signaling Center. Current Biology *19*, R526.

67. Anna D' Angelo, B.F. (2011). The primary cilium in different tissues—lessons from patients and animal models. Pediatric Nephrology *26*, 655-662.

68. Norihito Kishimoto, Y.C., Alice Park, Zhaoxia Sun (2008). Cystic Kidney Gene seahorse Regulates Cilia-Mediated Processes and Wnt Pathways. Developmental Cell *14*, 954-961.

69. Linda M. DiBella, A.P., Zhaoxia Sun (2008). Zebrafish Tsc1 reveals functional interactions between the cilium and the TOR pathway. Human Molecular Genetics *18*, 595-606.

70. Dyke P. McEwen, P.M.J., Jeffrey R. Martens (2008). Chapter 12 Olfactory Cilia: Our Direct Neuronal Connection to the External World. Current Topics in Developmental Bilogy *85*, 333-370.

71. Kevin C. Corbit, P.A., Veena Singla, Andrew R. Norman, Didier Y. R. Stainier, Jeremy F. Reiter (2005). Vertebrate Smoothened functions at the primary cilium. Nature *437*, 1018-1021.

72. Peng Huang, A.F.S. (2009). Dampened Hedgehog signaling but normal Wnt signaling in zebrafish without cilia. Development *136*, 3089-3098.

73. Laurel A. Rohde, C.P.H. (2007). Zebrafish Gastrulation: Cell Movements, Signals, and Mechanisms. International Review of Cytology *261*, 159-192.

74. Solnica-Krezel, L. (2006). Gastrulation in zebrafish — all just about adhesion? Current Opinion in Genetics & Development *16*, 433-441.

75. Charles B. Kimmel, W.W.B., Seth R. Kimmel, Bonnie Ullmann, Thomas F. Schilling (1995). Stages of embryonic development of the zebrafish. developmental Dynamics *203*, 253-310.

76. Rachel M.Warga, C.B.K. (1990). Cell movement during epiboly and gastrulation in zebrafish. Development *108*, 569-580.

77. Trinkaus, J.P. (1951). A study of the mechanism of epiboly in the egg of Fundulus heteroclitus. Journal of Experimental Zoology *118*, 269-320.

78. Lilianna Solnica-Krezel, W.D. (1994). Microtubule arrays of the zebrafish yolk cell: organization and function during epiboly. Development *120*, 2443-2455.

79. Jackie C. Cheng, A.L.M., Sarah E. Webb (2004). Organization and function of microfilaments during late epiboly in zebrafish embryos. Developmental Dynamics *231*, 313-323.

80. Hwei-Jan Hsu, M.-R.L., Chao-Tsen Chen, Bon-chu Chung (2005). Pregnenolone stabilizes microtubules and promotes zebrafish embryonic cell movement. Nature *439*, 480-483.

81. Ashley E.E. Bruce, C.H., Monica Dixon Fox, Robert K. Ho (2005). T-box gene eomesodermin and the homeobox-containing Mix/Bix gene mtx2 regulate epiboly movements in the zebrafish. Developmental Dynamics *233*, 105-114.

82. Susan Du, B.W.D., Marina Mione, Cecilia B. Moens, Ashley E. E. Bruce (2012). Differential regulation of epiboly initiation and progression by zebrafish Eomesodermin A. Developmental Biology *362*, 11-23.

83. Martina Lachnit, E.K., Wolfgang Driever (2008). Alterations of the cytoskeleton in all three embryonic lineages contribute to the epiboly defect of Pou5f1/Oct4 deficient MZspg zebrafish embryos. Developmental Biology *315*, 1-17.

84. Danielle M Webster, C.F.T., Yuhua Sun, Dorota Wloga, Steven Gay, Kimberly D Klonowski, Lance Wells, Scott T Dougan (2009). O-GlcNAc modifications regulate cell survival and epiboly during zebrafish development. BMC Developmental Biology *9*.

85. Swapnalee Sarmah, P.M., Courtney L. Curtis, Jeanette N. McClintick, Bryce B. Buente, David J. Holdgrafer, Osato Ogbeifun, Opeyemi C. Olorungbounmi, Liliana Patino, Ryan Lucas, Sonya Gilbert,Evan S. Groninger, Julia Arciero, Howard J. Edenberg, James A. Marr (2013). Ethanol exposure disrupts extraembryonic microtubule cytoskeleton and embryonic blastomere cell adhesion, producing epiboly and gastrulation defects Biology Open *2*, 1013-1021.

86. Donald A. Kane, K.N.M., Rachel M. Warga (2005). Mutations in half baked/E-cadherin block cell behaviors that are necessary for teleost epiboly. Development *132*, 1105-1116.

87. Sherry G. Babb, J.A.M. (2004). E-cadherin regulates cell movements and tissue formation in early zebrafish embryos. Developmental Dynamics *230*, 263-277.

88. Roberto Mayor, E.T. (2013). The neural crest. Development *140*, 2247-2257.

89. Timothy J. Stuhlmiller, M.I.G.-C. (2012). Current perspectives of the signaling pathways directing neural crest induction. Cellular and Molecular Life Sciences *69*, 3715-3737.

90. Paola Betancur, M.B.-F., and Tatjana Sauka-Spengler (2010). Assembling Neural Crest Regulatory Circuits into a Gene Regulatory Network. Annual Review of Cell and Developmental Biology *26*, 581-603.

91. Wen-Der Wang, D.B.M., Mercedes Montero-Balaguer, Antonis K. Hatzopoulos, Ela W. Knapik (2011). Tfap2a and Foxd3 regulate early steps in the

development of the neural crest progenitor population. Developmental Biology *360*, 173-185.

92. Martín L. Basch, M.B.-F., Martín I. García-Castro (2006). Specification of the neural crest occurs during gastrulation and requires Pax7. Nature *441*, 218-222.

CHAPTER 2

MGA IS A NOVEL REGULATOR OF NEURAL CREST DEVELOPMENT IN ZEBRAFISH

INTRODUCTION

During embryonic development in vertebrates, neural crest (NC) cells are a group of migratory multipotent cells that will give rise to a variety of different tissues, such as pigment cells, craniofacial cartilages, peripheral nervous system (PNS) and enteric nervous system (ENS) [1-3]. NC cells originate from the border between the neural plate (NP) and non-neural ectoderm at the end of the gastrulation. In zebrafish, NC cells delaminate from the dorsal part of the neural tube soon after the closure of the neural tube and start migrating to different regions in the body. After migrating to their destinations, NC cells undergo differentiation to become various cell types according to their cell fates and also local environmental cues that they receive [1].

Signaling pathways play essential roles during early embryonic patterning. Several signaling pathways, including bone morphogenic protein (BMP), Wnt, fibroblast growth factor (FGF), and Notch/Delta, have been suggested to participate in the early induction step of NC development in different organisms [1, 2]. Among all of these signaling pathways, BMP and Wnt signaling pathways play essential roles in NC induction [4-6].

The ventral to dorsal BMP signaling gradient begins to form in late blastula stages, and BMP signaling is cleared from the dorsal side of the embryo by the onset of gastrulation [7]. This ventral to dorsal BMP gradient is essential for the establishment of dorsoventral axis in developing embryos. In Xenopus, reduced levels of BMP signaling at the lateral edges of neural plate provide an initial, weak activity to specify NC fate. Additional signals from the adjacent non-neural ectoderm, the underlying mesoderm or both are required at later stages to enhance and maintain the NC induction [8]. In zebrafish, *swirl*/ *bmp2b* mutant exhibits a loss of BMP signaling as well as a reduced NC progenitor population, while *snailhouse* /*bmp7* or *somitabun* /*smad5* mutants have the decreased BMP activity and expanded NC domain [9, 10]. Maintaining intermediate levels of ventral BMP and dorsal Wnt signaling during the gastrulation is also important for defining the domain of prospective NC cells [4]. During NC development, BMP signaling antagonizes the sensory fate-inducing activity of Wnt/β-catenin during NC development. Wnt and BMP also act synergistically to suppress differentiation and to maintain NC stem cell marker expression and multipotency [5]. Wnt signaling has been shown to have a strong influence on NC induction in the mouse, chick, Xenopus, and zebrafish [1, 11]. Blocking Wnt signaling during the early development in zebrafish inhibits NC formation without blocking development of dorsal spinal neurons, suggesting that Wnt signaling plays a crucial, time sensitive role in NC induction [11]. Therefore, a fine tuning of BMP and Wnt signaling interplay is necessary for normal NC induction.

Max's giant associated protein (Mga) is a member of T-box6/Spadetail transcription factor family and has both T-box domain and bHLHzip domain for DNA

binding. It was first identified as an interacting protein of Myc associated factor X (Max) [12]. Max serves as a cofactor with different transcription factors for DNA binding. For example, Max and Myc form heterodimers to activate many different target genes, which are involved in promoting cell cycle progression [13]. *in vitro* study showed that Mga forms heterodimers with Max to promote exiting of cell cycle by antagonizing Myc activity [14]. Human *mga* mutations are found to be associated with Richter's Syndrome, an aggressive form of lymphoma, which occurs in some patients with chronic lymphocytic leukemia (CLL) [15]. This result suggests that Mga plays a role in regulating cell proliferation. Meanwhile, loss of *mga* leads to the death of proliferating pluripotent inner cell mass cells both *in vitro* and *in vivo*, and the death of embryonic stem cells *in vitro* [16]. In zebrafish, Mga is important to the development of brain, heart and gut in zebrafish embryos [17]. Mga also regulates BMP expression in the extra-embryonic yolk syncytial layer (YSL) and contributes to the dorsoventral pattern formation [18]. Therefore, Mga might contribute to different steps of the embryonic development through different mechanisms.

In this study, we identify Mga as a novel regulator of NC development in zebrafish. Mga might affect early NC formation by positively regulating BMP signaling. However, it is still possible that Mga controls NC formation by antagonizing Myc activity during the gastrulation. Further investigation is needed in order to explore the mechanism that Mga is involved in regulating NC development.

MATERIALS AND METHODS

Zebrafish husbandry and embryo collection

The wildtype zebrafish line WIK was used in all experiments. All fish were maintained in the fish facility at 28.5°C according to the Animal Use Protocol (AUP) A2011 08-015, approved annually by the University of Georgia IACUC committee. Embryos were obtained from either single or multiple pair matings. After collection, embryos were cultured in egg water (60μg/ml Instant Ocean Sea Salt Mix, 0.3μg/ml Methylene Blue) at 28.5°C. Embryos were staged periodically using Leica S6E stereomicroscope (Leica Microsystems, Wetzlar, Germany) as previously described (Kimmel et al., 1995).

Microinjection of antisense morpholino oligonucleotides (MOs)

1- to 2-cell stage embryos were used for microinjection as previously described [19]. For suppressing the expression of Mga, two translational blocker MOs were used for experiments. Meanwhile, two mismatch MOs (misMOs) corresponding to two *mga* MOs with few different nucleotides were also used as controls [18]. *p53*MO was also used in combination with other MOs to suppress the non-specific cell death caused by MOs in all microinjections [20]. The following MOs were used in microinjections: *mgaTL1MO*: 5'-ACCCTGTTTCTCTGTATCGGCC-3'; *mgaTL1misMO*: 5'-ACgCTcTTTgTCTcTATCGcCC-3'; *mgaTL3MO*: 5'-TCTGGATAGCTTCTGACCCTCTCAC-3'-Lissamine; *mgaTL3misMO*: 5'-TCaGcATAGgTTCTcACgCTCTCAC-3'; *p53MO*: 5'-GCGCCATTGCTTTGCAAGAATTG-3' (Gene Tools, Philomath, OR). All MOs were

dissolved in distilled water individually as 10μg/μl stocks and stored at room temperature. Prior to microinjections, MOs were diluted in 0.1M KCl to the desired concentration with 0.1% phenol red as the tracing dye for microinjections. 1nl of MO injection solution was injected into the yolk of each embryo. Each embryo received combined 1.6ng *mgaMOs* (*TL1* and *TL3*) with 2.4ng *p53MO* or 1.6ng *mgaMisMOs* (*TL1* and *TL3*) with 2.4ng *p53MO* in each microinjection. Injected embryos were kept in 100mm Petri dishes with egg water at 28.5°C. Damaged or unfertilized embryos were discarded around 4 to 5hpf. Survived embryos were collected at different stages for further analyses.

***in vitro* transcription and mRNA rescue**

Mouse full-length *mga* cDNA was cloned into the pCS2+ vector. For the control, pCS2+-*βgal* encoded the full-length *β-galactosidase* was used. Both plasmids were linearized with *Not*I for using as templates for *in vitro* transcription. Capped mRNAs were synthesized using Ambion mMessage mMachine SP6 Transcription Kit (AM1340, Life Technologies, Carlsbad, CA). Final concentration of mRNAs was determined by Nanodrop spectrophotometer. 100pg of Mouse *mga* mRNA or *βgal* mRNA was injected into each WIK embryo at 1- to 2-cell stage along with combined 1.6ng *mgaMOs* (*TL1* and *TL3*) and 2.4ng *p53MO* with 0.1M KCl and phenol red. Damaged or unfertilized embryos were discarded around 4 to 5hpf. Survived embryos were scored at 32hpf for their skin pigmentation under the Leica S6E stereomicroscope (Leica Microsystems, Wetzlar, Germany).

Western blot

Total embryonic lysates were prepared from 8hpf embryos. 100μl RIPA Buffer (R0278, Sigma-Aldrich, St. Louis, MO) was added to 200 deyolked embryos for the protein extraction. BCA Assay Kit (23227, Thermo Scientific, Rockford, IL) was used to determine the concentration of each lysate. SDS-PAGE was carried out on a 4%-20% precast gel (456-1094, Bio-Rad Laboratories, Hercules, CA), with 20μg total protein loaded in each lane. After transferring to Hybond-P PVDF membranes (RPN303f, GE Healthcare, Piscataway, NJ), the membranes were incubated with either polyclonal rabbit anti-Mga antibody (1:500, AbMart, Shanghai, China) or 12G10 mouse monoclonal anti-α-tubulin antibody (1:500) at 4°C overnight. Either HRP-conjugated goat-anti rabbit IgG (1:3,000, SC-2004, Santa Cruz Biotechnology, Dallas, TX) or HRP-conjugated goat-anti mouse IgG (1:3,000, A5278, Sigma-Aldrich, St. Louis, MO) was used as secondary antibodies. After antibody incubation, bands were developed and detected with the Western Blot ECL Substrate (170-5060, Bio-Rad Laboratories, Hercules, CA) and X-OMAT LS films (864-6770, Carestream, Rochester, NY).

Whole mount in situ hybridization (WISH)

WISH was carried out as previously described [19]. Digoxigenin (DIG)-labeled antisense RNA probes were synthesized by using DIG RNA Labeling Kit (SP6/T7) (11175025910, Roche Diagnostics, Basel, Switzerland). The following antisense probes were used: *tfap2a*, *mitfa*, *islet1* (from Schilling Lab, UCI, CA, USA), *hand2*, *snai1b* (from Yelon Lab, UCSD, CA, USA), *phox2bb* (from Shepherd Lab, Emory University, GA, USA), *ifabp*, *tfa* (from Gong Lab, NUS, Singapore), *sox10*, *foxd3*, *dlx2a*, *chordin* and *tbx6*. The

DIG-labeled probes were detected by applying Anti-Digoxigenin-AP, Fab Fragments (1:3,000, 11093274910, Roche Diagnostics). Signals were developed in NTMT solution (100mM Tris-HCl, pH9.5, 50mM $MgCl_2$, 100mM NaCl, 0.1% Tween-20) with BCIP/NBT (11383221001/11383213001, Roche Diagnostics) for 1 to 4 hours at room temperature until signals became significant.

Alcian Blue cartilage staining

Zebrafish larvae were collected at 120hpf. For maintaining optical clarity, 0.003% 1-phenyl 2-thiouracil (PTU) was added into the egg water at 22hpf to inhibit skin pigmentation. After collection, larvae were fixed with 4% paraformaldehyde in 1X PBS overnight at 4°C. Fixed larvae were stained overnight at room temperature with 0.1% Alcian Blue 8GX (A3157, Sigma-Aldrich, St Louis, MO) in acid alcohol. Stained larvae were differentiated in acid alcohol and rinsed with distilled water until background was clear. For whole mount imaging, stained larvae were cleared with glycerol in 1% KOH solution and mounted in 80% glycerol. For cartilage dissection, stained larvae were rehydrated and rinsed with saturated sodium tetraborate solution. Larvae were digested in trypsin solution at room temperature until tissues turned loose. Craniofacial cartilage dissection was carried out by gently removing surrounding tissues with fine forceps.

L-DOPA staining

22hpf embryos were dechorinated and fixed with 4% paraformaldehyde in 1X PBS at room temperature for 2 hours. Fixed embryos were rinsed 5 times with 1X PBS. Embryos were then incubated with 0.1% 3,4-Dihydroxy-L-phenylalanine (L-DOPA) (D9628,

Sigma-Aldrich, St. Louis, MO) in 1X PBS at 37°C for 1.5 to 2.5 hours. The reaction was stopped by rinsing embryos 3 times with 1X PBS when the staining reached desired intensity. Finally, embryos were stored in 80% glycerol for photography.

TUNEL assay

Cell death in embryos was detected by DeadEnd Fluorometric TUNEL system (G3250, Promega, Fitchburg, WI) following manufacturer's instruction. Briefly, embryos were collected and fixed with 4% paraformaldehyde in 1X PBS at 22hpf. After fixation, embryos were rinsed 2 times with 1X PBS and permeabilized with 20μg/ml Proteinase K solution at room temperature for 10 minutes. Permeabilized embryos were fixed again with 4% paraformaldehyde in 1X PBS to kill the activity of Proteinase K. Embryos were then incubated in Equilibration Buffer at room temperature for 10 minutes after rinsed 2 times with 1X PBS. Embryos were incubated in the mixture of fluorescein-12-dUTP and Terminal Deoxynucleotidyl Transferase (TdT) to label dead cells. The reaction was stopped by adding 2X SSC to embryos. Embryos' cell nuclei were also stained with DAPI (1:2,000) as the counterstain.

Microscopy

Live embryos and Alcian Blue-stained craniofacial cartilages were photographed using Leica MZ FLIII stereomicroscope and DFC450 CCD camera (Leica Microsystems, Wetzlar, Germany). WISH signals were photographed using Zeiss Axioplan 2 compound microscope (Carl Zeiss, Jena, Germany) and RETIGA EX CCD camera (QImaging, Surrey, Canada). For fluorescence imaging, Zeiss AXIO Imager D2 compound

fluorescence microscope with Colibri.2 LED light source and AxioCam HR CCD camera was used (Carl Zeiss, Jena, Germany).

RESULTS

Suppression of Mga expression leads to various defects during embryonic and larval development

Mga has been reported to participate in the developmental regulation of brain, heart, and gut [17]. Here we suppressed the expression of Mga by injecting antisense morpholino oligonucleotides (MO) into 1-cell stage zebrafish embryos. Two different translation blocker MOs (*mga*TL1MO and *mga*TL3MO) were combined with *p53*MO in a single injection to block the translation of Mga. Injecting these two *mga*MOs to suppress the expression of Mga in YSL resulted in the dorsoventral patterning defect in a previous study [18]. In addition, the same concentration of two mismatch *mga*MisTL1MO and *mga*MisTL3MO were used as the control. After injecting combined MOs at 1 cell stage, embryos were carefully monitored throughout the entire course of the development. Within the first 24 hours after injection, embryos injected with 1.6ng *mga*MOs developed slightly slower than those injected with 1.6ng *mga*MisMOs, roughly 1 to 2 hours delay. This developmental delay in *mga* morphants became not so evident after 24 hours. *mga* morphants exhibited a reduced, almost completely loss of skin pigmentation and the regression of yolk stalk extension at 32hpf, whereas control embryos showed grossly normal morphology at the same stage (Figure 2.1A-B). *mga* morphants had relatively larger, swollen heads, particularly in the brain region at 48hpf. Besides, the heart was also

not folded normally with a sign of mild heart edema (Figure 2.1C-D). By 72hpf, *mga* morphants exhibited reduced, or even completely loss of pectoral fins with more significant heart defect (Figure 2.1E-F, 2.1I-J). Later during the larval development, *mga* morphants showed reduced jaw structure as well as the severe heart defect with significant edema at 120hpf (Figure 2.1G-H, 2.1K-L). From 32hpf to 120hpf, some defects were observed during the entire course of the development, such as the regression of yolk stalk extension and the reduction of skin pigmentation. Instead of losing all the skin pigmentation, a few melanocytes, primarily concentrated on the head and yolk surface, could still be seen after 48hpf. However, the reduced skin pigmentation was not fully recovered by 120hpf in *mga* morphants. The swollen brain phenotype was significant at 48hpf but recovered later at 72hpf. The heart defect appeared at 48hpf and became evident after 72hpf. Other than the heart edema, hearts were severely misfolded along with the abnormal beating pattern and frequency in *mga* morphants. In agreement with a previous study, defects in the heart, brain, gut were also observed in our *mga* morphants [17]. The expression of gut markers *ifabp* and *tfa* were both reduced in the presumptive gut region of *mga* morphants at 96hpf, suggesting a possible gut defect as previously being reported (Figure 2.2A-D). However, here we also identified few other defects that were not mentioned in the previous report. The protein level of Mga was reduced, but not completely depleted in *mga* morphants at 8hpf, suggesting that our *mga*MOs could suppress the translation of Mga (Figure 2.1M). mRNA rescue experiment was performed to test whether those defects found in *mga* morphants were the result of suppressing Mga expression. For rescuing the defects in *mga* morphants, 100pg mouse full-length *mga* mRNA was injected along with 1.6ng *mga*MOs and 2.4ng *p53*MO in

each embryo at 1 cell stage. 100pg *β-galactosidase* (*βgal*) was used as the control. The mouse *mga* mRNA was chosen for the rescuing *mga* morphants because the sequence near the translation start site is different from the one in zebrafish *mga* mRNA. Therefore, our *mga*MOs should not be able to block the translation of the mouse mRNA in the experiment. Most of the *mga* morphants injected with *βgal* mRNA still exhibited pigmentation and yolk stalk extension defects (87.89%, N=408), whereas many of the *mga* morphants injected with the mouse *mga* mRNA showed normal development at the same stage (73.64%, N=465) (Figure 2.3A- C). This result suggests that Mga knockdown leads to various defects, and those defects could be rescued by overexpressing the mouse *mga* mRNA.

mga morphants exhibit defective NC development

According to the morphological defects found in *mga* morphants, many of them were closely related to NC-derived tissues, such as the reduced skin pigmentation and jaw structures. In order to know whether the development of NC-derived tissues was affected by *mga* knockdown before those defects were evident, we analyzed the developmental regulation of these tissues in *mga* morphants. Melanoblasts start to form around 18-somite stage in zebrafish embryos. These precursor cells will become melanocytes once they begin producing melanin and accumulating melanin to form melanophores [21]. Tyrosinase, an enzyme responsible for the production of the pigment melanin, is started to be expressed in melanoblasts shortly before melanophores can be seen by naked eyes [22]. When embryos stained with L-DOPA, the active tyrosinase can convert L-DOPA to melanin to make melanoblasts visible. In the control, melanoblasts were visible around

the head and dorsal anterior region of the embryos after stained with L-DOPA at 22hpf. However, very few visible melanoblasts were observed in *mga* morphants at the same stage (Figure 2.4A-D). The expression of a melanoblast/melanocyte marker *mitfa* was also reduced in *mga* morphants before and after melanophores was evident (Figure 2.4E-H). This suggests that the development of NC-derived melanocyte lineage is affected by Mga knockdown. We further examined the craniofacial cartilage development in *mga* morphants by Alician Blue staining. At 120hpf, *mga* morphants showed severely disorganized craniofacial cartilages comparing to those in the control. The size of Meckel's, palatoquadrate, hyosymplectic, and ceratohyal cartilages were greatly reduced, while ceratobrachial 1-5, basihyal, and basibrachial cartilages were missing. The reduced ceratohyal cartilage was flipped over toward the posterior, possibly because of the loss of structural support from those missing cartilages (Figure 2.5A-F). This suggests that the reduced jaw structures we observed in live *mga* morphants were indeed caused by defective craniofacial cartilages. In order to know whether the development of craniofacial cartilage was affected earlier in the development, the expression of two craniofacial cartilage precursor markers, *dlx2a* and *hand2*, was examined at 36hpf. In control embryos, both *dlx2a* and *hand2* were expressed in pharyngeal pouches, which will form craniofacial cartilages later in the development. However, the expression of *dlx2a* and *hand2* were restricted to the first and second pharyngeal pouches in *mga* morphants, suggesting a trend of posterior to anterior reduction of craniofacial cartilage precursors (Figure 2.5G-J). This result corresponds to our observation on defective craniofacial cartilages at 120hpf that most of the posterior cartilages were missing while anterior ones though greatly reduced, were still present. NC cells also contribute to the

development of PNS and ENS. Therefore, we examined the expression of *islet1* in PNS and *phox2bb* in ENS. Both *islet1* and *phox2bb* were reduced in their corresponding expression domains within PNS and ENS in 48hpf *mga* morphants, suggesting that the development of both nervous systems was also interfered by Mga knockdown (Figure 2.6A-D). Since the development of all three major NC-derived tissue types including melanocytes, craniofacial cartilages, and PNS and ENS were all affected in *mga* morphants, it is possible that *mga* is involved in controlling the early steps of general NC development.

Mga controls general NC development

Since *mga* is expressed both maternally and zygotically, it is very possible that Mga starts to affect NC development from very early steps. Therefore, we further examined the early NC development to understand whether it is affected by Mga knockdown. When NC cells form at the dorsal edge of neural tube, several transcription factors are expressed in NC cells to maintain the NC population, such as Foxd3, Sox10, Tfap2a, and Snai1b. These transcription factors can be used as markers to localize NC cells in developing embryos. In control embryos, all these four markers were expressed in NC cells along the anterior-posterior axis with stronger expression in the anterior region at 3-somite stage (Figure 2.7A, E, I, and M). However, the expression was greatly reduced in *mga* morphants, particularly in the more posterior region while the anterior region still remained the relatively stronger expression (Figure 2.7B, F, J, and N). The NC marker expression was also reduced in *mga* morphants at 8-somite stage, suggesting that this reduction persisted through the early steps of NC formation. The reduction of NC marker

was not due to the general developmental delay in *mga* morphants because all embryos with exactly the same number of somites were collected for the experiment. Therefore, Mga might affect NC formation before NC cells migrate and differentiate. Since *mga* morphants exhibited lower expression level of NC markers during NC formation, it is possible that those cells with reduced or absent expression of NC markers might undergo programmed cell death at some point later during the development. Indeed, significant apoptosis was observed in cranial and dorsal regions of *mga* morphants at 22hpf, whereas control embryos only had few apoptotic cells in the same regions at the same stage (Figure 2.8A-D). Those apoptotic cells observed in *mga* morphants concentrated in regions contained pre-migratory and migratory NC cells, suggesting that some NC cells might not adapt their cell fate properly and eventually undergo apoptosis.

BMP signaling is altered when the expression of Mga is surpressed

BMP signaling has been shown to play an important role during NC development [4, 23]. It is also known that Mga can regulate the expression of *bmp2b* in the YSL of zebrafish embryos [18]. Therefore, we hypothesize that Mga affects NC formation by regulating BMP signaling during early development. Here we examined whether BMP signaling was altered in *mga* morphants shortly before NC cells form. The expression domain of a BMP antagonist, *chordin*, was slightly expanded ventrolaterally in *mga* morpahnts at 8hpf (Figure 2.9A-D). The expression of *tbx6*, a BMP downstream target gene, was also reduced from its dorsal expression domain in *mga* morphants at the same stage (Figure 2.9E-M). These results indicate that *mga* morphants might exhibit weaker BMP signaling during the period when BMP signaling is essential for defining the prospective NC

domain. However, BMP signaling is also known to control the formation of dorsoventral axis at the stage. Weaker BMP signaling might cause the dorsalization of developing embryos. Although *mga* morphants did not exhibit significant dorsoventral patterning defect after 24hpf stage, it is still possible that some molecular changes of dorsoventral patterning occur earlier during the embryonic development. Thus, it is important to know whether the dorsalization occurs during early steps of development when the expression of *mga* is suppressed. The expression of *egr2b*, a marker of hindbrain rhombomere 3 and 5, was neither expanded nor reduced in any direction in *mga* morphants at 22hpf (Figure 2.9N-O). During the segmentation, the expression of *myod* is commonly used as the marker to label somites. At 8-somite stage, *mga* morphants showed normally developed somites without any sign of ventral expansion (Figures 9P and 9Q). Taken together, suppression of *mga* does not result in dorsoventral patterning defect even though the level of BMP signaling is reduced.

DISCUSSION

It has been mentioned in a previous study that suppressing the expression of Mga results in the absence of skin pigmentation, which is contributed by one of the NC lineages [17]. However, the correlation between Mga and NC development has never been analyzed. Here we show that Mga is a novel regulator required for normal NC development. Suppressing the expression of Mga by injecting MOs resulted in significant and board impact on general NC defects affecting several NC lineages. The earliest NC-specific defect we observed was the reduction of NC marker expression during NC formation at

3-somite stage. *mga* mRNA is known to be expressed ubiquitously in zebrafish embryos from 1 cell to the end of the gastrulation [17, 18]. The spatiotemporal expression pattern of *mga* also overlaps the time and region required for normal NC development, suggesting that Mga might participate in NC formation or even earlier steps for defining prospective NC cells. Nevertheless, it is still not clear how Mga regulates NC development. One possible role that Mga might play to control the formation of NC cells is to fine tune the BMP signaling. It has been suggested that an intermediate level of BMP signaling during the gastrulation is required for normal NC development [4, 24]. Our result supports this model as the strength of BMP signaling was reduced in *mga* morphants during the gastrulation. Previous study has suggested that Mga controls the expression of *bmp2b* in the YSL during the gastrulation [18]. Therefore, it is possible that Mga also controls the expression of *bmp*2b in the embryonic tissue during the gastrulation. However, we still cannot rule out the possibility that the mild reduction of BMP signaling we observed was due to the suppression of Mga expression in YSL as Mga was also knocked down in YSL after injecting MOs at 1-cell stage. It is shown that Mga knockdown in YSL leads to the loss of ventral tailfin in zebrafish embryos by reducing the strength of BMP signaling [18]. One possible reason why dorsoventral patterning defect was not observed in our *mga* morphants is that we injected lower dosage of MOs in embryos comparing to previous study. Thus, a milder reduction of BMP signaling during the gastrulation is expected in our *mga* morphants. Taken together, early NC development might be more sensitive than the dorsoventral patterning to the change of BMP signaling stength during the gastrulation. Another possible regulatory mechanism is that Mga regulates NC development through competing Max with Myc.

Myc is known to participate in many biological processes such as cell survival, cell death, and cell cycle progression. Loss of Mga might result in the increase of Max-Myc heterodimer formation, which will lead to the elevation of Myc activity. In Xenopus and chicks, c-Myc is expressed in the premigratory NC cells. The expression c-Myc is dependent on Wnt signaling, and knockdown with MOs results in the loss of NC cell markers as well as NC derivatives in Xenopus embryos [25]. Zebrafish Mych is also required for NC cell survival during the gastrulation [26, 27]. Therefore, the defective NC development in *mga* morphants could also be a result of the increasing Myc activity that affects the cell survival of developing NC cells.

REFERENCES

1. Timothy J. Stuhlmiller, M.I.G.-C. (2012). Current perspectives of the signaling pathways directing neural crest induction. Cellular and Molecular Life Sciences *69*, 3715-3737.
2. Paola Betancur, M.B.-F., and Tatjana Sauka-Spengler (2010). Assembling Neural Crest Regulatory Circuits into a Gene Regulatory Network. Annual Review of Cell and Developmental Biology *26*, 581-603.
3. Nicole M. Le Douarin, S.C., Gérard Couly, Elisabeth Dupin (2004). Neural crest cell plasticity and its limits. Development *131*, 4637-4650.
4. Wen-Der Wang, D.B.M., Mercedes Montero-Balaguer, Antonis K. Hatzopoulos, Ela W. Knapik (2011). Tfap2a and Foxd3 regulate early steps in the development of the neural crest progenitor population. Developmental Biology *360*, 173-185.

5. Maurice Kléber , H.-Y.L., Heiko Wurdak , Johanna Buchstaller, Martin M. Riccomagno, Lars M. Ittner, Ueli Suter, Douglas J. Epstein, Lukas Sommer (2005). Neural crest stem cell maintenance by combinatorial Wnt and BMP signaling. Journal of Cell Biology *169*, 309-320.

6. David W. Raible, J.W.R. (2005). Reiterated Wnt and BMP signals in neural crest development. Seminars in Cell & Developmental Biology *16*, 673-682.

7. Yvette G Landon, M.C.M. (2011). Maternal and zygotic control of zebrafish dorsoventral axial patterning. Annual Review of Genetics *45*, 357-377.

8. Carole LaBonne, M.B.-F. (1998). Neural crest induction in Xenopus: evidence for a two-signal model. Development *125*, 2403-2414.

9. Bettina Schmid, M.F., Stephanie A. Connors, Jamie Trout, Bernard Thisse, Christine Thisse, Mary C. Mullins (2000). Equivalent genetic roles for bmp7/snailhouse and bmp2b/swirl in dorsoventral pattern formation. Development *127*, 957-967.

10. Vu H. Nguyen, B.S., Jamie Trouta, Stephanie A. Connorsa, Marc Ekker, Mary C. Mullins (1998). Ventral and Lateral Regions of the Zebrafish Gastrula, Including the Neural Crest Progenitors, Are Established by a bmp2b/swirl Pathway of Genes. Developmental Biology *199*, 93-110.

11. Jessica L. Lewis, J.B., Melinda Modrell, Jared W. Ragland, Randall T. Moon, Richard I. Dorsky, David W. Raible (2004). Reiterated Wnt signaling during zebrafish neural crest development. Development *131*, 1299-1308.

12. Peter J. Hurlin, E.S., Neal G. Copeland, Nancy A. Jenkins, Robert N. Eisenman (1999). Mga, a dual-specificity transcription factor that interacts with Max and contains a T-domain DNA-binding motif. EMBO Journal *18*, 7019-7028.

13. Peter J. Hurlin, J.H. (2006). The MAX-interacting transcription factor network. Seminars in Cancer Biology *16*, 265-274.

14. Hidesato Ogawa, K.-i.I., Stefan Gaubatz, David M. Livingston, Yoshihiro Nakatani (2002). A Complex with Chromatin Modifiers That Occupies E2F- and Myc-Responsive Genes in G0 Cells Science *296*, 1132-1136.

15. Lorenzo De Paoli, M.C., Sara Monti, Silvia Rasi, Valeria Spina, Alessio Bruscaggin, Mariangela Greco, Carmela Ciardullo, Rosella Famà, Stefania Cresta, Rossana Maffei, Marco Ladetto, Maurizio Martini, Luca Laurenti, Francesco Forconi, Roberto Marasca, Luigi M. Larocca, Francesco Bertoni, Gianluca Gaidano, Davide Rossi (2013). MGA, a suppressor of MYC, is recurrently inactivated in high risk chronic lymphocytic leukemia. Leukemia & Lymphoma *54*, 1087-1090.

16. Andrew J. Washkowitz, C.S., Kun Zhang, Wolfgang Wurst, Thomas Floss, Jesse Mager, Virginia E. Papaioannou (2015). Mga is essential for the survival of pluripotent cells during peri-implantation development. Development *142*, 31-40.

17. Amir Rikin, T.E. (2010). The tbx/bHLH transcription factor mga regulates gata4 and organogenesis. Developmental Dynamics *239*, 535-547.

18. Yuhua Sun, W.-C.T., Xiang Fan, Rebecca Ball, Scott T. Dougan (2014). Extraembryonic Signals under the Control of MGA, Max, and Smad4 Are Required for Dorsoventral Patterning. Developmental Cell *28*, 322-334.

19. Yuhua Sun, D.W., Scott T. Dougan (2011). Embryological Manipulations in Zebrafish. Methods in Molecular Bilogy *770*, 139-184.

20. Mara E Robu, J.D.L., Soraya Beiraghi, Charles Brenner, Steven A Farber, Stephen C Ekker (2007). p53 Activation by Knockdown Technologies. PLoS Genetics *3*, e78.

21. Robert N. Kelsha, M.L.H., Sarah Colanesia, Carol A. Erickson (2009). Stripes and belly-spots—A review of pigment cell morphogenesis in vertebrates. Seminars in Cell & Developmental Biology *20*, 90-104.

22. Esther Camp, M.L. (2001). Tyrosinase gene expression in zebrafish embryos. Development Genes and Evolution *211*, 150-153.

23. Jennifer A. Schumacher , M.H., Vu H. Nguyen, Mary C. Mullins (2011). An Intermediate Level of BMP Signaling Directly Specifies Cranial Neural Crest Progenitor Cells in Zebrafish. PLoS ONE *6*, e27403.

24. Sabine Reichert, R.A.R., Caroline S. Hill (2013). A BMP regulatory network controls ectodermal cell fate decisions at the neural plate border. Development *140*, 4435-4444.

25. Amy Bellmeyer, J.K., Julie Lindgren, Carole LaBonne (2003). The Protooncogene c-Myc Is an Essential Regulator of Neural Crest Formation in Xenopus. Developmental Cell *4*, 827-839.

26. Kay Kotkamp, E.K., Björn Wendik, Bożena K. Polok, Shifra Ben-Dor, Daria Onichtchouk, Wolfgang Driever (2014). Pou5f1/Oct4 Promotes Cell Survival via Direct Activation of mych Expression during Zebrafish Gastrulation. PLoS ONE *9*, e92356.

27. Sung-Kook Hong, M.T., Igor B. Dawid (2008). The Mych Gene Is Required for Neural Crest Survival during Zebrafish Development. PLoS ONE *3*, e2029.

FIGURES AND FIGURE LEGENDS

Figure 2.1. *mga* morphants exhibit various developmental defects. The same embryos injected with either *mga*MisMOs or *mga*MOs at 1 cell stage are photographed at 32hpf **(A and B)**, 48hpf **(C and D)**, 72hpf **(E and F)**, and 120hpf **(G and H)** respectively. *mga* morphants show a variety of developmental defects at different stages, including reduced skin pigmentation, reduced yolk stalk extension, atrophic pectoral fins **(I and J)**, heart edema and reduced jaw **(K and L)**. Meanwhile, embryos injected with *mga*MisMOs develop normally. The protein level of Mga is decreased but not completely depleted in *mga* morphants at 8hpf **(M)**. Arrow: pectoral fin.

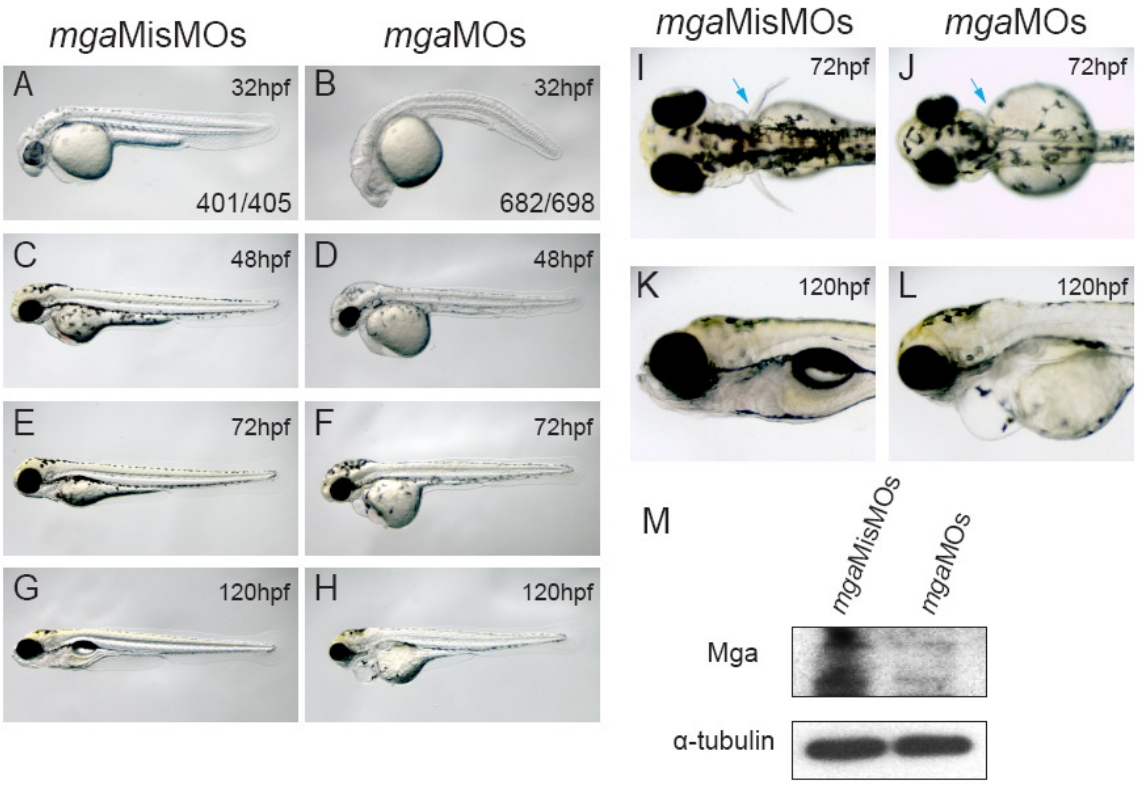
mgaMisMOs
mgaMOs
A
32hpf
401/405
B
32hpf
682/698
C
48hpf
D
48hpf
E
72hpf
F
72hpf
G
120hpf
H
120hpf
mgaMisMOs
mgaMOs
I
72hpf
J
72hpf
K
120hpf
L
120hpf
M
mgaMisMOs
mgaMOs
Mga
α-tubulin

Figure 2.2. Gut development is affected in *mga* morphants. The mRNA expression of two gut markers *ifabp* **(A and B)** and *tfa* **(C and D)** at 96hpf are detected by *in situ* hybridization (ISH). Notice that the expression of both gut markers is reduced in *mga* morphants.

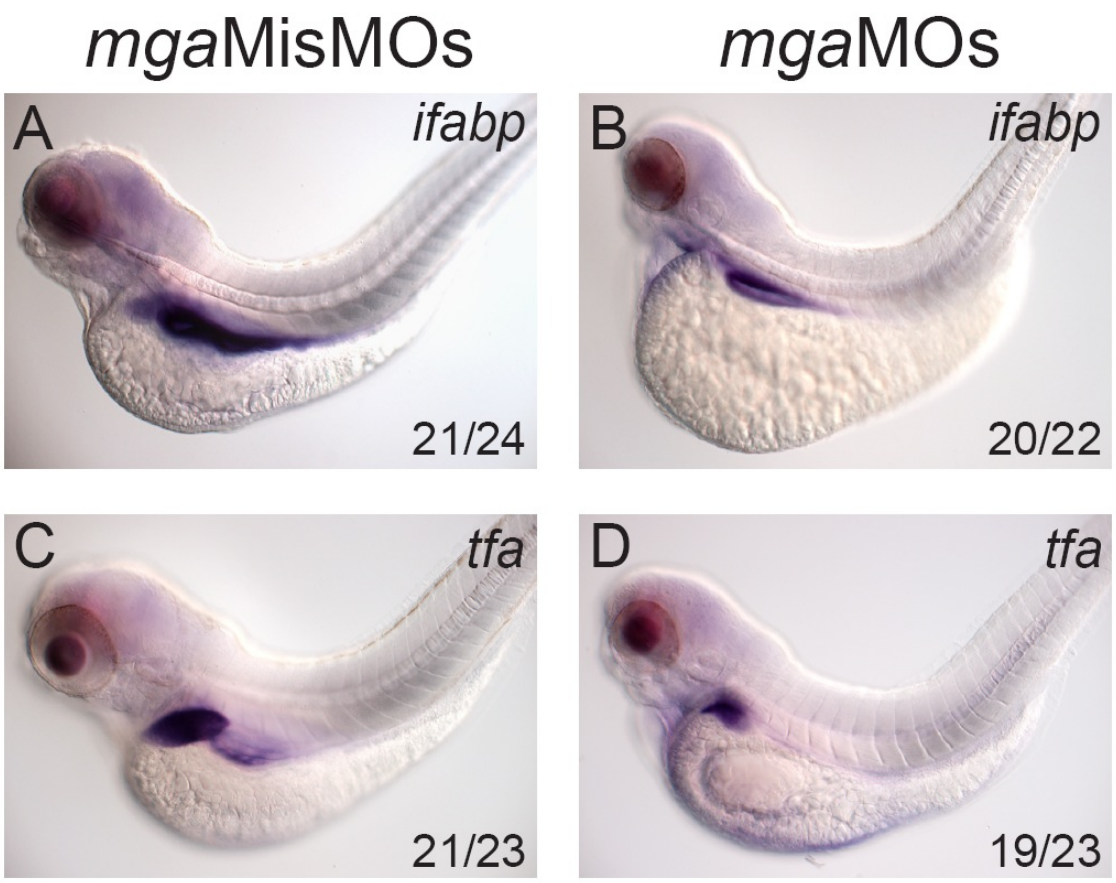
mgaMisMOs
mgaMOs
A
ifabp
21/24
B
ifabp
20/22
C
tfa
21/23
D
tfa
19/23

Figure 2.3. Pigmentation defect in *mga* morphants can be rescued by injecting mouse *mga* mRNA. *mga* morphants injected with *βgal* **(A)** or mouse *mga* mRNA **(B)** are photographed at 32hpf. Skin pigmentation is greatly reduced in *mga* morphants injected with *βgal* mRNA comparing with those injected with mouse *mga* mRNA. The skin pigmentation phenotype is scored as normal or reduced at 32hpf and shown as percentage **(C)**. **: $p<0.001$, Student's t-test.

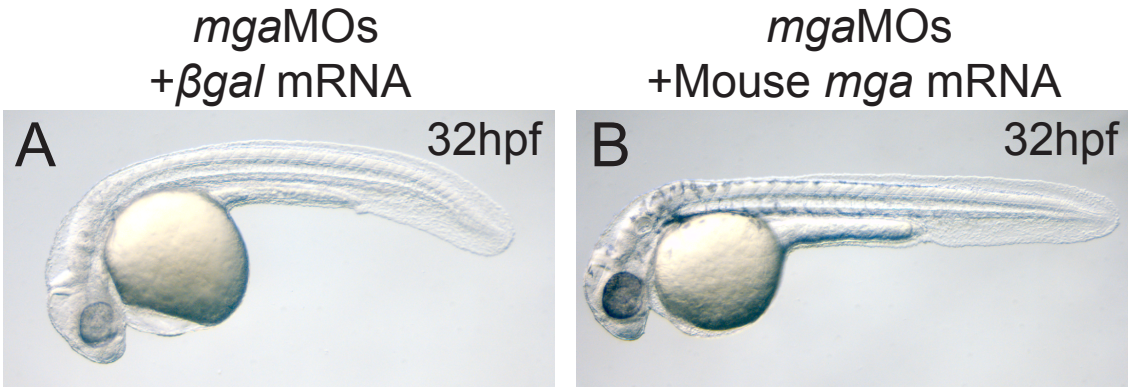
mgaMOs
+βgal mRNA
mgaMOs
+Mouse mga mRNA
A
32hpf
B
32hpf

C

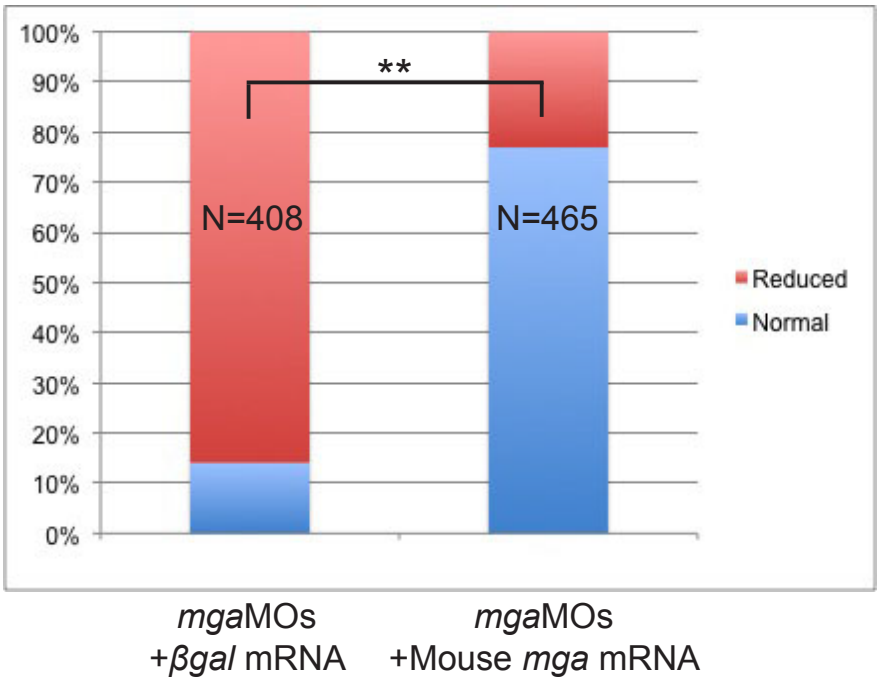
100%
90%
80%
70%
60%
50%
40%
30%
20%
10%
0%
**
N=408
N=465
Reduced
Normal
mgaMOs
+βgal mRNA
mgaMOs
+Mouse mga mRNA

Figure 2.4. Early development of melanocytes is suppressed in *mga* morphants. Tyrosinase-positive melanoblasts are greatly reduced in *mga* morphants stained with L-DOPA at 22hpf **(A-D)**. The expression of an early pigmentation marker *mitfa* is also reduced in *mga* morphants at 22hpf **(E and F)** and 26hpf **(G and H)**, respectively.

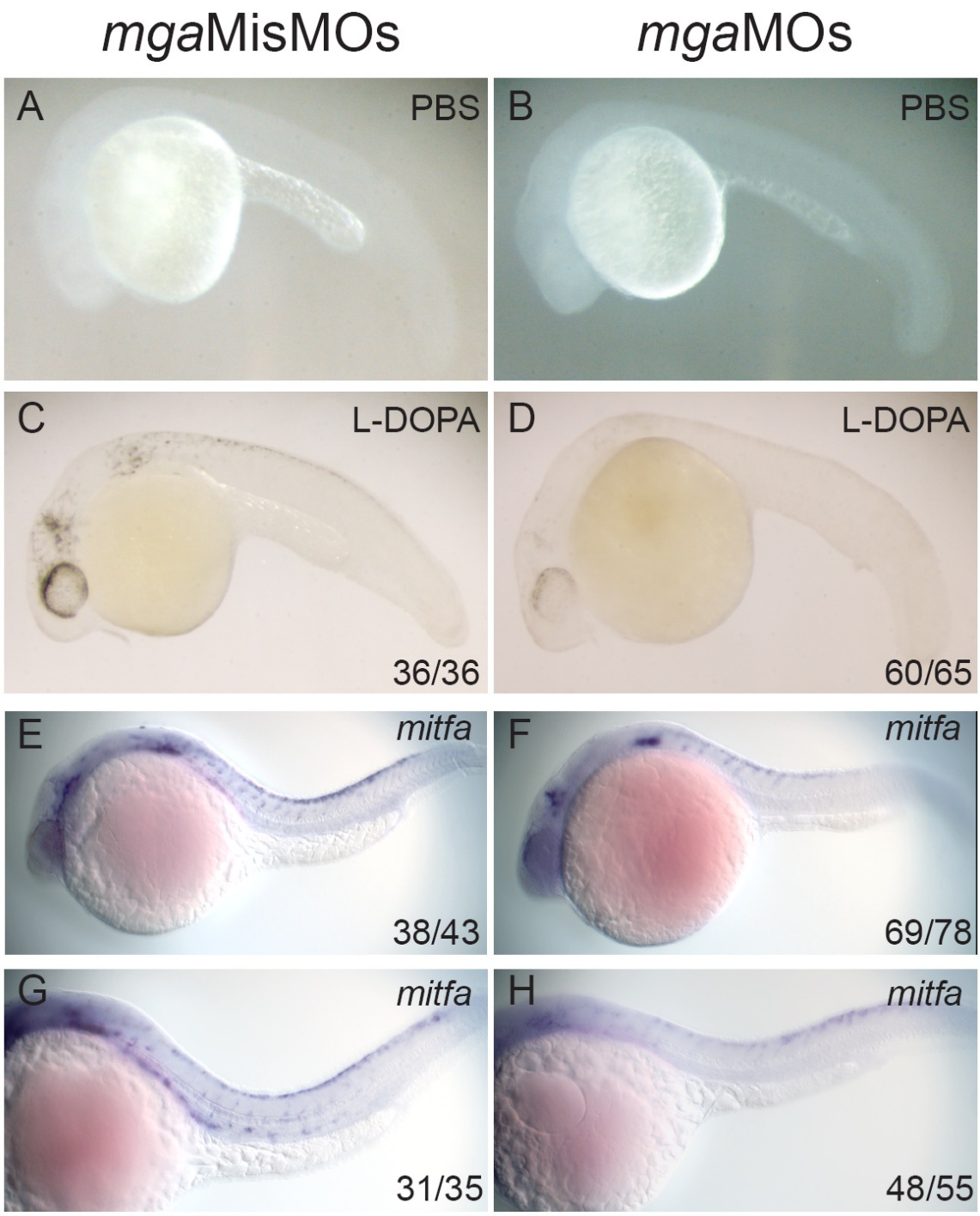
*mga*MisMOs
*mga*MOs
A
PBS
B
PBS
C
L-DOPA
36/36
D
L-DOPA
60/65
E
mitfa
38/43
F
mitfa
69/78
G
mitfa
31/35
H
mitfa
48/55

Figure 2.5. Reduced craniofacial cartiliage development is observed in *mga* morphants. Alcian Blue stained 120hpf larvae are shown in ventral view. Craniofacial cartilages in *mga* morphants are abnormal in terms of their organization and size **(A and B)**. Ventral and lateral images of dissected craniofacial cartilages from the same larvae are shown in higher magnification **(C-F)**. In *mga* morphants, mRNA expression of craniofacial cartilage precursor markers *dlx2a* **(G and H)** and *hand2* **(I and J)** is reduced specifically in pharyngeal arch area at 36hpf. T: Trabeculae; M: Meckel's; P: Palatoquadrate; HS: Hyosymplectic; CH: Ceratohyal. Scale bar=100μm.

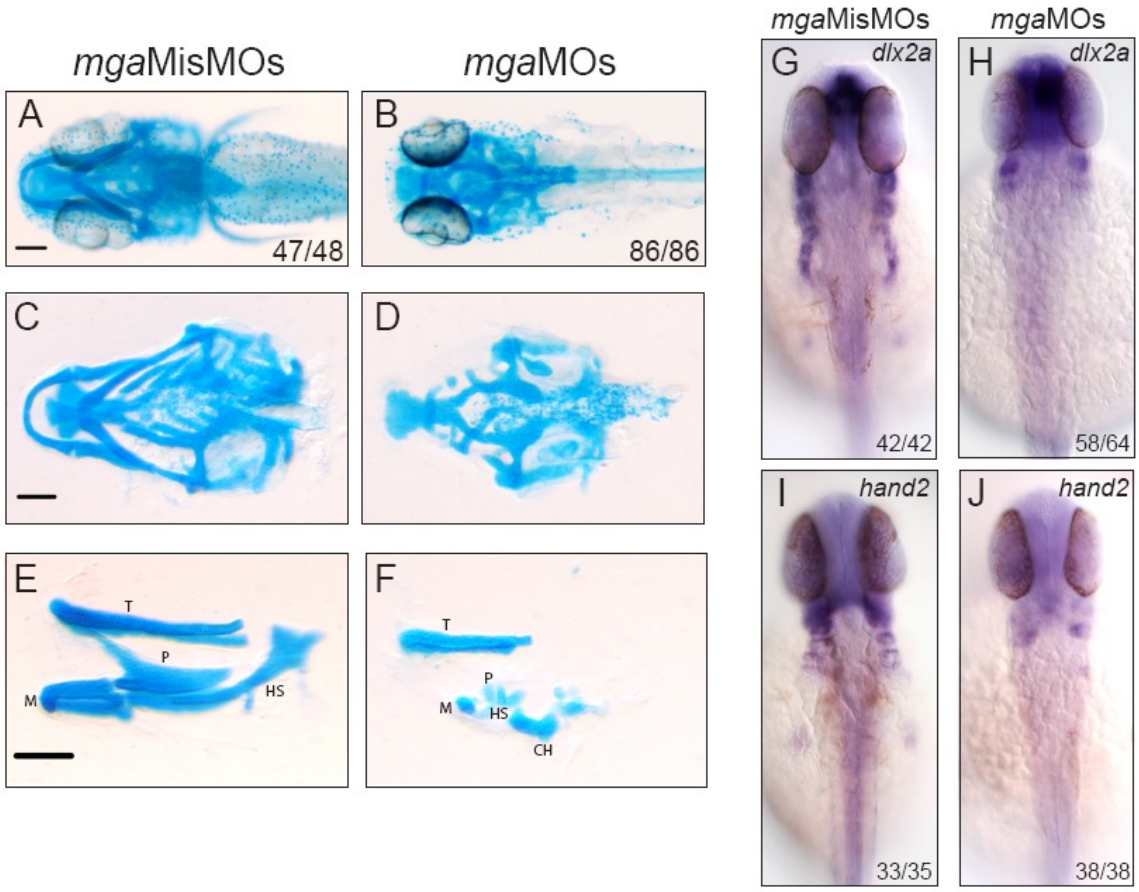
mgaMisMOs
mgaMOs
A
47/48
B
86/86
C
D
E
T
P
M
HS
F
T
P
M
HS
CH
mgaMisMOs
mgaMOs
G
dlx2a
42/42
H
dlx2a
58/64
I
hand2
33/35
J
hand2
38/38

Figure 2.6. Abnormal development of peripheral and enteric nervous system in *mga* morphants. *islet1* mRNA expression in peripheral nerves is reduced in *mga* morphants at 48hpf **(A and B)**. *phox2bb* mRNA expression is significantly reduced in *mga* morphants at 48hpf as well **(C and D)**.

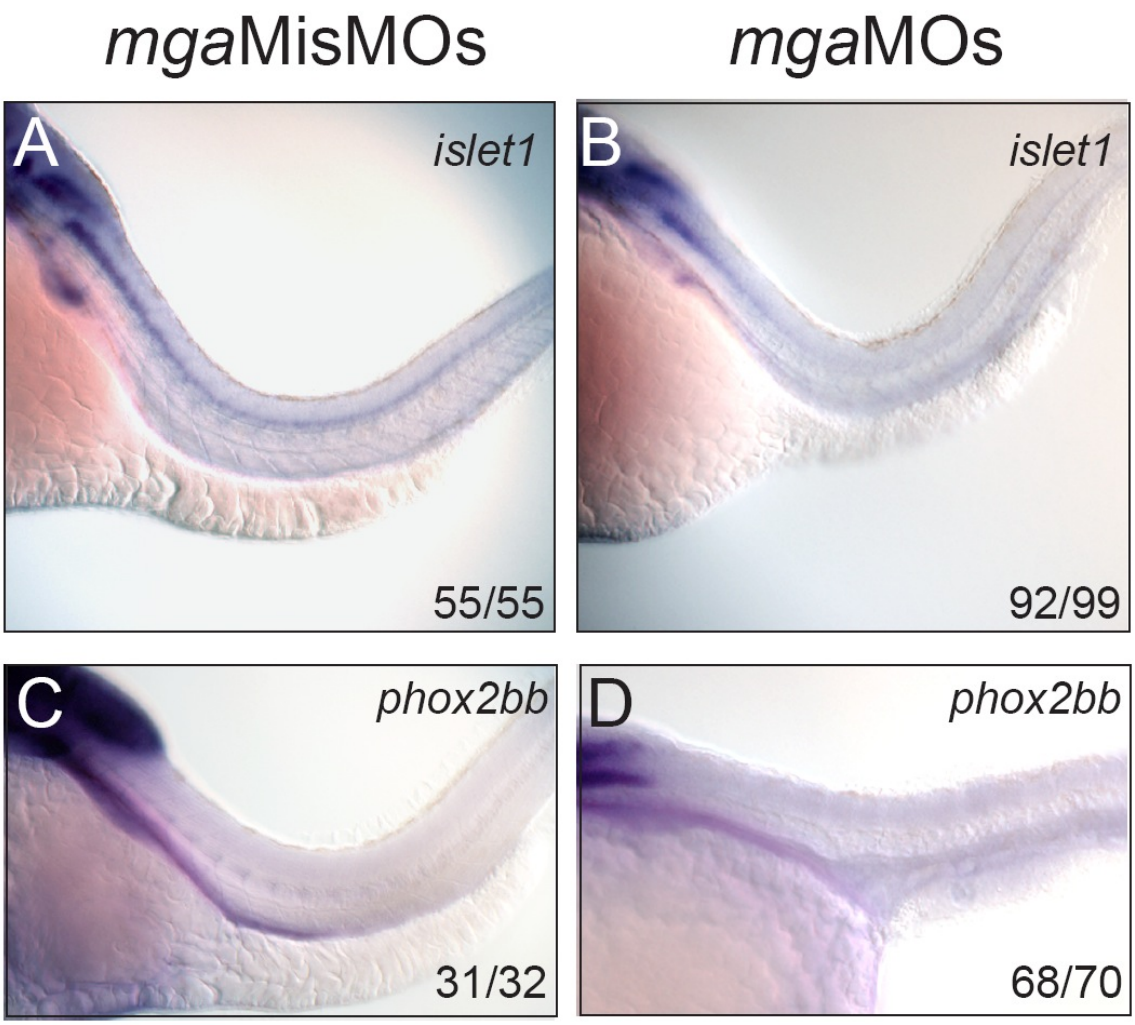
mgaMisMOs
mgaMOs
A
islet1
55/55
B
islet1
92/99
C
phox2bb
31/32
D
phox2bb
68/70

Figure 2.7. The expression of early NC cell markers is down-regulated in *mga* morphants. The expressions of early NC cell markers including *foxd3* **(A-D)**, *sox10* **(E-H)**, *tfap2a* **(I-L)** and *snai1b* **(M-P)** are detected by whole mount *in-situ* hybridization at 3 and 8 somite stages, respectively. The expression of all four NC marker genes is reduced in *mga* morphants at both 3- and 8-somite stages.

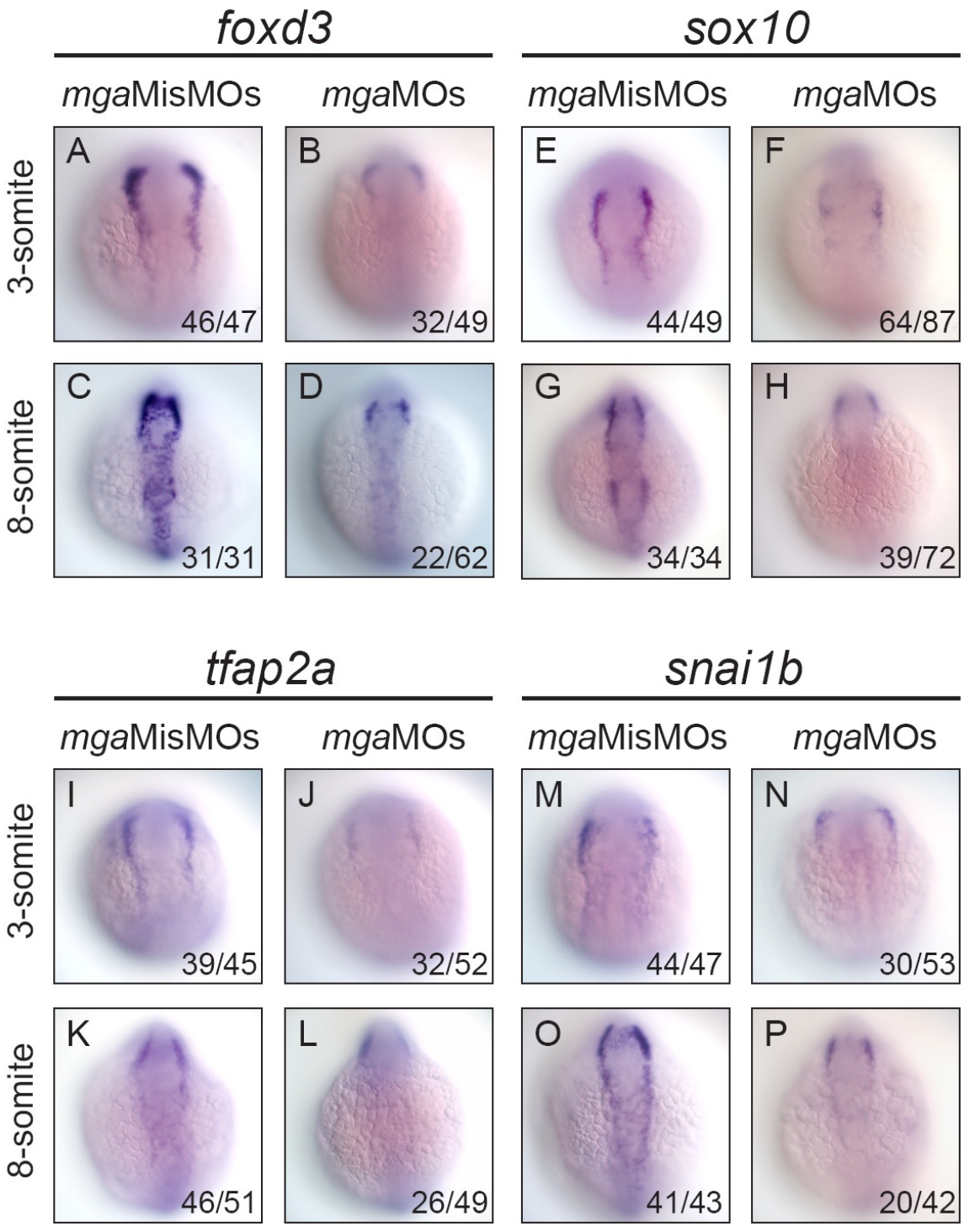
foxd3
sox10
mgaMisMOs
mgaMOs
mgaMisMOs
mgaMOs
3-somite
8-somite
A
B
E
F
C
D
G
H
46/47
32/49
44/49
64/87
31/31
22/62
34/34
39/72
tfap2a
snai1b
mgaMisMOs
mgaMOs
mgaMisMOs
mgaMOs
3-somite
8-somite
I
J
M
N
K
L
O
P
39/45
32/52
44/47
30/53
46/51
26/49
41/43
20/42

Figure 2.8. Increased apoptosis is observed in the dorsal region of *mga* morphants. Images of 22hpf embryos analyzed by TUNEL assays are shown in dorsal view **(A and B)** and later view **(C and D)**, respectively. Apoptotic cells (green) are labeled with FITC, and cell nuclei (blue) are labeled with DAPI. Scale bar=100μm.

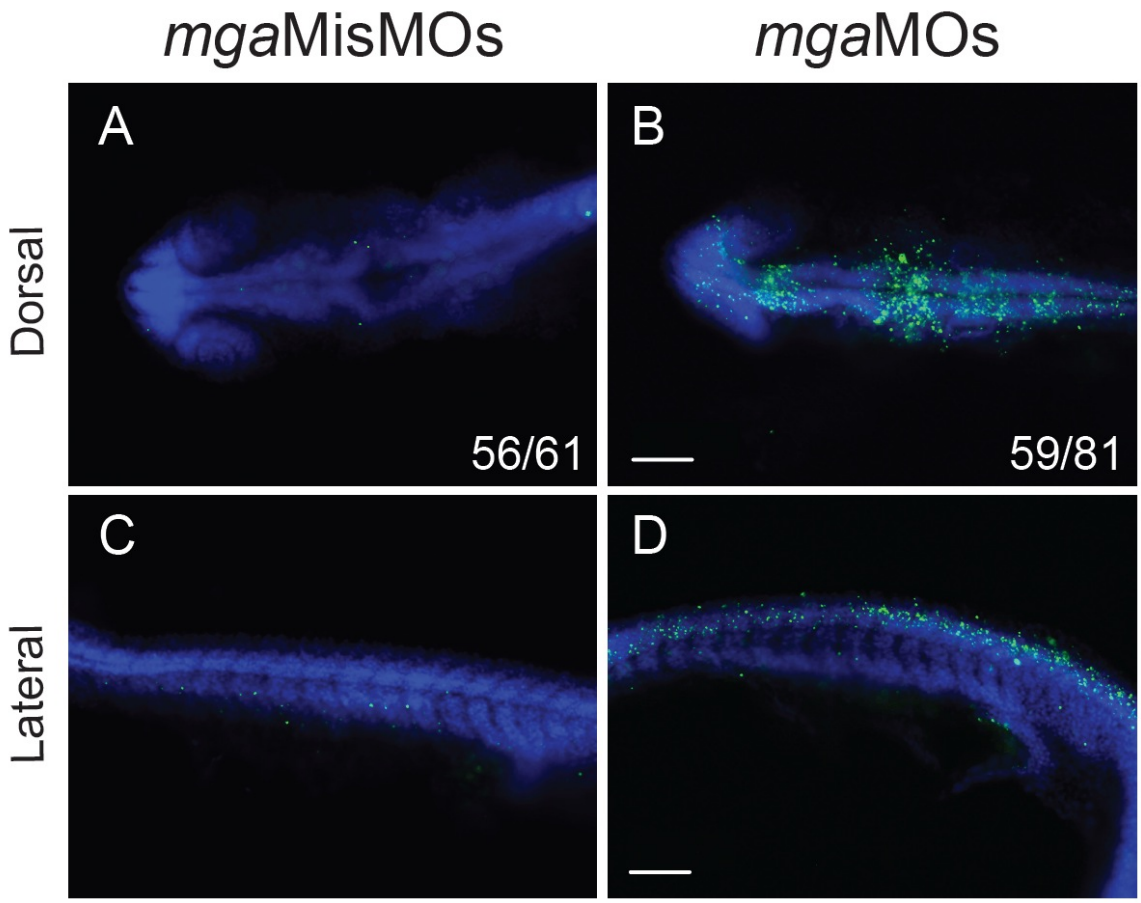
mgaMisMOs
mgaMOs
A
B
C
D
Dorsal
Lateral
56/61
59/81

Figure 2.9. BMP signaling is altered in *mga* morphants. The expression of BMP antagonist *chd* is expanded in *mga* morphants at 8hpf **(A- D)**. The expression of BMP downstream target gene *tbx6* is also reduced in *mga* morphants at 8hpf **(E-M)**. However, the expression of *egr2b* at 22hpf **(N and O)** and *myod* at 8-somite stage **(P and Q)** is not altered in *mga* morphants. No typical dorsoventral patterning defect is observed. Arrowhead: lateral expression boarder of *chd.*

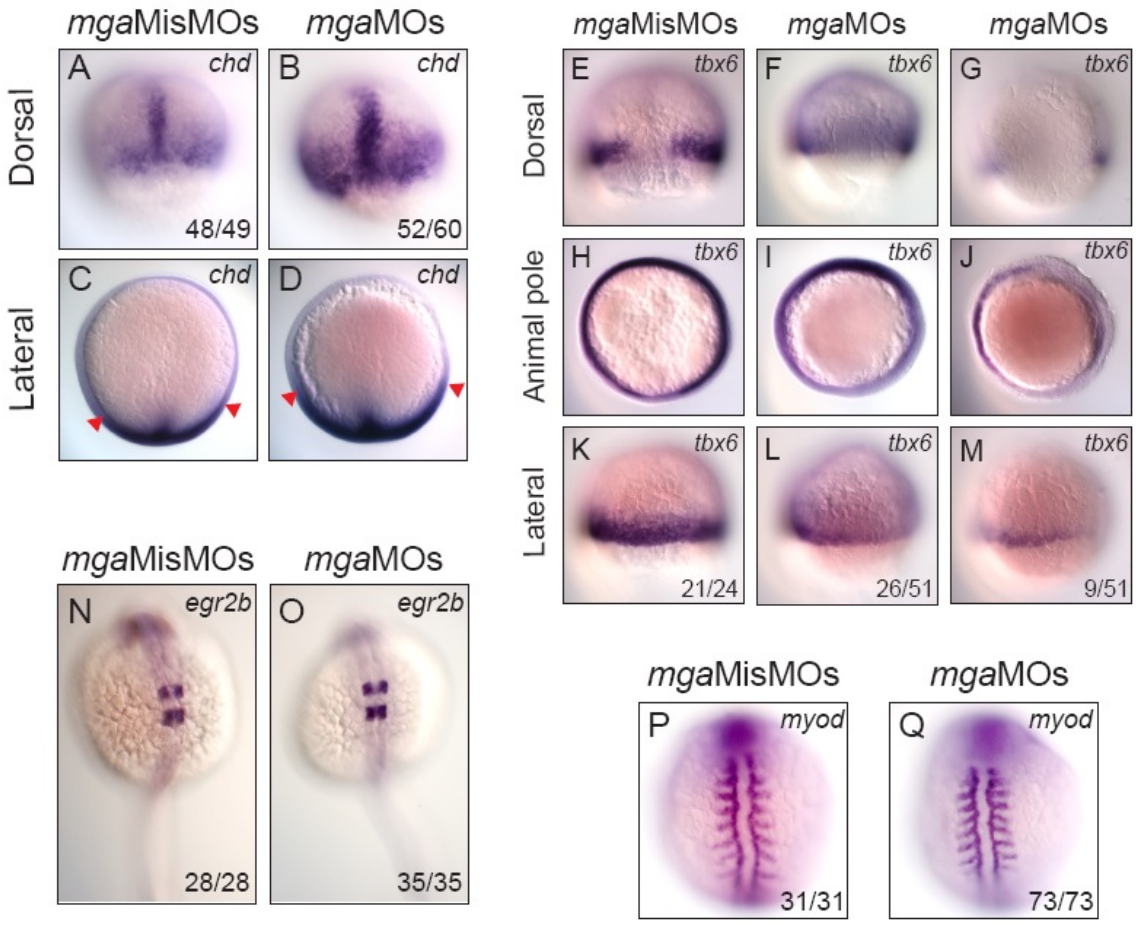
mgaMisMOs
mgaMOs
Dorsal
Lateral
A chd
B chd
C chd
D chd
48/49
52/60
mgaMisMOs
mgaMOs
N egr2b
O egr2b
28/28
35/35
mgaMisMOs
mgaMOs
mgaMOs
Dorsal
Animal pole
Lateral
E tbx6
F tbx6
G tbx6
H tbx6
I tbx6
J tbx6
K tbx6
L tbx6
M tbx6
21/24
26/51
9/51
mgaMisMOs
mgaMOs
P myod
Q myod
31/31
73/73

CHAPTER 3

SITE-SPECIFIC GENE TARGETING IN ZEBRAFISH

INTRODUCTION

To understand functions of genes, it is essential to have the ability to manipulate the genome, especially for generating mutants. ENU-based mutagenesis has been extensively used as a tool of forward genetics to generate zebrafish mutants. However, unlike generating gene-knockout mice, it was almost not possible to generate gene-knockout zebrafish due to the lack of equivalent tools such as embryonic stem cells for zebrafish. Therefore, knocking down gene expression using antisense morpholino oligonucleotides (MOs) has long been a major way to study loss-of-function effects of genes in zebrafish. It is a fast and easy method to study functions of genes, but it has limitations and also possibly causes some potential problems. For example, it is easy to knock down gene expression in zebrafish embryos by simply injecting antisense MOs at 1 cell stage, but it is difficult to access functions of genes in adults due to the half-life of MOs. It is still not clear how long it will last, so the knockdown efficiency at different stages might be a concern. Moreover, MOs have been shown to have the ability to induce p53-mediated apoptosis in zebrafish embryos, resulting in non-specific cell death-related phenotype observed in morphants that possibly not associated with the gene of interest [1]. It has been reported that morphants of a large number of genes exhibited some defects while

mutants of these genes showed normal phenotypes [2, 3]. This result also raises the concern that the specificity of MOs might not be as high as people thought before.

Not long ago, a new gene targeting strategy using synthetic zinc finger nucleases (ZFNs) had made it possible modify specific genetic loci in zebrafish genome. These ZFNs can bind, cut, and induce the non-homologous end joining (NHEJ) during repairing, suggesting that they increase the possibility to generate mutations around the target site. Zinc fingers are found in eukaryotic transcription factors and have abilities to bind to sequence-specific regions in the genome. Their sequence-specific DNA binding abilities make them a great tool to target genetic loci. ZFN technology utilizes engineered zinc fingers to recognize different DNA triplets [4, 5]. Based on the DNA sequence of the target site, several zinc fingers can be aligned to form an array for site-specific binding. Each array is then linked to a *Fok*I endonuclease half domain, which induces DNA double-strand breaks once meets another *Fok*I half domain. Therefore, ZFN technology requires the usage of two zinc finger arrays recognizing two different DNA strands to target one locus in the genome [4]. Many zebrafish mutants have been generated using ZFNs since the technology was developed [6-11]. However, it can be challenging to engineer ZFNs because of the complexity of context-dependent design for each zinc finger array [12]. In addition, due to the limited selection of publicly available synthetic zinc fingers, some genes in zebrafish might be difficult to be targeted [13, 14].

A more recently described method utilizing the transcription activator-like effector nucleases (TALENs) to edit the genome of cultured human cells has became a popular

way to target genes in zebrafish [12, 15]. TALENs technology utilizes the design similar to ZFNs that links two different DNA sequence-specific binding arrays to *Fok*I half domains to target a single locus (Figure 3.1A). Each array consists of a combination of many engineered transcription activator–like effector (TALE) repeats that each TALE repeat specifically binds to one of the four nucleotides of DNA to increase the binding specificity [12, 16, 17]. Therefore, choosing target sites for genome editing becomes more flexible by arranging many different combinations of TALE repeats because of the one TALE repeat to one nucleotide recognition mechanism. In fact, it has been reported that target sites are as frequent as 1 in 35 bp of random DNA sequence [18]. Like ZFNs, TALENs cut double-strand DNA and induce error-prone DNA damage repair for the efficient mutagenesis. These error-prone repairs occurred within loci are usually small insertions or deletions, which often result in frame-shift, null mutations [12, 19].

Another new system using the clustered regularly interspaced short palindromic repeats (CRISPR) RNA-guided CRISPR-associated 9 (Cas9) nuclease (RGN) has been widely utilized as a tool for gene targeting in many different organisms due to the simplicity of the method [4, 20-22]. CRISPR/Cas systems are originally the adaptive immune systems found in bacteria and archaea for defending against intruding viruses and plasmid DNAs [23-25]. Cas9, a dual RNA-guided endonuclease from *Streptococcus pyogenes*, is directed by CRISPR RNA (crRNA) and the trans-activating CRISPR RNA (tracrRNA) to mediate site-specific DNA double-strand breaks [26]. For gene targeting, a synthetic single guide RNA (sgRNA) composed of a site-specific sequence for target DNA recognition via complimentary and a tracrRNA is utilized to guide Cas9 to the

target locus (Figure 3.1B). sgRNA interacts with the complementary strand of the DNA target site containing a 3′ protospacer adjacent motif (PAM) sequence (NGG) [20]. Once being guided to the target site, Cas9 cleaves the double-strand DNA and induces error-prone NHEJ during DNA damage repairs for efficient gene targeting. RGN system provides a quick, efficient, and flexible way to manipulate zebrafish genome that both gene knockin and knockout can be easily achieved by using this method [27, 28]. Furthermore, it has been shown that multiple genomic loci can be targeted simultaneously, resulting in multiple loss-of-function phenotypes in the same injected zebrafish [22]. Therefore, RGN system has became the most popular method for genome editing among all existing methods.

Here we demonstrate gene targeting in zebrafish using two different genome-editing systems. Two null mutant alleles of *α- tubulin acetyltransferase 1* (*atat1*) are generated by using TALENs. Five potentially null mutant alleles of max's giant associate protein (*mga*) are generated by using RGN system. Therefore, both TALENs and RGN system are reliable and efficient tools to generate heritable and precise mutations in zebrafish genome.

MATERIALS AND METHODS

Transcription Activator-like Effector Nucleases (TALENs) design

Two TALENs (left and right) were designed to target the first exon of zebrafish *atat1* gene. Left TALEN target sequence (5'-GGGAAATCCATTGCAGA-3') and right

TALEN target sequence (5'-GCTTTTCCCCGAGAGGA-3') were selected to design two TALEN arrays.

sgRNA design and cloning

The sequence (5'-GGGCGTGACTGCCCCAACACTGG-3') located within zebrafish *mga* exon 2 was identified as the potential binding target of sgRNA to generate indels. Two DNA oligo primers (Forward: 5'-TAGGGCGTGACTGCCCCAACAC-3'; Reverse: 5'-AAACGTGTTGGGGCAGTCACGC-3') containing core-targeting sequence were annealed and subsequently cloned into pT7-gRNA plasmid as previously described [22]. The construct was sequenced to confirm the accuracy of insert sequence.

RNA synthesis and microinjection

For *atat1* gene targeting, two plasmids containing left TALEN and right TALEN inserts were linearized with *Not*I and purified using phenol-chloroform extraction method. Linearized plasmids were used as templates for mRNA *in vitro* transcription. Capped mRNAs were synthesized using Ambion mMessage mMachine SP6 Transcription Kit (AM1340, Life Technologies, Carlsbad, CA). For the microinjection, a mixture of both left TALEN and right TALEN mRNAs (150pg each) together with 0.1M KCl and 0.1% phenol red was injected into the yolk of each WIK embryo at 1-cell stage. For *golden* gene targeting, the BamHI-linearized pT7goldRNA plasmid was used as the template for sgRNA synthesis. For *mga* gene targeting, the plasmid containing *mga* exon 2 targeting sequence was first linearized with *Bam*HI and purified as the template for in vitro

transcription. sgRNA synthesis was carried out using MEGAshortscript T7 Kit (AM1354, Life Technologies, Carlsbad, CA) with 1μg linearized plasmid following manufacturer's instruction. sgRNA was further purified using *mir*Vana miRNA Isolation Kit (AM1560, Life Technologies, Carlsbad, CA) and concentrated by ethanol precipitation. Final sgRNA was dissolved in ~20μl RNase-free water to reach the concentration around 1μg/μl as the stock. Capped *cas9* mRNA was synthesized as previously described using *Not*I-linearized pCS2+-nls-zCas9-nls plasmid as the template. Both sgRNA and *cas9* mRNA stocks were stored at -80°C before use. For microinjection, a mixture of 150pg *cas9* mRNA and ~100pg sgRNA together with 0.1M KCl and 0.1% phenol red was injected into the cell (not the yolk) of each 1-cell stage WIK embryos. Damaged or unfertilized embryos were discarded around 4 to 5hpf. Survived embryos were raised to adulthood and named as F0.

T7 endonuclease I (T7EI) assay and mutation identification

For atat1 gene targeting, TALENs mRNA injected F0 adult zebrafish were outcrossed to wildtype WIK adults to obtain F1 embryos. Twelve F0 adults were randomly selected from two F0 stocks containing ~30 adults to outcross to wildtype adults individually. Embryos from each pair mating were collected and cultured at 28°C. 20 larvae were randomly selected from each batch of larvae (>80) obtained from each pair mating to extract their genomic DNA at 72hpf. Genotyping PCR was carried out using forward primer TALENTESTF3 (5'-CATTGATAAGACCGCTACTACA-3') and reverse primer TALENTESTR3 (5'-GTGCATGTAGCGAACCAGAT-3') under the PCR condition as shown here (initial denaturing: 94°C for 2 minutes, denaturing: 94°C for 30 seconds,

annealing: 57°C for 30 seconds, extension: 72°C for 1 minute, 35 cycles, final extension: 72°C for 5 minutes). PCR products were then digested with T7 endonuclease I (M0302, New England BioLabs, Ipswich, MA) at 37°C for 2 hours after boiling and cooling slowly. T7E1-digested PCR products were resolved on 2% agarose gels to identify any potential changes (insertion, deletion or substitution) in the targeting region. For *mga* gene targeting, *mga* sgRNA/*cas9* mRNA injected F0 adult zebrafish were outcrossed to wildtype WIK adults to obtain F1 embryos. Five adult F0 females were randomly selected from a F0 stock containing ~30 adults to outcross to five WIK adult males individually. Embryos from each pair mating were collected and cultured at 28°C. 16 larvae were randomly selected from each batch of larvae (>80) obtained from each pair mating to extract their genomic DNA at 72hpf. Genomic DNA from these larvae was extracted with DNA extraction buffer (10 mM Tris pH 8.2, 10 mM EDTA, 200 M NaCl, 0.5% SDS, and 200 ug/ml proteinase K) and diluted 20 times as the template for genotyping PCR. Genotyping PCR was carried out using forward primer mgaT7EF (5'-GATGTAGACCTGATATACCC-3') and reverse primer mgaT7ER (5'-CTAATTGCCATTAGATTAGCC-3') under the PCR condition as shown here (initial denaturing: 94°C for 2 minutes, denaturing: 94°C for 30 seconds, annealing: 52°C for 30 seconds, extension: 72°C for 30 seconds, 45 cycles, final extension: 72°C for 5 minutes). PCR products were then processed for T7E1 assay as previously described. In both cases, their F1 embryos were raised to adulthood and screened again individually using genomic DNA extract from fin-clips and T7E1 assay once potential F0 founders were identified. Genotyping PCR products from individuals identified as potential mutation carriers were

subsequently cloned into pGEM-T Easy vector (A1360, Promega, Fitchburg, WI) for sequencing.

Genotyping

For allele *atat1*^{ga4}, genotyping PCR was carried out as previously described using the primer pair TALENTESTF3 and TALENTESTR3 with genomic DNA from either larvae or adult fin-clips as the template. PCR products were then digested with *Bsm*I (R0134, New England BioLabs, Ipswich, MA) at 65°C for 8 hours. For allele *atat1*^{ga21}, genotyping PCR was carried out using forward primer MecC17-StuI-F (5'-CAGATCTGCAATGGATTTCCCTTAGGCC-3') and reverse primer TALENTESTR3 (5'-GTGCATGTAGCGAACCAGAT-3') under the same PCR condition for *atat1*^{ga4} allele. PCR products were then digested with *Stu*I (R0187, New England BioLabs, Ipswich, MA) at 37°C for 8 hours. Genotyping PCR for all four recovered *mga* mutant alleles (*mga*^{ga37}, *mga*^{ga94}, *mga*^{ga98}, and *mga*^{ga112}) was carried out as previously described using the primer pair mgaT7EF and mgaT7ER with genomic DNA from either larvae or adult fin-clips as the template. PCR products were then digested with BslI (R0555, New England BioLabs, Ipswich, MA) at 55°C for 8 hours. For all *atat1* and *mga* alleles, restriction enzyme digested PCR products were resolved on 2% agarose gels for identifying each individual's genotype.

RESULTS

Design of *atat1*-specific TALENs for gene targeting

Atat1 (Mec-17) is an acetyltransferase that responsible for adding acetyl groups onto Lysine 40 (K40) residue of polymerized α-Tubulin [29]. In zebrafish, a single *atat1* gene (Gene ID: 406389) is located within the chromosome 19. *atat1* consists of 11 exons encoding a 305aa ATAT1 protein. In order to generate potentially null mutants, a target sequence within the exon 1 (5'-TCTGCAATGGATTTCCCTTACGACCTGAATGCGCTTTTCCCCGAGAGGA-3') spanning the translation start site (ATG) was chosen for designing TALEN arrays. Within the target site, a sequence (5'- TCTGCAATGGATTTCCC-3) from the antisense strand was used as the left TALEN site, and a sequence (5'-GCTTTTCCCCGAGAGGA-3') from the sense strand was selected as the right TALEN site. The site (5'-TTACGACCTGAATGC-3') in between those two 17 nucleotides long TALEN recognition sites is the target site for *Fok*I to induce DNA double-strand breaks. This site was chosen for *atat1* gene targeting because of its proximity to the translation start site, suggesting a potential to obtain null mutations. A restriction emzyme *Bsm*I site located within the target site also facilitate the process for mutation screening.

atat1-specific TALENs induces heritable error-prone NHEJ within target site

For targeting *atat1*, a combination of both left and right TALEN mRNAs (150pg each) was injected into 1-cell stage embryos. Most of the injected embryos (F0) developed normally with some others developed with various degrees of defects. To test the

efficiency of error-prone NHEJ, T7E1 assay or *Bsm*I digest was applied to detect any possible mutation happened within the target site [30]. However, we found no sign of any potential insertion, deletion, or substitution within the target site in F0 embryos. This result suggests that the percentage of cells containing mutations might too low to be detected by either assay. Alternatively, F0 embryos were raised to adulthood and outcrossed to wildtype fish individually to obtain embryos (F1) for T7E1 assay or *Bsm*I digest. This strategy can greatly increase the presence of mutant DNA in any mutation carrying individual because these individuals should be heterozygous. The screening using F1 embryos as materials was utilized to confirm which F0 adult carried potential mutation(s) in the germ line. Indeed, potential mutations were found in the offspring of two F0 adults (2/12). F1 adults from both F0 parents were screened by either *Bsm*I digest or T7E1 assay. Finally, one allele from a single F1 adult was discovered by *Bsm*I digest (Figure 3.2A), whereas another allele was identified by T7E1 assay from a different F1 adult (Figure 3.2B). Both alleles were subsequently sequenced to confirm the types of mutations and named *atat1*^{ga4} and *atat1*^{ga21}, respectively (Figure 3.3A-B). *atat1*^{ga4} is a single nucleotide deletion losing a G, and *atat1*^{ga21} is also a single nucleotide deletion losing a C. Both mutations result in frame-shift, potentially null mutations. This result suggests that TALENs can precisely induce mutations occurred within the target site.

Design of *mga*-specific sgRNA for gene targeting

Zebrafish *mga* (*mgaa*, Gene ID: 569620) encodes a T-box domain containing transcription factor required for many developmental processes in embryos [31, 32]. Here we attempted to generate *mga* null mutants by utilizing RGN system. In RGN system, a

potential site for gene targeting is a stretch of 23 nucleotides sequence in the genome that begins with two GG residues at the 5′ end and ends with PAM sequence, NGG, which is required for Cas9 binding [33]. Zebrafish *mga* contains 25 exons, and its translation start site (ATG) is located within the exon 2. In order to increase the possibility of generating null mutants, a single site (5'-GGGCGTGACTGCCCCAACACTGG-3') located within *mga* exon 2 was selected as the sgRNA target site. Therefore, *mga*-sgRNA should be able to interact with the antisense strand DNA of the target site and guide Cas9 endonuclease to induce DNA double-strand breaks.

mga-sgRNA/Cas9 induces high frequency mutagenesis within the target site

For validating the RGN system, *golden*-specific sgRNA was used to target *golden* gene. Zebrafish *golden* encodes a cation exchanger SLC24A5, which is required for normal skin and retinal pigment epithelium (RPE) pigmentation. Homozygous *golden* mutants exhibit hypopigmentation phenotype starting at embryonic stage [34]. Therefore, the same phenotype is expected to be observed in embryos injected with *golden*-sgRNA/Cas9 mRNA because any somatic loss-of-function mutations occurred in pigment cells should affect their pigmentation. Indeed, many larvae showed mosaic hypopigmentation in RPE and skin after being co-injected with *golden*-sgRNA/*cas9* mRNA (100pg/150pg per embryo) at 1-cell stage (Figure 3.4A). The hypopigmentation phenotype was first seen at 48hpf, and became evident by 56hpf (Figure 3.4B-C). We next targeted *mga* by injecting *mga*-sgRNA/*cas9* mRNA (100pg/150pg per embryos) into 1-cell stage embryos. Most of the injected embryos (F0) developed normally without any noticeable defect. We were also not able to detect any possible mutations in F0 embryos

via T7E1 assay. This might be due to the same situation as we encountered when using TALENs to target *atat1* that mutant DNA was too less to be detected by T7E1 assay. Again, F0 embryos were raised to adulthood and outcrossed to wildtype adults individually to obtain embryos (F1) for mutation screening. Surprisingly, germ-line transmission rate in F0 was high as three out of five F0 adults (F0 #1, #2, and #3) we used for screening carried potential mutations (60%, N=5) (Figure 3.5A). F1 embryos from F0 #1, #2, and #3 were raised to adulthood and screened by T7E1 assay. We screened a total of 98 F1 adults from F0 #1, #2, and #3 by T7E1 assay and found 38 T7E1-positive individuals (Figure 3.5B). However, three F0 adults exhibited different degrees of ability to pass their mutations to F1 as we examined the F1 screening result from T7E1 assay (from F0 #1: 28%, N=25; from F0 #2: 20.75%, N=53; from F0 #3: 100%, N=20). This result indicates that each F0 might have different degrees of mosaicism in the germ-line. These potential mutations were cloned and sequenced to confirm the types of mutations. Finally, we identified five different alleles potentially resulting in null mutations. The types of mutations in these alleles are small deletions (mga^{ga37} and mga^{ga98}), small deletions and substitution (mga^{ga71} and mga^{ga94}), and single nucleotide insertion and substitution (mga^{ga112}) (Figure 3.6A-B). Among all these alleles, four out of five (mga^{ga37}, mga^{ga94}, mga^{ga98}, and mga^{ga112}) were recovered in F2. Overall, our result suggests that RGN system is an efficient way to induce site-specific mutagenesis.

DISCUSSION

The recently developed genome editing techniques have made it possible to precisely target certain loci in zebrafish genome. Here we decided to target two genes, *atat1* and *mga*, which are thought to play important roles during embryonic development in zebrafish. Both *atat1* and *mga* knockout mice have been generated using classic homologous recombination [35-37]. However, there are no null zebrafish mutants of either gene available currently. Therefore, generating null *atat1* and *mga* mutants is crucial in terms of understanding both genes' possible roles in zebrafish embryonic development. *atat1* was targeted by TALENs, whereas *mga* was targeted by RGN system. It has been shown that the mutagenesis rate can be evaluated as early as in F0 embryos with assays such as T7E1 digest [22]. But we did not detect any possible mutations in F0 embryos by either *Bsm*I digest or T7E1 assay. This might be due to the lower efficiency of TALENs and CRISPR/Cas9, and might be improved by simply increasing the concentration of mRNA/sgRNA injected into embryos. However, increasing the RNA dosage might also elevate the risk of killing more somatic/germ cells in F0 and the possibility of non-specific targeting. If there are more dead cells due to mutations in F0, it increases the possibility that fewer F0 individuals can survive and develop into fertile adults. This might affect the screening as many F0 mutation-carrying individuals die at some points during the development. Hence, it might be more efficient in terms of establishing mutant lines by not losing too many cells in F0 due to gene targeting. Indeed, we were still able to find F0 adults that carry mutations in their germ-lines even we failed to identify any possible mutations from F0 embryos. It is reported that phenotypes caused

by targeting some genes might be observed in F0 [22]. Therefore, this can be utilized as an alternative way to access the efficiency of gene targeting. But this may not be quite useful for genes with unknown functions as their phenotypes might be variable or not significant in F0. We did not find any consistent phenotypes in F0 embryos for both genes, suggesting that this alternative method may not be able to be applied to our cases. Meanwhile, off-target effect might still have to be taken into account if higher dosage of RNA is used for the injection even though its influence is minimal under normal condition [4, 28, 38]. This might be a more significant issue in RGN system because some secondary targets with multiple mismatches to sgRNAs are mutated at rates similar to that of the desired target [4].

Both TALENs and RGN system utilize endonucleases with sequence-specific guide protein/RNA to induce DNA double-strand breaks precisely [4]. Theoretically, these frequent DNA double-strand breaks should induce random, error-prone NHEJ that occurs during DNA damage repair. Hence, the mosaic distribution of cells carrying different mutations is expected in both somatic and germ cells. However, we found that these error-prone DNA repairs might not be random as we identified the same mutation in F1 embryos and adults from different F0 parents. This result suggests that the DNA repairs might be affected by local micro-environment such as DNA sequence.

TALENs and RGN system provide excellent tools to edit particular loci in the genome. It is much easier to identify target sites in the genome that are suitable for gene targeting with TALENs [18]. However, it is more complex in terms of assembling TALE

arrays via cloning. RGN system, on the other hand, the target sites are limited by the presence of PAM sequence and first two "GG" 18 bp upstream to it. But it is relatively easy to design sgRNA for one target site as only one sgRNA is needed for targeting a single site. Therefore, these gene targeting techniques have widen the possibility in search of functions of many unexplored genes, and potentially provide comparisons with gene functions identified by using MOs.

REFERENCES

1. Mara E Robu, J.D.L., Soraya Beiraghi, Charles Brenner, Steven A Farber, Stephen C Ekker (2007). p53 Activation by Knockdown Technologies. PLoS Genetics *3*, e78.
2. Fatma O. Kok, M.S., Chih-Wen Ni, Ankit Gupta, Ann S. Grosse, Andreas van Impel, Bettina C. Kirchmaier, Josi Peterson-Maduro, George Kourkoulis, Ira Male, Dana F. DeSantis, Sarah Sheppard-Tindell, Lwaki Ebarasi, Christer Betsholtz, Stefan Schulte-Merker, Scot A. Wolfe, Nathan D. Lawson (2015). Reverse Genetic Screening Reveals Poor Correlation between Morpholino-Induced and Mutant Phenotypes in Zebrafish. Developmental Cell *32*, 97-108.
3. Didier Y.R. Stainier, Z.K., Andrea Rossi (2015). Making Sense of Anti-Sense Data. Developmental Cell *32*, 7-8.
4. Carroll, D. (2014). Genome Engineering with Targetable Nucleases. Annual Review of Biochemistry *83*, 409-439.

5. John R. Desjarlais, J.M.B. (1993). Use of a zinc-finger consensus sequence framework and specificity rules to design specific DNA binding proteins. Proceedings of the National Academy of Sciences USA *90*, 2256-2260.

6. Raman Sood, B.C., Kevin Bishop, MaryPat Jones, Alberto Rissone, Fabio Candotti, Settara C. Chandrasekharappa, Paul Liu (2013). Efficient Methods for Targeted Mutagenesis in Zebrafish Using Zinc-Finger Nucleases: Data from Targeting of Nine Genes Using CompoZr or CoDA ZFNs. PLoS ONE *8*, e57239.

7. Frauke van Bebber, A.H., Michael Willem, Bettina Schmid, Christian Haass (2013). Loss of Bace2 in zebrafish affects melanocyte migration and is distinct from Bace1 knock out phenotypes. Journal of Neurochemistry *127*, 471-481.

8. Andrew Taibi, K.P.M., Justine Noel, Ejike V. Okoye, Carolyn R. Milano, Benjamin L. Martin, Howard I. Sirotkin (2013). Zebrafish churchill regulates developmental gene expression and cell migration. Developmental Dynamics *242*, 614-621.

9. Lingyan Xing, K.H., David J. Grunwald, Esther Fujimoto, Tyler S. Quist, Jacob Sneddon, Chi-Bin Chien, Tamara J. Stevenson, Joshua L. Bonkowsky (2012). Zebrafish foxP2 Zinc Finger Nuclease Mutant Has Normal Axon Pathfinding. PLoS ONE *7*, e43968.

10. Fatma O. Kok, A.T., Sarah J. Wanner, Xiayang Xie, Cara E. Moravec, Crystal E. Love, Victoria E. Prince, Jeff S. Mumm, Howard I. Sirotkin (2012). Zebrafish rest regulates developmental gene expression but not neurogenesis. Development *139*, 3838-3848.

11. Jin Ben, S.E., Ashley Shu Mei Ng, Freek van Eeden, Philip W. Ingham (2011). Targeted mutation of the talpid3 gene in zebrafish reveals its conserved requirement for ciliogenesis and Hedgehog signalling across the vertebrates. Development *138*, 4969-4978.

12. Jeffry D Sander, L.C., Cyd Khayter, Deepak Reyon, Randall T Peterson, J Keith Joung, Jing-Ruey J Yeh (2011). Targeted gene disruption in somatic zebrafish cells using engineered TALENs. Nature Biotechnology *29*.

13. Jeffry D Sander, E.J.D., Mathew J Goodwin, Lindsay Cade, Feng Zhang, Daniel Cifuentes, Shaun J Curtin, Jessica S Blackburn, Stacey Thibodeau-Beganny, Yiping Qi, Christopher J Pierick, Ellen Hoffman, Morgan L Maeder, Cyd Khayter, Deepak Reyon, Drena Dobbs, David M Langenau, Robert M Stupar, Antonio J Giraldez, Daniel F Voytas, Randall T Peterson, Jing-Ruey J Yeh, J Keith Joung (2011). Selection-free zinc-finger-nuclease engineering by context-dependent assembly (CoDA). Nature Methods *8*, 67-69.

14. Jonathan E. Foley, J.-R.J.Y., Morgan L. Maeder, Deepak Reyon, Jeffry D. Sander, Randall T. Peterson, J. Keith Joung (2009). Rapid Mutation of Endogenous Zebrafish Genes Using Zinc Finger Nucleases Made by Oligomerized Pool ENgineering (OPEN). PLoS ONE *4*, e4348.

15. Jeffrey C Miller, S.T., Guijuan Qiao, Kyle A Barlow, Jianbin Wang, Danny F Xia, Xiangdong Meng, David E Paschon, Elo Leung, Sarah J Hinkley, Gladys P Dulay, Kevin L Hua, Irina Ankoudinova, Gregory J Cost, Fyodor D Urnov, H Steve Zhang, Michael C Holmes, Lei Zhang, Philip D Gregory, Edward J Rebar

(2011). A TALE nuclease architecture for efficient genome editing. Nature Biotechnology *29*, 143-148.

16. Matthew J. Moscou, A.J.B. (2009). A Simple Cipher Governs DNA Recognition by TAL Effectors. Science *326*, 1501.

17. Jens Boch, H.S., Sebastian Schornack, Angelika Landgraf, Simone Hahn, Sabine Kay, Thomas Lahaye, Anja Nickstadt, Ulla Bonas (2009). Breaking the Code of DNA Binding Specificity of TAL-Type III Effectors. Science *326*, 1509-1512.

18. Tomas Cermak, E.L.D., Michelle Christian, Li Wang, Yong Zhang, Clarice Schmidt, Joshua A. Baller, Nikunj V. Somia, Adam J. Bogdanove, Daniel F. Voytas (2011). Efficient design and assembly of custom TALEN and other TAL effector-based constructs for DNA targeting. Nucleic Acids Research *39*, e82.

19. Lindsay Cade, D.R., Woong Y. Hwang, Shengdar Q. Tsai, Samir Patel, Cyd Khayter, J. Keith Joung, Jeffry D. Sander, Randall T. Peterson, Jing-Ruey Joanna Yeh (2012). Highly efficient generation of heritable zebrafish gene mutations using homo- and heterodimeric TALENs. Nucleic Acids Research *40*, 8001-8010.

20. Woong Y. Hwang, Y.F., Deepak Reyon, Morgan L. Maeder, Prakriti Kaini, Jeffry D. Sander, J. Keith Joung, Randall T. Peterson, Jing-Ruey Joanna Yeh (2013). Heritable and Precise Zebrafish Genome Editing Using a CRISPR-Cas System. PLoS ONE *8*, e68708.

21. Woong Y Hwang, Y.F., Deepak Reyon, Morgan L Maeder, Shengdar Q Tsai, Jeffry D Sander, Randall T Peterson, J-R Joanna Yeh, J Keith Joung (2013). Efficient genome editing in zebrafish using a CRISPR-Cas system. Nature Biotechnology *31*, 227-229.

22. Li-En Jao, S.R.W., Wenbiao Chen (2013). Efficient multiplex biallelic zebrafish genome editing using a CRISPR nuclease system. Proceedings of the National Academy of Sciences USA *110*, 13904-13909.

23. Blake Wiedenheft, S.H.S., Jennifer A. Doudna (2012). RNA-guided genetic silencing systems in bacteria and archaea. Nature *482*.

24. Michael P Terns, R.M.T. (2011). CRISPR-based adaptive immune systems. Current Opinion in Microbiology *14*, 321-327.

25. Philippe Horvath, R.B. (2010). CRISPR/Cas, the Immune System of Bacteria and Archaea. Science *327*.

26. Martin Jinek, K.C., Ines Fonfara, Michael Hauer, Jennifer A. Doudna, Emmanuelle Charpentier (2012). A Programmable Dual-RNA–Guided DNA Endonuclease in Adaptive Bacterial Immunity. Science *337*, 816-821.

27. James A. Gagnon, E.V., Summer B. Thyme, Peng Huang, Laila Ahkmetova, Andrea Pauli, Tessa G. Montague, Steven Zimmerman, Constance Richter, Alexander F. Schier (2014). Efficient Mutagenesis by Cas9 Protein-Mediated Oligonucleotide Insertion and Large-Scale Assessment of Single-Guide RNAs. PLoS ONE *9*, e98186.

28. Alexander Hruscha, P.K., Alexandra Rechenberg, Verena Heinrich, Jochen Hecht, Christian Haass, Bettina Schmid (2013). Efficient CRISPR/Cas9 genome editing with low off-target effects in zebrafish. Development *140*, 4982-4987.

29. Jyothi S. Akella, D.W., Jihyun Kim, Natalia G. Starostina, Sally Lyons-Abbott, Naomi S. Morrissette, Scott T. Dougan, Edward T. Kipreos, Jacek Gaertig (2010). MEC-17 is an α-tubulin acetyltransferase. Nature *467*, 218-222.

30. Ankit Gupta, V.L.H., Fatma O. Kok, Masahiro Shin, Joseph C. McNulty, Nathan D. Lawson, Scot A. Wolfe (2013). Targeted chromosomal deletions and inversions in zebrafish. Genome Research *23*, 1008-1017.

31. Yuhua Sun, W.-C.T., Xiang Fan, Rebecca Ball, Scott T. Dougan (2014). Extraembryonic Signals under the Control of MGA, Max, and Smad4 Are Required for Dorsoventral Patterning. Developmental Cell *28*, 322-334.

32. Amir Rikin, T.E. (2010). The tbx/bHLH transcription factor mga regulates gata4 and organogenesis. developmental Dynamics *239*, 535-547.

33. F. J. M. Mojica, C.D.-V., J. García-Martínez, C. Almendros (2009). Short motif sequences determine the targets of the prokaryotic CRISPR defence system. Microbiology *155*, 733-740.

34. Rebecca L. Lamason, M.-A.P.K.M., Jason R. Mest, Andrew C. Wong, Heather L. Norton, Michele C. Aros, Michael J. Jurynec, Xianyun Mao, Vanessa R. Humphreville, Jasper E. Humbert, Soniya Sinha, Jessica L. Moore, Pudur Jagadeeswaran, Wei Zhao, Gang Ning, Izabela Makalowska, Paul M. McKeigue, David O'Donnell, Rick Kittles, Esteban J. Parra, Nancy J. Mangini, David J. Grunwald, Mark D. Shriver6, Victor A. Canfield4, Keith C. Cheng (2005). SLC24A5, a Putative Cation Exchanger, Affects Pigmentation in Zebrafish and Humans. Science *310*, 1782-1786.

35. Andrew J. Washkowitz, C.S., Kun Zhang, Wolfgang Wurst, Thomas Floss, Jesse Mager, Virginia E. Papaioannou (2015). Mga is essential for the survival of pluripotent cells during peri-implantation development. Development *142*, 31-40.

36. Nereo Kalebic, S.S., Emerald Perlas, Giulia Bolasco, Concepcion Martinez, Paul A. Heppenstall (2013). αTAT1 is the major α-tubulin acetyltransferase in mice. Nature Communications *4*, 1962.

37. Go-Woon Kim, L.L., Mohammad Gorbani, Linya You, Xiang-Jiao Yang (2013). Mice lacking α-tubulin acetyltransferase 1 are viable but display α-tubulin acetylation deficiency and dentate gyrus distortion. The Journal of Biological Chemistry *288*, 20334-20350.

38. Timothy J. Dahlem, K.H., Michael J. Jurynec, Derrick Gunther, Colby G. Starker, Alexandra S. Locke, Allison M. Weis, Daniel F. Voytas, David Jonah Grunwald (2012). Simple Methods for Generating and Detecting Locus-Specific Mutations Induced with TALENs in the Zebrafish Genome. PLoS Genetics *8*, e1002861.

FIGURES AND FIGURE LEGENDS

Figure 3.1. Schematic diagrams of zebrafish gene targeting methods. Two most popular gene targeting methods, TALENs-mediated gene targeting and RGN-mediated gene targeting, are shown, respectively. For targeting a single site using TALENs, left and right TALE arrays linked to *FokI* endonuclease domains bind to target sequences and induce DNA double-strand breaks. Each TAL domain in the array recognizes one nucleotide **(A)**. For targeting a single site using RGN, a sgRNA binds to the complementary strand of target sequence and introduces Cas9 endonuclease to cut the target region **(B)**.

A

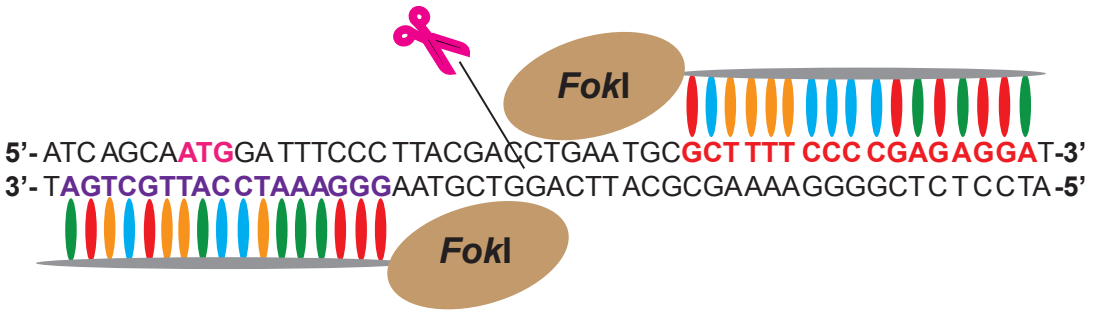
FokI
5'- ATC AGCAATGGA TTTCCC TTACGACCTGAA TGCGCT TTT CCC CGAG AGGAT-3'
3'- TAGTCGTTAC CTAAAGGGAATGCTGGACTT ACGCGAAAAGGGGCT C T CCTA-5'
FokI

B

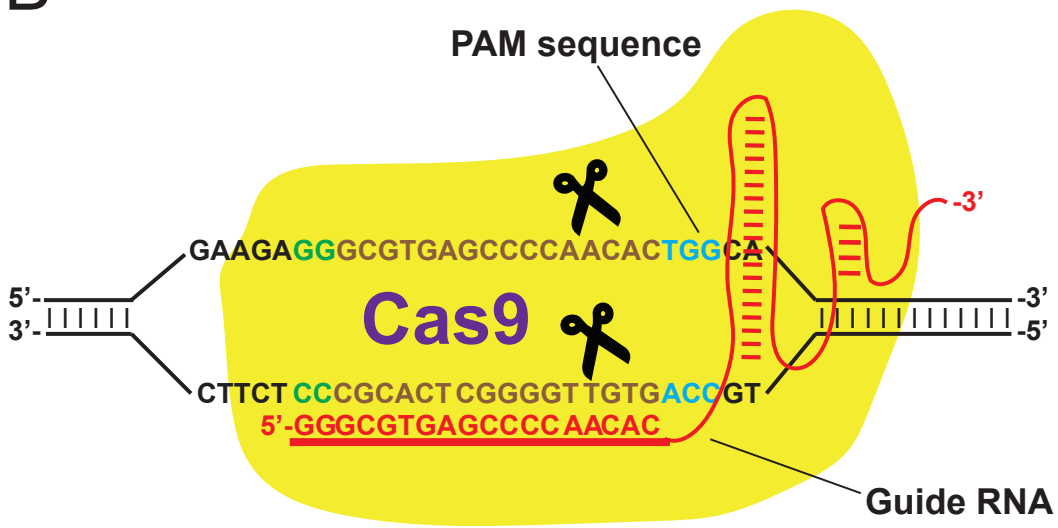
PAM sequence
GAAGAGGGCGTGAGCCCCAACACTGGCA
Cas9
5'-
3'-
-3'
-3'
-5'
CTTCT CCCGCACT CGGGGT TGTGACCGT
5'-GGGCGTGAGCCCC AACAC
Guide RNA

Figure 3.2. *atat1*-specific TALENs-induced mutations are detected in F1. 11 F1 adult individuals (A1-A11) are randomly chosen for *Bsm*I digest. *Bsm*I cuts wildtype PCR product but not mutant PCR product **(A)**. 8 F1 adult individuals (A1'-A8') are randomly chosen for T7E1 assay to screen mutations that don't affect *Bsm*I site **(B)**. Genomic DNA from a known heterozygous *mga*^{sa865} mutant is used as a positive control.

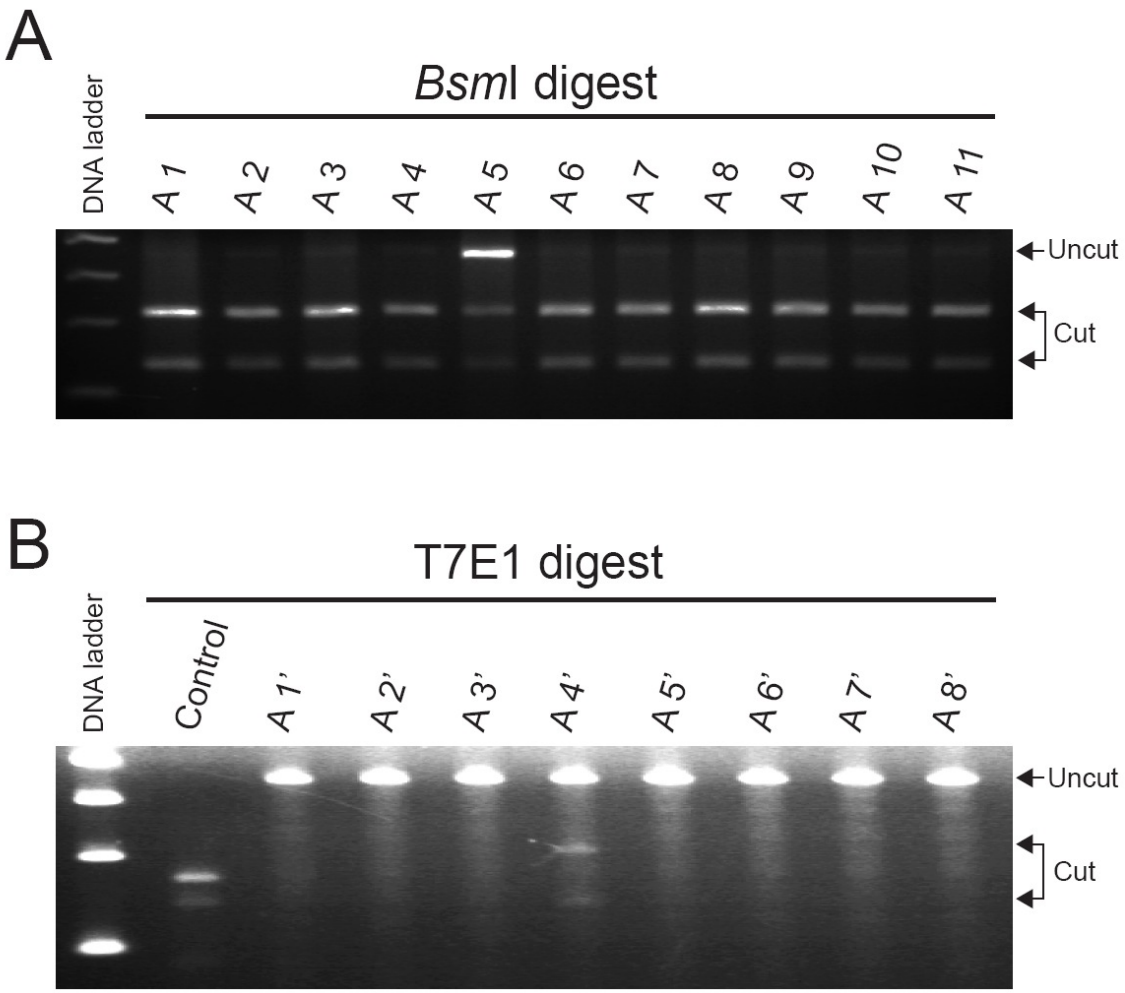
A
BsmI digest
DNA ladder
A 1
A 2
A 3
A 4
A 5
A 6
A 7
A 8
A 9
A 10
A 11
Uncut
Cut
B
T7E1 digest
DNA ladder
Control
A 1'
A 2'
A 3'
A 4'
A 5'
A 6'
A 7'
A 8'
Uncut
Cut

Figure 3.3. Potential *atat1* null mutants identified from mutation screening. Two *atat1* mutant alleles, $atat1^{ga4}$ and $atat1^{ga21}$, are identified in F1 adults **(A)**. Chromatograms of wildtype and mutant DNA sequences between magenta dash lines in (A) are shown **(B)**. Red dash: deletion.

A


Left TALEN site
Right TALEN site
atat1 wt
5'-ATCTGCAATGGATTTCCCTTACGACCTGAATGCGCTTTTCCCCGAGAGGAT-3'
atat1 ga4
5'-ATCTGCAATGGATTTCCCTTACGACCT-AATGCGCTTTTCCCCGAGAGGAT-3'
atat1 ga21
5'-ATCTGCAATGGATTTCCCTTACGA-CTGAATGCGCTTTTCCCCGAGAGGAT-3'

B

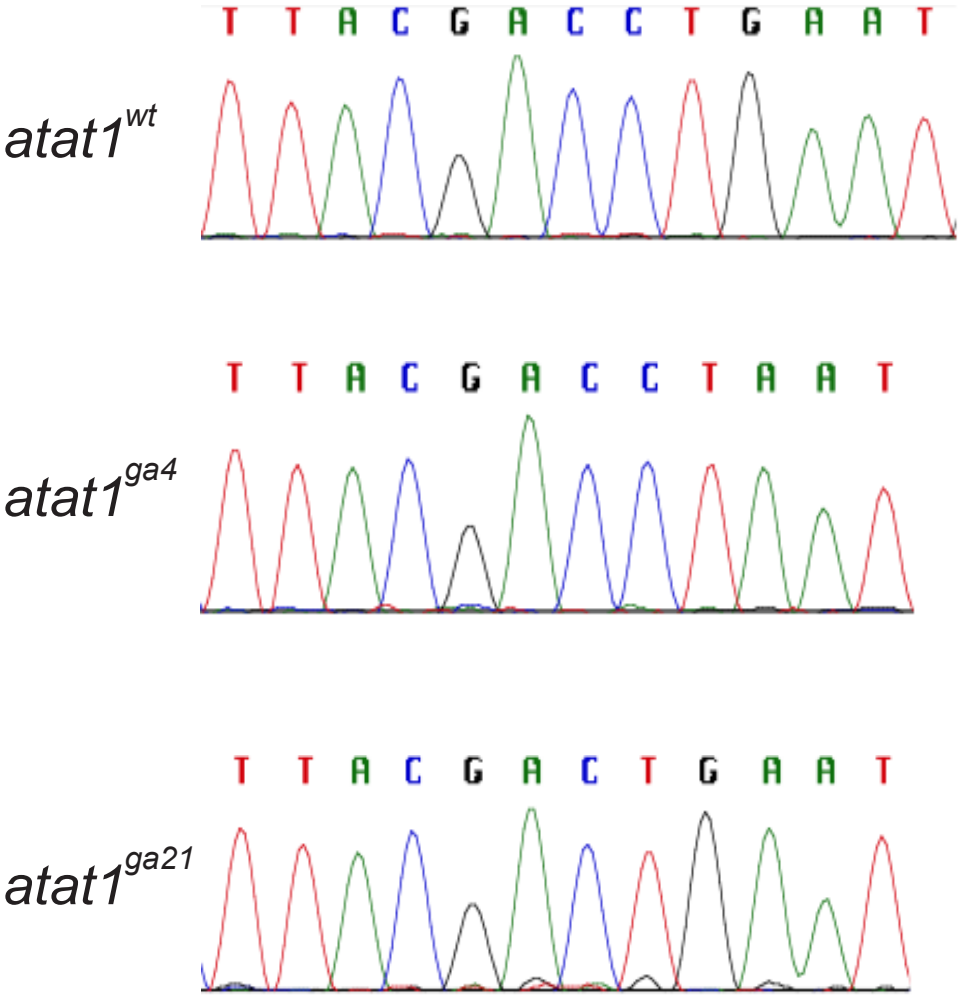
atat1 wt
T T A C G A C C T G A A T
atat1 ga4
T T A C G A C C T A A T
atat1 ga21
T T A C G A C T G A A T

Figure 3.4. RGN-mediated gene targeting leads to gene-specific phenotype in F0. Schematic drawing shows that both gene-specific sgRNA and *cas9* mRNA are required to be co-injected into 1-cell stage embryos **(A)**. The embryo shows normal pigmentation at 56hpf **(B)**, whereas the embryo injected with *golden* sgRNA and *cas9* mRNA exhibits reduced pigmentation **(C)**.

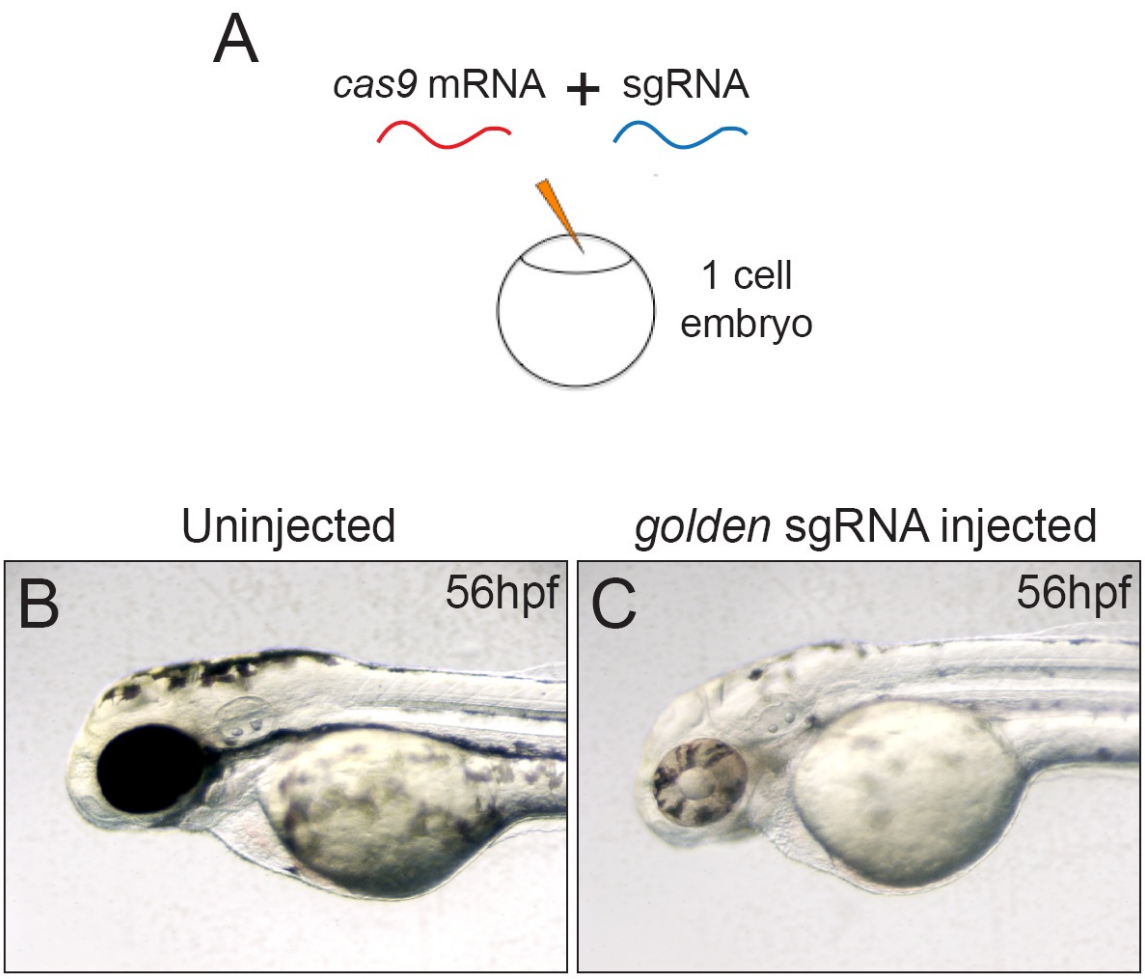
A
cas9 mRNA + sgRNA
1 cell
embryo
Uninjected
golden sgRNA injected
B
56hpf
C
56hpf

Figure 3.5. *mga*-specific RGN-mediated mutations are detected in F1. 16 F1 embryos (E1-E16) are randomly chosen for T7E1 assay **(A)**. 16 F1 adult individuals (A1-A16) are randomly chosen for T7E1 assay **(B)**.

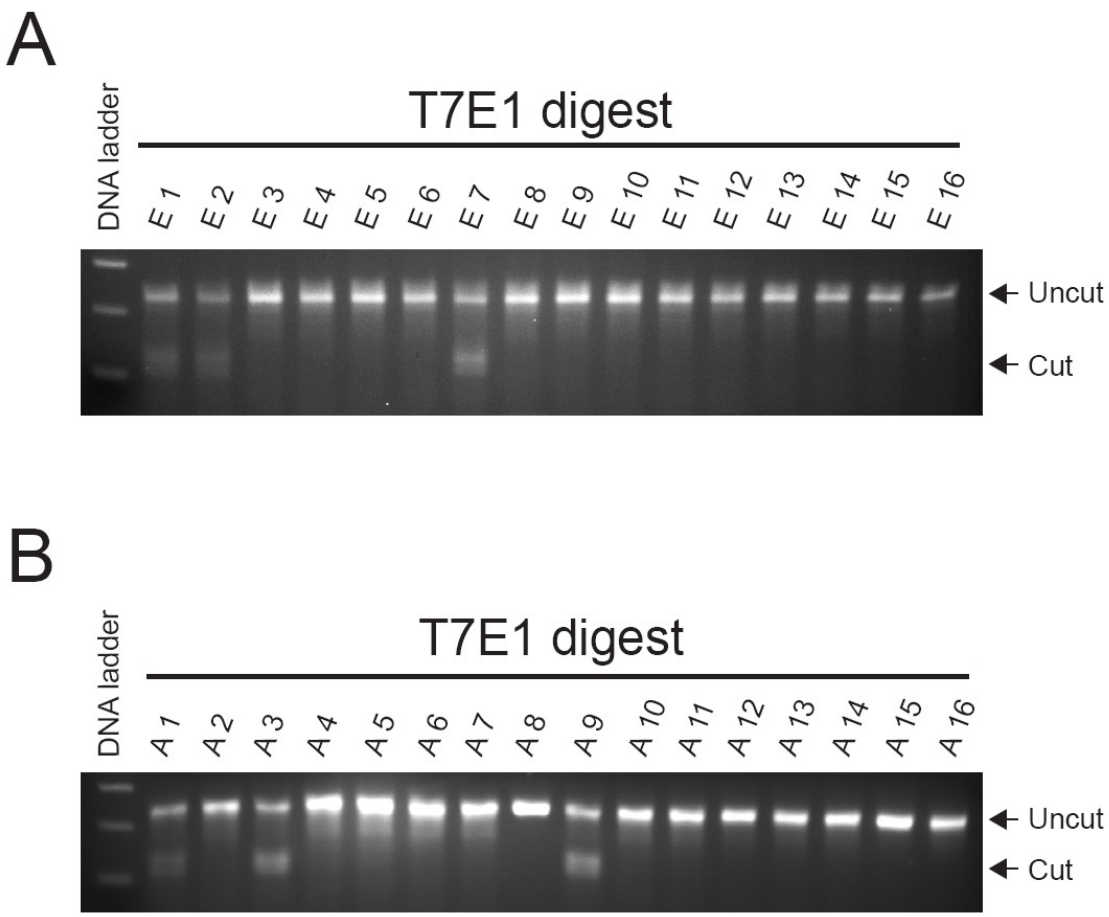
A
T7E1 digest
DNA ladder
E 1
E 2
E 3
E 4
E 5
E 6
E 7
E 8
E 9
E 10
E 11
E 12
E 13
E 14
E 15
E 16
Uncut
Cut
B
T7E1 digest
DNA ladder
A 1
A 2
A 3
A 4
A 5
A 6
A 7
A 8
A 9
A 10
A 11
A 12
A 13
A 14
A 15
A 16
Uncut
Cut

Figure 3.6. Potential *mga* null mutants identified from mutation screening. Five *atat1* mutant alleles, mga^{ga37}, mga^{ga71}, mga^{ga94}, mga^{ga98}, and mga^{ga112}, are identified in F1 adults **(A)**. Chromatograms of wildtype and mutant DNA sequences between magenta dash lines in (A) are shown **(B)**. Red dash: deletion; Orange letter: substitution; Purple letter: insertion.

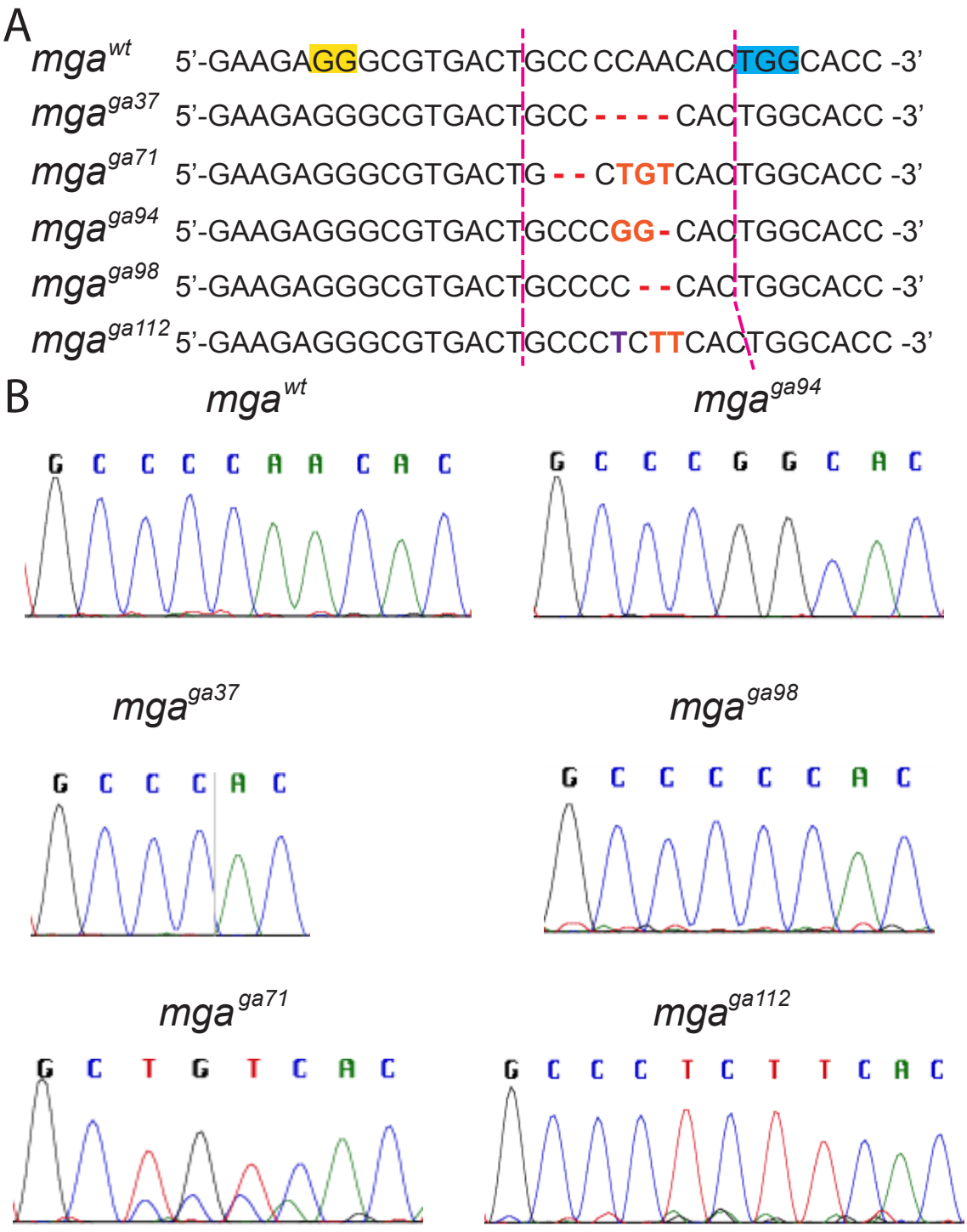
A
mga^wt 5'-GAAGAGGGCGTGACTGCC CCAACACTGGCACC -3'
mga^ga37 5'-GAAGAGGGCGTGACTGCC - - - - CACTGGCACC -3'
mga^ga71 5'-GAAGAGGGCGTGACTG - - CTGTCACTGGCACC -3'
mga^ga94 5'-GAAGAGGGCGTGACTGCCCGG - CACTGGCACC -3'
mga^ga98 5'-GAAGAGGGCGTGACTGCCCC - - CACTGGCACC -3'
mga^ga112 5'-GAAGAGGGCGTGACTGCCCTCTTCACTGGCACC -3'
B
mga^wt
mga^ga94
mga^ga37
mga^ga98
mga^ga71
mga^ga112

CHAPTER 4

ATAT1 IS THE MAJOR α-TUBULIN ACETYLTRANSFERASE IN ZEBRAFISH

INTRODUCTION

Microtubules are a type of highly conserved cytosketeton found in all eukaryotic cells. They are involved in various biological processes such as the formation of mitotic spindles, intracellular transport, axonal outgrowth, and motility of cilia and flagella [1, 2]. Microtubules are polymers that consist of α- and β-tubulin heterodimers, and their diverse biological distributions and functions are achieved by a variety of regulations, including the interaction with microtubule-associated proteins, differential expression of tubulin isoforms, and tubulin post-translational modifications (PTMs). Among these regulations, tubulin PTMs are one of the least understood, and has been shown to play important roles in many microtubule-based structures [3-5].

Both α- and β-tubulin are selectively modified by many different PTMs to increase their functional diversity. Common tubulin PTMs include acetylation, glycylation, glutamylation, palmitoylation, detyrosination/tyrosination, and Δ2 modification [3, 4, 6]. The combinations of different PTMs are thought to form a 'tubulin code' that can be recognized by microtubule-interacting proteins [7, 8]. Most of tubulin PTMs are reversible except Δ2 modification, and some of them may or may not occur at the same

time or at the same location. For example, tubulin glycylation is abundant in microtubules of cilia, flagella and basal bodies, whereas tubulin acetylation is enriched in structures that contain stable microtubules such as cilia, flagella, and neuronal processes [4, 9, 10]. Tubulin PTMs might distribute differently in terms of their subcellular localizations even in a single cell. Tyrosinated microtubules are abundant in dendrites of neurons, but acetylated, glutamylated, and detyrosinated microtubules are more concentrated in axons of neurons [3]. In addition, different tubulin PTMs might either compete or collaborate with each other to regulate the function of microtubules. It has been reported that microtubules lacking both glycylation and glutamylation significantly impairs the motility of cilia in zebrafish [11]. Therefore, regulating proteins responsible for adding or removing tubulin PTMs is the key to control the spatiotemporal diversity and functions of microtubules. [4].

Most of tubulin PTMs occur at the C-terminal tail (CTT) domains of α- and β-tubulin, and are located on the outer surface of microtubules [4]. However, unlike other tubulin PTMs, acetylation is the only known PTM that is found on the luminal surface of microtubules [4, 9, 12]. Acetylation is a PTM that an acetyl group is added onto Lysine 40 (K40) residue of α-tubulin, which is distant away from CTT domain [13]. A ciliate *Tetrahymena thermophila* α-tubulin K40R mutant has no detectable acetylated lysine in cytoskeletons, suggesting that α-tubulin K40 is the major, if not the only, site for acetylation on microtubules. *in vitro* studies have also shown that acetylation of α-tubulin K40 might be involved in regulating intrcellular transport by promoting the binding of motor protein Kinesin-1[14, 15]. A recent study also suggests that α-tubulin acetylation is

elevated in metastatic and basal-like breast cancer cells and possibly involved in invasive cell migration [16].

α-tubulin acetyltransferase 1 (ATAT1) and its ortholog Mec-17 have been characterized as the major enzyme responsible for adding the acetyl group onto α-tubulin K40 residue in ciliates, worms, and mice [9, 17, 18]. Tubulin acetyltransferase scans the luminal surface of microtubules bidirectionally and acetylates stochastically without preference for ends [19]. Animals lacking functional ATAT1/Mec-17 result in nearly complete depletion of α-tubulin K40 acetylation. In cultured cells, ATAT1 catalyzes α-tubulin at clathrin-coated pits, promoting directional locomotion and chemotaxis [20]. Additionally, ATAT1 can also destabilize microtubules independently of its acetylation activity, suggesting its importance in regulating the structure and function of microtubules [21]. In *Caenorhabditis elegans*, acetylated α-tubulin is abundant in touch receptor neurons. Mec-17 has been shown to be essential for touch sensitivity and the integrity of axons in worms [9, 22]. In ciliate *Tetrahymena thermophila*, genetic ablation of *mec-17* leads to the slower growth rate after being treated with microtubule-depolymerizing drugs and the increased rate of axoneme depolymerization. Suppression of ATAT1expression by injecting antisense morpholino oligonucleotides (MOs) results in ciliary and neurological defects in zebrafish, including curved body axis, hydrocephalus, and neuromascular deficiencies [9]. However, *atat1* knockout mice that lose α-tubulin acetylation completely are viable and exhibit only subtle phenotypic changes, such as changes in dentate gyrus and sperms [18, 20]. Taken together, these

results suggest that more complicated mechanisms are possibly involved in regulating ATAT1, tubulin PTMs, and even other microtubule-associated proteins.

In this study, we show that ATAT1 is the major α-tubulin acetyltransferase responsible for tubulin acetylation in zebrafish. Zebrafish lacking functional ATAT1 are viable and fertile with no overt defects. Interestingly, ATAT1 and tubulin monoglycylase TTLL3 might interact genetically to fine tune tubulin PTMs on microtubules. Therefore, this result indicates a possible regulatory mechanism that maintains the structure and function of microtubules.

MATHERIALS AND METHODS

Zebrafish husbandry and embryo collection

All fish lines were maintained according to The University of Georgia IACUC guidelines as previously described. Embryos were obtained from either single or multiple pair matings and cultured in egg water (60μg/ml Instant Ocean Sea Salt Mix, 0.3μg/ml Methylene Blue) at 28.5°C. Embryos were staged periodically to confirm their developmental progression before being collected for all experiments as previously described (Kimmel et al., 1995).

Genotyping

For allele *atat1*^{ga4}, genotyping PCR was carried out as previously described using the primer pair TALENTESTF3 and TALENTESTR3 with genomic DNA from either larvae

or adult fin-clips as the template. PCR products were then digested with *Bsm*I (R0134, New England BioLabs, Ipswich, MA) at 65°C for 8 hours. For allele *atat1*^{ga21}, genotyping PCR was carried out using forward primer MecC17-StuI-F (5'-CAGATCTGCAATGGATTTCCCTTAGGCC-3') and reverse primer TALENTESTR3 (5'-GTGCATGTAGCGAACCAGAT-3') under the same PCR condition for *atat1*^{ga4} allele. PCR products were then digested with *Stu*I (R0187, New England BioLabs, Ipswich, MA) at 37°C for 8 hours. Restriction enzyme digestion products were resolved on 2% agarose gels for identifying each individual's genotype.

RT-PCR

Total RNA from embryos and larvae were extracted using TRIzol Reagent (15596018, Life Technologies, Carlsbad, CA) following manufacturer's instruction. After extraction, total RNA was treated with DNase to eliminate genomic DNA contamination using TURBO DNA-*free* Kit (AM1907, Life Technologies, Carlsbad, CA). 200ng DNase-treated total RNA was used as the template for reverse transcription to synthesize cDNAs. This reaction was carried out using iScript cDNA Synthesis Kit (170-8890, Bio-Rad Laboratories, Hercules, CA) following manufacturer's instruction. For PCR, forward primer MEC17EX1F (5'-GGTCGGAAAGCGCATGGGAG-3') and reverse primer MEC17EX5R2 (5' -GAAGTCGAAGAGCTCTGAGCC-3') were used to amplify *atat1* cDNA under the condition as shown here (initial denaturing: 94°C for 2 minutes, denaturing: 94°C for 30 seconds, annealing: 65°C for 30 seconds, extension: 72°C for 30 seconds, 35 cycles, final extension: 72°C for 5 minutes). For the control, *gapdh* cDNA was amplified using forward primer zGAPDH-Long F1 (5'-

CGTCTGGTGACCCGTGCTGC-3') and reverse primer zGAPDH-Long R1 (5'-TGGGGGTGGGGACACGGAAG-3') under the condition as shown here (initial denaturing: 94°C for 2 minutes, denaturing: 94°C for 30 seconds, annealing: 63°C for 30 seconds, extension: 72°C for 45 seconds, 35 cycles, final extension: 72°C for 5 minutes). PCR products were resolved on 1.5% agarose gels.

Immunofluorescence

Zebrafish embryos and larvae were fixed with 4% paraformaldehyde in 1X PBS at 4°C overnight. Fixed samples were subsequently blocked in blocking solution (2% BSA, 1% DMSO, 0.5% Triton X-100, 0.5% normal goat serum in 1X PBS) at room temperature for 1 hour after being rinsed extensively with 1X PBT (0.5% Triton X-100 in 1X PBS). Samples were incubated with 6-11 B-1 mouse monoclonal anti-acetylated α-tubulin K40 antibody (1:1,000) or TAP952 mouse monoclonal anti-monoglycylated tubulin antibody (1:1,000) at 4°C overnight. Samples were rinsed extensively with 1X PBT and incubated with secondary antibody goat anti-mouse IgG-TRITC (T5393, Sigma-Aldrich, St. Louis, MO) at 4°C overnight. After incubation with secondary antibody, samples were rinsed several times in 1X PBT and 1X PBST (0.1% Tween-20 in 1X PBS) to remove unbound antibodies. For immunofluorescence imaging, Zeiss AXIO Imager D2 compound fluorescence microscope, Colibri.2 LED light source, and AxioCam HR CCD camera were used (Carl Zeiss, Jena, Germany).

Western blot

Western blot was performed as previously described [23]. Zebrafish embryos and larvae were collected according to their developmental stages for the protein extraction. 10μg total protein was loaded into each well on 4-20% polyacrylamide gels for SDS-PAGE. Proteins on each gel were transferred to a Hybond-P PVDF membrane (RPN303f, GE Healthcare, Piscataway, NJ) for further blotting. The blots were incubated at 4°C overnight with following primary antibodies: 6-11 B-1 mouse monoclonal anti-acetylated α-tubulin K40 antibody (1:500), TAP952 mouse monoclonal anti-monoglycylated tubulin antibody (1:1,000), R2302 rabbit polyclonal anti-polyglycylation antibody (1:1,000), GT335 mouse monoclonal anti-glutamylation antibody (1: 1,000) and R2304 rabbit polyclonal anti-polyglutamylation antibody (1:1,000). Blots were then rinsed extensively with 1X TBST and incubated with secondary antibodies HRP-conjugated goat anti-rabbit IgG (1:3,000, SC-2004, Santa Cruz Biotechnology, Dallas, TX) or HRP-conjugated goat anti-mouse IgG (1:3,000, A5278, Sigma-Aldrich, St. Louis, MO) for further detection. Protein bands were developed and detected with the Western Blot ECL Substrate (170-5060, Bio-Rad Laboratories, Hercules, CA) and X-OMAT LS films (864-6770, Carestream, Rochester, NY). Alternatively, separate polyacrylamide gels loaded with the same amount of proteins for blots were stained with Imperial Protein Stain (24615, Thermo Scientific, Rockford, IL) as loading controls.

***in vitro* transcription and mRNA rescue**

Both zebrafish and mouse *atat1* cDNA sequences were used in mRNA rescue experiments. Zebrafish full-length *atat1* cDNA (NM_213258.1) and two different

versions of mouse *atat1-eyfp* fusion cDNA, *atat1-eyfp* and *atat1*-GGL-*eyfp* [21], were subcloned into the *Eco*RI site on the pCS2+ vector for *in vitro* mRNA synthesis. pCS2+-*βgal* encoded the full-length *β-galactosidase* was used as the control. Plasmids were sequenced to confirm the accuracy of cloning. All plasmids were linearized with *Not*I for being used as templates for *in vitro* transcription. Capped mRNAs were synthesized using Ambion mMessage mMachine SP6 Transcription Kit (AM1340, Life Technologies, Carlsbad, CA). Final concentration of mRNA was determined by Nanodrop spectrophotometer. For mRNA rescue, 100pg mRNA was injected into each embryo at 1- to 2-cell stage with 0.1M KCl and phenol red. Damaged or unfertilized embryos were discarded around 4 to 5hpf. Survived embryos were collected and fixed at 72hpf for immunofluorescence detecting the signal of acetylated α-tubulin K40.

Behavioral assays

Behavior analysis was done as previously described [24-27]. Zebrafish larvae were raised to 5 dpf at 29ºC on a 14-h:10-h light:dark cycle in E3 media. For all experiments larvae were placed in individual wells of a 4x4 grid and after testing were transferred to 96-well plates for genotyping. Acoustic stimuli were 3 ms duration sinusoids with 1000 Hz frequency and variable intensity. Stimulus intensities were calibrated using a PCB Piezotronics accelerometer (model #355B04) and signal conditioner (#482A21). Dark-flash induced O-bends were induced and measured as described previously [27]. For behavior imaging, a 96-bulb infrared LED array (IR100 Illuminator removed from its housing; YYTrade)

was positioned below a 3 mm-thick sheet of white acrylic to diffuse the IR light. A white LED bulb (PAR38 LED light; LEDlight.com) was positioned above the testing area to provide white light illumination during acoustic startle and spontaneous movement testing. High-speed video was recorded using a Motionpro camera (Redlake) with a 50 mm macro lens at 1000 frames/sec at 512 × 512 pixel resolution. Spontaneous movement was analyzed after first habituating larvae to the testing arena for 15 min. Unstimulated movements during a 160 sec period were then captured at 100 frames/sec. All behavioral analysis was carried out with the FLOTE software package [24-27]. Statistical analysis was done using t-tests with GraphPad Prism 5.0. All data is presented as mean ± SEM.

Pactitaxel treatment

Embryos were treated with either 100μM Paclitaxel (T7191, Sigma-Aldrich, St. Luois, MO) or DMSO in egg water starting from sphere stage (4hpf) in glass Petri dishes. Paclitaxel was dissolved in DMSO to make a 10mM stock. Embryos were maintained in egg water with either Paclitaxel or DMSO through the entire course of experiment and imaged at different stages.

Microinjection of morpholino oligonucleotides (MO)

1- to 2-cell stage embryos were used for microinjection as previously described. Translational blocker MOs were used to suppress the expression of TTLL3 and ATAT1. Meanwhile, a mismatch MO (MisMO) corresponding to either *ttll3* MO or *atat1*MO with 5 different nucleotides were also used as the control. *p53* MO was also used in

combination with other MOs to suppress the non-specific cell death possibly caused by MOs in all microinjections [28]. Additionally, an MO *alk8morph2* against mRNA of BMP receptor ACVR1L was used as a positive control to test the specificity of MO injection. The following MOs were used in microinjections: *TTLL3TLMO*: 5'-GTGTTGGTGCATGTTTGAGTTAACC-3'; *TTLL3TLMisMO*: 5'-GTcTTGcTGCATcTTTcAGTTAAaC-3'; *MEC17TLMO*: 5'CATTCAGGTCGTAAGGGAAATCCAT-3'; *MEC17TLMisMO*: 5'-CATTgAcGTCcTAAGGcAAATgCAT-3'; *p53MO*: 5'-GCGCCATTGCTTTGCAAGAATTG-3'; *alk8lmorph2*: 5'-GATTCATGTTTGTGTTCAATTTCC-3' (Gene Tools, Philomath, OR) [4, 9, 11, 29]. All MOs were dissolved in distilled water individually as 10μg/μl stocks and stored at room temperature. Prior to microinjections, MOs were diluted in 0.1M KCl to the desired concentration with 0.1% phenol red as the tracing dye for microinjections. 1nl of MO injection solution was injected into the yolk of each embryo. For TTLL3 knockdown, each embryo received 1ng *ttll3MO* with 1.5ng *p53MO* or 1ng *ttll3MisMO* with 1.5ng *p53MO* in each microinjection. For ATAT1 knockdown, each embryo received 1ng *atat1MO* with or without 1.5ng *p53MO* or 1ng *atat1MisMO* with or without1.5ng *p53MO* in each microinjection. For ACVR1L knockdown, each embryo received 2ng alk8morph2 in each injection. For rescuing *ttll3* morphants, additional 100pg *β-gal* or zebrafish *atat1* mRNA was included in each injection. Injected embryos were kept in 100mm Petri dishes with egg water at 28.5°C. Damaged or unfertilized embryos were discarded around 4 to 5hpf. Survived embryos were collected at different stages for further analyses.

RESULTS

Acetylated α-tubulin is a common tubulin PTM in developing zebrafish embryos

Acetylated α-tubulin has been widely utilized as a marker for labeling cilia and the nervous system [9, 17, 18]. In zebrafish, acetylated α-tubulin is found in most ciliated structures and the nervous system. Starting from 24hpf, acetylated α-tubulin was seen in the pronephros, neural tube, and some nerve fibers (Figure 4.1A). By 48hpf, acetylated α-tubulin was abundant in many tissues, including olfactory placode, pronephros, spinal cord, and nerves (Figure 4.1B-D). Acetylated α-tubulin remained abundant in olfactory placode and nerves by 72hpf and was also detected in neuromasts, which are sensory organs in the lateral line system (Figure 4.1E-G). Together, α-tubulin acetylation is a common tubulin PTM found in many types of tissues in developing zebrafish embryos and larvae, especially in tissues that are rich in microtubules and cilia. The distribution of acetylated α-tubulin also implies that enzymes responsible for this tubulin PTM could potentially affect the development of these tissues when their expression is altered.

Acetylated α-tubulin is not detected in *atat1*$^{-/-}$ embryos

It has been shown that knockdown of ATAT1 by MOs in zebrafish leads to many developmental defects [9]. To determine whether ATAT1 is the major α-tubulin acetyltransferase in zebrafish, we generated zebrafish *atat1* null mutants using transcription activator-like effector nucleases (TALENs) for gene targeting [30]. Zebrafish has a single *atat1* gene (Gene ID: 406389), which is located within the

chromosome 19. We aimed to generate null mutants by targeting a site right downstream of the translation start site (ATG) in exon 1. Through the mutation screening, two potential null *atat1* mutant alleles were identified namely *atat1*^{ga4} and *atat1*^{ga21}. Both mutant alleles had a single base pair deletion and resulted in frame-shift mutations that potentially generated many downstream pre-mature stop codons. We first obtained heterozygotes by incrossing either *atat1*$^{ga4/+}$ or *atat1*$^{ga21/+}$ independently to examine the phenotype of homozygous mutants. Surprisingly, no significant developmental defect was observed during embryonic and larval development. However, we found a significant portion of embryos from the incrosses were void of acetylated α-tubulin that were examined by 6-11B-1 anti-acetylated α-tubulin antibody staining at 72hpf (incross of *atat1*$^{ga4/+}$: 21.37%, N=117; incross of *atat1*$^{ga21/+}$: 20.65%, N=92), whereas their siblings showed normal acetylated α-tubulin signal in tissues such as the olfactory placode and peripheral nerves (Figure 4.2A-D, 4.2A'-B'). We further divided these embryos into two groups: one was 6-11B-1 positive and the other was 6-11B-1 negative. Embryos from each group were randomly selected and genotyped to confirm their genotypes. All 6-11B-1 negative embryos we genotyped were *atat1*$^{-/-}$, but 6-11B-1 positive embryos were either *atat1*$^{+/+}$ or $^{+/-}$ (Figure 4.2E). This result suggests that α-tubulin acetylation is down-regulated in *atat1*$^{-/-}$ embryos. Although most of the embryos from *atat1*$^{+/-}$ incrosses were normal during the embryonic development, we did observe very few embryos exhibited cyclopia (incross of *atat1*$^{ga4/+}$: 3.27%, N=153) (Supplementary Figure S4.1A-F). Astonishingly, all of the cyclopic embryos we found were *atat1-/-*, whereas other normal embryos were atat1$^{+/+}$, $^{+/-}$, or even $^{-/-}$ (Supplementary Figure S4.1G). It suggests that cyclopia might be associated with the loss of ATAT1 with

extremely low penetrance. Since *atat1*$^{-/-}$ did not develop any significant defect during embryonic and larval development, we tried to raise them to adulthood. *atat1*$^{-/-}$ survived to adulthood and developed in almost the same rate as their *atat1*$^{+/+}$ or $^{+/-}$ siblings. Previously, it has been reported that *atat1* knockout mice exhibit defects in sperm morphology and motility [17]. However, *atat1*$^{-/-}$ zebrafish reproduced normally with no overt effect on their fertility. We further examined the level of acetylated α-tubulin in *atat1*$^{-/-}$ and found no detectable signal from 72hpf embryonic lysate (Figure 4.2F). Due to the lack of anti-ATAT1 antibody for zebrafish, we were unable to examine the protein expression of ATAT1. Instead, we examined the mRNA expression of *atat1* by RT-PCR in both *atat1*$^{+/+}$ and $^{-/-}$ embryos. In zebrafish embryos, *atat1* mRNA was expressed both maternally and zygotically (Figure S4.2A-B). The expression of *atat1* was almost identical in both *atat1*$^{+/+}$ and $^{-/-}$, indicating that non-sense mediated mRNA decay did not occur.

atat1$^{-/-}$ zebrafish restore tubulin acetylation when overexpressing _atat1_ mRNA

To examine whether the loss of tubulin acetylation in *atat1*$^{-/-}$ was due to the loss of ATAT1, we injected *atat1* mRNA into 1 cell stage *atat1*$^{-/-}$ embryos. When *atat1*$^{-/-}$ embryos received 100ng *atat1* mRNA per embryo at 1 cell stage, they developed normally without any defect. However, *atat1* mRNA-injected *atat1*$^{-/-}$ embryos exhibit normal tubulin acetylation comparing to *atat1*$^{+/+}$ at 72hpf, whereas *βgal* mRNA-injected embryos still showed no sign of α-tubulin acetylation (Figure 4.3A-C, 4.3A'-C', 4.3F-H, and 4.3K-M). We further tested the hypothesis that the restoration of tubulin acetylation in *atat1*$^{-/-}$ was due to the acetyltransferase activity of ATAT1 by injecting mouse

wildtype *atat1-eyfp* fusion mRNA and mouse *atat1-GGL-eyfp* mRNA [21], an enzyme-dead version of *atat1*, into *atat1*$^{-/-}$ embryos at 1 cell stage. Indeed, *atat1*$^{-/-}$ larvae restored their tubulin acetylation after receiving mouse wildtype *atat1-eyfp* mRNA, but they still exhibited the loss of tubulin acetylation when receiving *atat1-GGL-eyfp* mRNA (Figure 4.3D-E, 4.3D'-E', 4.3I-J, 4.3N-O). Interestingly, we found that enzyme-dead version of *atat1*possibly degraded faster than the wildtype version, suggesting a possibility that acetyltransferase activity might be required for the stability of ATAT1 (Figure S4.3A-X). To sum up, our result suggests that ATAT1 is the major acetyltransferase responsible for tubulin acetylation in zebrafish.

atat1$^{-/-}$ larvae show normal behavioral responses

Previous study shows that the dentate gyrus region of hippocampus in *atat1* knockout mice is slightly deformed [18]. Thus, it is very likely that *atat1*$^{-/-}$ zebrafish also exhibit some mild defects in the nervous system. Although another group has shown that adult *atat1* knockout mice display normal behavior [17], it is still possible that *atat1*$^{-/-}$ zebrafish develop neurological or behavioral defects during larval development. Here we examined behavioral responses of *atat1*$^{-/-}$ larvae after receiving stimulations at 5dpf. The same stage *atat1*$^{+/-}$ larvae were also used as the control in all experiments. *atat1*$^{+/-}$ and $^{-/-}$ larvae displayed very similar responses to acoustic stimuli (Figure 4.4A-B). Although *atat1*$^{-/-}$ were slightly less responsive to pre-pulse inhibition and more sensitive to weaker acoustic stimuli (Figure 4.4C), the differences between *atat1*$^{+/-}$ and $^{-/-}$ larvae were not statistically significant ($p>0.05$, Student's t-test). We also tested the behavioral response after stimulating fish with visual stimuli. However, both *atat1*$^{+/-}$ and $^{-/-}$ larvae responded

almost identically (Figure 4.5). We further examined their spontaneous movement without any stimulation. Again, both *atat1*$^{+/-}$ and $^{-/-}$ larvae displayed almost identical behavior in terms of their spontaneous moving distance and movement frequency (Figure 4.6A-B). Overall, *atat1*$^{-/-}$ larvae did not exhibit significant behavioral changes.

atat1$^{-/-}$ embryos are more sensitive to microtubule-stabilizing agent

Tubulin acetylation is generally enriched on stable microtubules in cells [7]. In addition, ATAT1 has been suggested to participate in maintaining the stability of microtubules [19, 21]. Therefore, we hypothesized that *atat1*$^{-/-}$ embryos might behave differently in terms of the microtubule stability and dynamics under abnormal conditions. Here we examined the epiboly movement, a developmental process during the gastrulation that is highly associated with yolk microtubules, in both *atat1*$^{+/+}$ and $^{-/-}$ embryos [31]. The epiboly begins at sphere stage (4hpf) in zebrafish embryos when the yolk cell domes into the blastoderm. During the epiboly, the blastoderm becomes thinner and extends from animal pole all the way to vegetal pole until embryonic cells cover the entire yolk. The epiboly movement can be delayed when microtubule stability is altered, suggesting that the epiboly is a good developmental process for observing the effect of microtubule stability *in vivo* [31]. Both *atat1*$^{+/+}$ and $^{-/-}$ embryos developed normally without any sign of epiboly delay when they were treated with DMSO starting from sphere stage (Figure 4.7A-B, 4.7E-F). However, *atat1*$^{+/+}$ embryos exhibited slower epiboly progression at 2-somite stage after being treated with 100μM Paclitaxel, an agent known to stabilize microtubules (Figure 4.7C). The epiboly delay in Paclitaxel-treated *atat1*$^{+/+}$ embryos was recovered later as we did not observe any overt defect at 24hpf (Figure 4.7G).

Interestingly, Paclitaxel-treated *atat1*$^{-/-}$ embryos exhibited significantly slower epiboly progression at 2-somite stage, and the effect of epiboly delay ("openback" phenotype) can still be seen even at 24hpf (Figure 4.7D-H) [32]. Although epiboly progression was delayed in both *atat1*$^{+/+}$ and $^{-/-}$ embryos when being treated with Paclitaxel, the gastrulation was not affected by the treatment. Hence, yolk microtubules in *atat1*$^{-/-}$ embryos might be more stable than those in *atat1*$^{+/+}$ embryos after microtubule-stabilizing agent treatment.

ATAT1 genetically interacts with the tubulin monoglycylase TTLL3

ATAT1 is the major acetyltransferase that mediates tubulin acetylation, which is the only known tubulin PTM that occurs on the luminal side of microtubules. Therefore, it is essential to know whether other PTMs are affected when tubulin acetylation is depleted. We examined the levels of different tubulin PTMs in adult testes, the microtubule-rich organs, by Western blot. In *atat1*$^{+/+}$ testes, several tubulin PTMs were detected, including monoglycylation, polyglycylation, glutamylation, polyglutamylation, and acetylation. All these PTMs except acetylation were also detected in *atat1*$^{-/-}$ testes (Figure 4.8). Surprisingly, the level of monoglycylation was greatly increased, whereas the level of polyglycylation was greatly decreased in *atat1*$^{-/-}$ testes. The level of glutamylation was slightly reduced while the level of polyglutamylation remained almost the same in *atat1*$^{-/-}$ testes. Despite these changes of tubulin PTMs in *atat1*$^{-/-}$ testes, we did not discover any significant fertility change in *atat1*$^{-/-}$ adult males. This result suggests that tubulin glycylation might be associated with tubulin acetylation in order to maintain the integrity of microtubules. Therefore, it is crucial to understand whether the elevation of tubulin

monoglycylation is to compensate the loss of tubulin acetylation. Here we injected antisense morpholino oligonucleotides (MO) against *ttll3*, a gene encodes a glycylase responsible for tubulin monoglycylation, into 1-cell stage *atat1*$^{+/+}$ and $^{-/-}$ embryos. It is reported that suppressing TTLL3 expression by injecting MO into zebrafish embryos results in the depletion of tubulin monoglycylation. However, tubulin monoglycylation is dispensable that most TTLL3-knockdown zebrafish develop normally [11]. When TTLL3 was suppressed in *atat1*$^{+/+}$ embryos, only very few individuals showed cilia-related defects such as curved body axis at 48hpf (5.105±0.455%, N=115). However, the frequency of cilia-related defects in *ttll3*MO-injected *atat1-/-* embryos (68.835±6.165%, N=135) was increased significantly ($p<0.05$, Student's t-test), whereas controls that received mismatch *ttll3*MO (*ttll3*MisMO) had no overt effect (Figure 4.9A-E). We also discovered that tubulin monoglycylation was increased in pronephric cilia of *ttll3*MisMO-injected *atat1*$^{-/-}$ embryos at 48hpf comparing with those in *atat1*$^{+/+}$ embryos (Figure 4.9F-G). Tubulin monoglycylation was not detected in pronephric cilia in either *atat1*$^{+/+}$ or $^{-/-}$ embryos that were injected with *ttll3*MO (Figure 4.9H-I). To test whether ATAT1 is sufficient to rescue the curved body axis phenotype, we co-injected either *βgal* or zebrafish atat1mRNA with *ttll3*MO into *atat1*$^{-/-}$ embryos. Indeed, *βgal* -injected embryos (74.76±1.43%, N=93) showed higher frequency of curved body axis phenotype comparing with *atat1*- injected embryos (57.66±5.16%, N=118). Together, TTLL3-mediated tubulin monoglycylation might play an important role in compensating the loss of tubulin acetylation, suggesting a possible mechanism that ATAT1 genetically interacts with TTLL3 in zebrafish embryos.

atat1$^{-/-}$ embryos are not more sensitive to MO injection

In a previous study, zebrafish embryos injected with *atat1*MO exhibit several developmental defects such as smaller head and neuromuscular defect [9]. However, similar defects were not observed in our *atat1*$^{-/-}$ zebrafish. To test the specificity of *atat1*MO, we injected both *atat1*$^{+/+}$ and $^{-/-}$ embryos with 1ng *atat1*MO with or without 1.5ng *p53*MO. The same experiment with *atat1*MisMO was used as the control. Embryos injected with different combinations of MOs showed a range phenotype from normal to severe. Normal embryos were morphologically identical to *atat1*$^{+/+}$ embryos. Moderate embryos showed reduced yolk stalk extension, mild brain defect, and slightly disorganized trunk. Severe embryos exhibited reduced yolk stalk extension, hydrocephalus, and shorter or curved body axis (Figure S4.4A-C). Embryos injected with *atat1*MO alone [(*atat1*$^{+/+}$: moderate: 83.245±3.245%; severe: 16.755±3.245%, N=67) (*atat1*$^{-/-}$: moderate: 29.575±9.613%; severe: 70.425±9.613%, N=81)] exhibited stronger phenotypes than embryos injected with *atat1*MO+ *p53*MO [(*atat1*$^{+/+}$: normal: 54.59±0.97%; moderate: 45.41±0.97%, N=96) (*atat1*$^{-/-}$: normal: 3.225±3.225%; moderate: 58.305±2.985%; severe: 38.47±6.21%, N=78)], suggesting that stronger phenotype might be partially caused by MO-induced p53-dependent cell death. Interestingly, *atat1*$^{+/+}$ embryos injected with different combinations of MOs showed weaker phenotypes, whereas *atat1*$^{-/-}$ embryos injected with the same MO combinations exhibited stronger phenotypes (Figure S4.4D). To explore whether *atat1*$^{-/-}$ embryos are more sensitive to MO injection, we injected *alk8*MO against BMP receptor *acvr1l* into both *atat1*$^{+/+}$ and $^{-/-}$ embryos. Blocking BMP signaling has been shown to affect the development of ventral structures in zebrafish [29, 33]. All *alk8*MO-injected *atat1*$^{+/+}$ and

$^{-/-}$ embryos exhibited dorsalized phenotypes, and these phenotypes can be categorized into a milder class lost-a-fin (C1) and slightly stronger class more dorsalized (C2) (Figure S4.5A-F) [33]. The difference between *alk8*MO-injected *atat1*$^{+/+}$ (C1: 92.325±3.755%; C2: 7.675±3.755%, N=86) and $^{-/-}$ (C1: 87.455±0.785%; C2: 12.545±0.785%, N=81) embryos was not significant ($p>0.05$, Student's t-test). No significant difference between two groups was found (Figure S4.5G), suggesting the *atat1*$^{-/-}$ zebrafish might not be more sensitive to MO injection.

DISCUSSION

In this study, we demonstrate that tubulin acetylation is completely undetectable in *atat1* $^{-/-}$ embryos and adult testes, suggesting that ATAT1 is responsible for this type of tubulin PTM. It has been shown that ATAT1 is the major α-tubulin acetyltransferase in mice [17, 18]. Furthermore, ATAT1 is known to acetylate itself other than its major target α-tubulin [21]. ATAT1also play roles in regulating microtubule stability independent of its acetyltransferase function [21]. Surprisingly, we discover that ATAT1 degrades faster when it loses its acetyltransferase activity *in vivo*. *in vitro* study has shown that human αTAT requires its acetyltransferase activity to maintain the protein stability [34]. Although there are other acetyltransferases that exist in zebrafish such as Nat10 and Nat15, they are unlikely to be significant contributors of tubulin acetylation. Our result shows that tubulin acetylation in zebrafish is mediated by ATAT1 via its acetyltransferase activity directly. Taken together, ATAT1 is the major α-tubulin acetyltranferase that mediates tubulin acetylation in zebrafish.

A previous study shows that depletion of ATAT1 using *atat1*MO results in various defects such as smaller head and neuromuscular defect [9]. However, zebrafish lacking functional ATAT1 are still viable and fertile without any significant developmental defect. Our result is in agreement with previous findings in *atat1* knockout mice [17, 18]. Therefore, the defects identified in *atat1*MO-injected zebrafish embryos and larvae might be non-specific, and some of them might be due to the p53-dependent cell death that is triggered by MO injection [28]. It has been reported that MO might also lead to many defects caused by the off-target effect [35]. It is known that the loss of α-tubulin acetyltransferase Mec-17 in *C. elegans* results in severe axonal degeneration [22]. Although *atat1* knockout mice exhibit the mild distortion of the dentate gyrus, no overt behavioral change has been documented [17, 18]. Our *atat1*$^{-/-}$ zebrafish also show no sign of behavioral change during the larval developemt, suggesting that the regulation between ATAT1 and microtubules in zebrafish is possibly more similar to the one in mice. Despite the fact that ATAT1 is the major α-tubulin acetyltransferase, it might not be physiologically important in terms of regulating neuronal functions in vertebrates.

Interestingly, *atat1*$^{-/-}$ embryos exhibit hypersensitivity to the microtubule-stabilizing agent Paclitaxel during the epiboly. Yolk microtubules are one of the key players of epiboly movement in zebrafish embryos [31]. When embryos are treated with 100μM Paclitaxel starting from sphere stage, *atat1*$^{-/-}$ embryos exhibit much slower epiboly progression, suggesting that their yolk microtubules might not be as dynamic as those in *atat1*$^{+/+}$ embryos. In culture cells, small siRNA-mediated depletion of mouse

ATAT1 increases microtubule stability and reduces microtubule dynamics [21]. There are also more stable microtubules in embryonic fibroblasts from *atat1* knockout mice when treating these cells with microtubule-destabilizing agent Nocodazole [17]. In contrast, it has been reported that depletion of α-tubulin acetyltransferase Mec-17in ciliates *Tetrahymena thermophila* results in the increase of microtubule dynamic after Paclitaxel treatment [9]. One possible explanation is that α-tubulin acetyltransferase might regulate microtubule dynamics differently in vertebrates as a consequence of evolution.

Although tubulin acetylation is the only known tubulin PTM that occurs on the luminal side of microtubules, neither the architecture of microtubules nor the tubulin conformation is altered by tubulin acetylation. Therefore, it has been proposed that the influence of tubulin acetylation might be highly localized and affects interaction with proteins that bind directly to the luminal side of microtubules [36]. *in vitro* study has shown that tubulin acetylation increases and CTT domains of α- and β-tubulin decrease axonemal dynein motility, indicating that axonemal dynein directly deciphers the tubulin code [37]. However, *atat1*$^{-/-}$ zebrafish lacking tubulin acetylation do not exhibit any significant defect under normal conditions, suggesting the possible existence of a compensatory mechanism that might act to alleviate the effect of tubulin acetylation depletion. To examine more regional effects of tubulin acetylation, we discover that Tubulin acetylation alters the level of some other tubulin PTMs that occur on the exterior surface of microtubules, including mono- and polyglycylation. Tubulin glycylation is found predominantly in cilia and requires the monoglycylase to add a single glycine onto

the CTT domains of tubulin and the polyglycylase to add multiple glycine residues onto the existing monoglycylated CTT domain of tubulin [8, 10]. Thus, the elevation of tubulin monoglycylation might be a way to reduce the effect of tubulin acetylation depletion in *atat1*$^{-/-}$ zebrafish. Interestingly, it is reported that ATAT1 binds to the exterior surface of microtubules and interacts with CTT domains of tubulin *in vitro*, suggesting a possible mechanism for coordinating tubulin acetylation and other tubulin PTMs [36]. Depletion of tubulin monoglycylation along is not sufficient to cause severe cilia-related defects in zebrafish. Nevertheless, the frequency of cilia-related defects is significantly increased when both tubulin monoglycylation and glutamylation are depleted [11], implying that different tubulin PTMs might work together and contribute to maintain the normal structure and function of microtubules. Indeed, zebrafish *atat1*$^{-/-}$ embryos exhibit severe cilia-related defects when the monoglycylase TTLL3 is suppressed by MO injection, whereas most *ttll3*MO-injected *atat1*$^{+/+}$ embryos develop normally with low frequency of cilia-related defects. Our result is in agreement with a recent study that ATAT1/Mec-17 interacts with Kinesin-13 genetically in ciliates to maintain the structure and function of cilia [38]. Taken together, our result indicates that ATAT1 also interacts with TTLL3 genetically to regulate the integrity of microtubules.

Here we demonstrate that ATAT1 is the major α-tubulin acetyltransferase responsible for tubulin acetylation in zebrafish by generating the first two *atat1* null mutants. *atat1*$^{-/-}$ lacking all detectable tubulin acetylation develop and reproduce normally. However, *atat1*$^{-/-}$ embryos exhibit hypersensitivity to the altered microtubule stability. We also provide the first ever *in vivo* evidence that tubulin acetylation, the only

known microtubule luminal PTM, affects other tubulin PTMs on the exterior surface of microtubules. Zebrafish embryos depleted both ATAT1 and TTLL3 exhibit severe cilia-related defects, suggesting that tubulin acetylation and glycylation might contribute synergistically to structural and functional regulations of microtubules in cilia. Our result also highlights the importance and complexity of tubulin PTM code in maintaining the microtubule dynamics and stability.

REFERENCES

1. Vale, R.D. (1987). Intracellular Transport Using Microtubule-Based Motors. Annual Review of Cell Biology *3*, 347-378.
2. Joanna B Olmsted, G.G.B. (1973). Microtubules. Annual Review of Biochemistry *42*, 507-540.
3. Carsten Janke, J.C.B. (2011). Post-translational regulation of the microtubule cytoskeleton: mechanisms and functions. Nature Reviews Molecular Cell Biology *12*, 773-786.
4. Dorota Wloga, J.G. (2010). Post-translational modifications of microtubules. Journal of Cell Science *123*, 3447-3455.
5. Ludueña, R.F. (1997). Multiple Forms of Tubulin: Different Gene Products and Covalent Modifications. International Review of Cytology *178*, 207-275.
6. Karel Soucek, A.K., Anh D. Phung, Luka Kubala, J. Chloe Bulinski, Richart W. Harper, Jason P. Eiserich (2006). Normal and prostate cancer cells display distinct

molecular profiles of alpha-tubulin posttranslational modifications. Prostate *66*, 954-965.

7. Janke, C. (2014). The tubulin code: Molecular components, readout mechanisms, and functions. Journal of Cell Biology *206*, 461-472.
8. Kristen J. Verhey, J.G. (2007). The Tubulin Code. Cell Cycle *6*, 2152-2160.
9. Jyothi S. Akella, D.W., Jihyun Kim, Natalia G. Starostina, Sally Lyons-Abbott, Naomi S. Morrissette, Scott T. Dougan, Edward T. Kipreos, Jacek Gaertig (2010). MEC-17 is an α-tubulin acetyltransferase. Nature *467*, 218-222.
10. Dorota Wloga, D.M.W., Krzysztof Rogowski, Marie-Hélène Bré, Nicolette Levilliers, Maria Jerka-Dziadosz, Carsten Janke, Scott T. Dougan, Jacek Gaertig (2009). TTLL3 Is a Tubulin Glycine Ligase that Regulates the Assembly of Cilia. Developmental Cell *16*, 867-876.
11. Narendra Pathak, C.A.A., Iain A. Drummond (2011). Tubulin Tyrosine Ligase-like Genes ttll3 and ttll6 Maintain Zebrafish Cilia Structure and Motility. The Journal of Biological Chemistry *286*, 11685-11695.
12. Eva Nogales, S.G.W., Kenneth H. Downing (1998). Structure of the alpha beta tubulin dimer by electron crystallography. Nature *391*, 199-203.
13. S. W. L'Hernault, J.L.R. (1985). Chlamydomonas alpha-tubulin is posttranslationally modified by acetylation on the epsilon-amino group of a lysine. Biochemistry *24*, 473-478.
14. Jim P. Dompierre, J.D.G., Bénédicte C. Charrin, Fabrice P. Cordelières, Stephen J. King, Sandrine Humbert, Frédéric Saudou (2007). Histone Deacetylase 6

Inhibition Compensates for the Transport Deficit in Huntington's Disease by Increasing Tubulin Acetylation. The Journal of Neuroscience *27*, 3571-3583.

15. Nathan A. Reed, D.C.T.L.B., Gloria T. Jih, Edgar Meyhofer, Jacek Gaertig, Kristen J. Verhey (2006). Microtubule Acetylation Promotes Kinesin-1 Binding and Transport. Current Biology *16*, 2166-2172.

16. Amanda E. Boggs, M.I.V., Rebecca A. Whipple, Monica S. Charpentier, Olga G. Goloubeva, Olga B. Ioffe, Kimberly C. Tuttle, Jana Slovic, Yiling Lu, Gordon B. Mills, Stuart S. Martin (2015). α-Tubulin Acetylation Elevated in Metastatic and Basal-like Breast Cancer Cells Promotes Microtentacle Formation, Adhesion, and Invasive Migration Cancer Research *75*, 203-215.

17. Nereo Kalebic, S.S., Emerald Perlas, Giulia Bolasco, Concepcion Martinez, Paul A. Heppenstall (2013). αTAT1 is the major α-tubulin acetyltransferase in mice. Nature Communications *4*, 1962.

18. Go-Woon Kim, L.L., Mohammad Gorbani, Linya You, Xiang-Jiao Yang (2013). Mice lacking α-tubulin acetyltransferase 1 are viable but display α-tubulin acetylation deficiency and dentate gyrus distortion. The Journal of Biological Chemistry *288*, 20334-20350.

19. Agnieszka Szyk, A.M.D., Jeffrey Spector, Benjamin Goodman, Max L. Valenstein, Natasza E. Ziolkowska, Vasilisa Kormendi, Nikolaus Grigorieff, Antonina Roll-Mecak (2014). Molecular Basis for Age-Dependent Microtubule Acetylation by Tubulin Acetyltransferase. Cell *157*, 1405-1415.

20. Guillaume Montagnac, V.M.-Y., Marie Irondelle, Antonio Castro-Castro, Michel Franco, Toshinobu Shida, Maxence V. Nachury, Alexandre Benmerah, Jean-

Christophe Olivo-Marin, Philippe Chavrier (2013). αTAT1 catalyses microtubule acetylation at clathrin-coated pits. Nature *502*, 567-570.

21. Nereo Kalebic, C.M., Emerald Perlasa, Philip Hublitza, Daniel Bilbao-Cortesa, Karol Fiedorczuka, Annapaola Andolfob, Paul A. Heppenstall (2013). Tubulin Acetyltransferase αTAT1 Destabilizes Microtubules Independently of Its Acetylation Activity. Molecular and Celluler Biology *33*, 1114-1123.
22. Brent Neumann, M.A.H. (2014). Loss of MEC-17 Leads to Microtubule Instability and Axonal Degeneration. Cell Report *6*, 93-103.
23. Yuhua Sun, D.W., Scott T. Dougan (2011). Embryological Manipulations in Zebrafish. Methods in Molecular Bilogy *770*, 139-184.
24. Marc A. Wolman, R.A.J., Laura Liss, Michael Granato (2011). Chemical modulation of memory formation in larval zebrafish. Proceedings of the National Academy of Sciences USA *108*, 15468-15473.
25. H. A. Burgess, S.L.J., M. Granato (2009). Unidirectional startle responses and disrupted left–right co-ordination of motor behaviors in robo3 mutant zebrafish. Genes, Brain and Behavior *8*, 500-511.
26. Harold A. Burgess, M.G. (2007). Sensorimotor gating in larval zebrafish. The Journal of Neuroscience *27*, 4984-4994.
27. Harold A. Burgess, M.G. (2007). Modulation of locomotor activity in larval zebrafish during light adaptation The Journal of Experimental Biology *210*, 2526-2539.

28. Mara E Robu, J.D.L., Soraya Beiraghi, Charles Brenner, Steven A Farber, Stephen C Ekker (2007). p53 Activation by Knockdown Technologies. PLoS Genetics *3*, e78.

29. Hermann Bauer, Z.L., Gerd-Jörg Rauch, Robert Geisler, Matthias Hammerschmidt (2001). The type I serine/threonine kinase receptor Alk8/Lost-a-fin is required for Bmp2b/7 signal transduction during dorsoventral patterning of the zebrafish embryo. Development *128*, 846-858.

30. Li-En Jao, S.R.W., Wenbiao Chen (2013). Efficient multiplex biallelic zebrafish genome editing using a CRISPR nuclease system. Proceedings of the National Academy of Sciences USA *110*, 13904-13909.

31. Lilianna Solnica-Krezel, W.D. (1994). Microtubule arrays of the zebrafish yolk cell: organization and function during epiboly. Development *120*, 2443-2455.

32. Federico Coluccio Leskow, B.A.H., HongBin Wang, Mary C. Mullins, Marcelo G. Kazanietz (2006). The zebrafish homologue of mammalian chimerin Rac-GAPs is implicated in epiboly progression during development. Proceedings of the National Academy of Sciences USA *103*, 5373-5378.

33. Yasuyuki Kishimoto, K.-H.L., Len Zon, Matthias Hammerschmidt, Stefan Schulte-Merker (1997). The molecular nature of zebrafish swirl: BMP2 function is essential during early dorsoventral patterning. Development *124*, 4457-4466.

34. Satoru Yuzawa, S.K., Junya Hayase and Hideki Sumimoto (2015). Structural basis of cofactor-mediated stabilization and substrate recognition of the α-tubulin acetyltransferase αTAT1. Biochemical Journal.

35. Fatma O. Kok, M.S., Chih-Wen Ni, Ankit Gupta, Ann S. Grosse, Andreas van Impel, Bettina C. Kirchmaier, Josi Peterson-Maduro, George Kourkoulis, Ira Male, Dana F. DeSantis, Sarah Sheppard-Tindell, Lwaki Ebarasi, Christer Betsholtz, Stefan Schulte-Merker, Scot A. Wolfe, Nathan D. Lawson (2015). Reverse Genetic Screening Reveals Poor Correlation between Morpholino-Induced and Mutant Phenotypes in Zebrafish. Developmental Cell *32*, 97-108.

36. Stuart C. Howesa, G.M.A., Toshinobu Shidac, Maxence V. Nachuryc, Eva Nogales (2014). Effects of tubulin acetylation and tubulin acetyltransferase binding on microtubule structure. Molecular Biology of the Cell *25*, 257-266.

37. Joshua D. Alper, F.D., Bernice Agana, Jonathon Howard (2014). The motility of axonemal dynein is regulated by the tubulin code. Biophysical Journal *107*, 2872-2880.

38. Krishna Kumar Vasudevan, Y.-Y.J., Karl F. Lechtreck, Yasuharu Kushida, Lea M. Alford, Winfield S. Sale, Todd Hennessey, Jacek Gaertig (2015). Kinesin-13 regulates the quantity and quality of tubulin inside cilia. Molecular Biology of the Cell *26*, 478-494.

FIGURES AND FIGURE LEGENDS

Figure 4.1. The distribution of acetylated α-tubulin in developing zebrafish.

Acetylated α-tubulin is detected by 6-11B1 antibody at 24hpf **(A)**, 48hpf **(B-D, B')**, AND 72hpf **(E-G, E')**. At 24hpf, acetylated α-tubulin is detected in neural tube and pronephros (A). At 48 hpf, acetylated α-tubulin is detected in olfactory placode (B and B'), spinal cord and peripheral nerves (C), and pronephros (D). At 72 hpf, acetylated α-tubulin is detected in olfactory placode (E and E'), neuromasts (F), and peripheral nerves (G). Scale bar=50μm. Blue arrowhead: neural tube; White arrowhead: pronephros; Yellow arrowhead: neuromast; Arrow: olfactory placode.

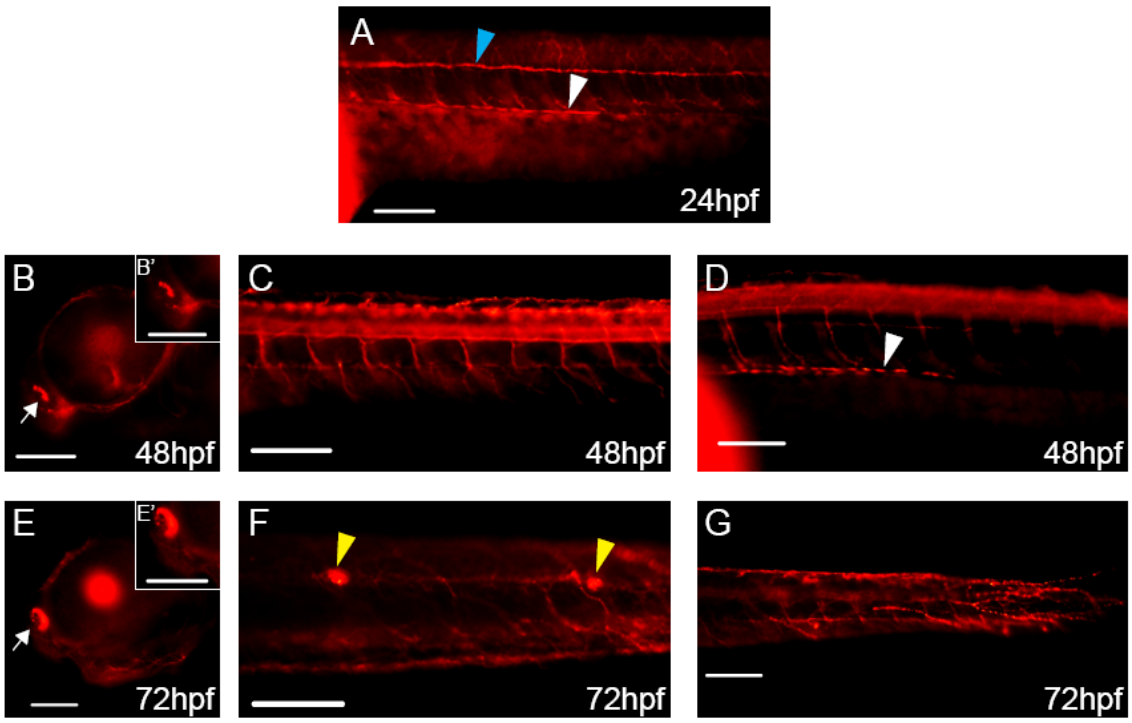
A
24hpf
B
B'
48hpf
C
48hpf
D
48hpf
E
E'
72hpf
F
72hpf
G
72hpf

Figure 4.2. Acetylated α-tubulin is not detected in *atat1*$^{-/-}$ embryos. 72hpf embryos taken from incrosses of *atat1*$^{+/-}$ adults are stained with 6-11B-1 anti- acetylated α-tubulin antibody **(A-D, A'-B')**. Most embryos show 6-11B-1 positive signals in olfactory placode (A and A') and peripheral nerves (C). Some other embryos are complete void of 6-11B-1 signal (B, B', and D). 6-11B-1 antibody-stained embryos are sorted and genotyped. All 6-11B-1 negative embryos are *atat1*$^{-/-}$ **(E)**. Western blot using lysate from 72hpf *atat1*$^{-/-}$ embryos shows no detectable acetylated α-tubulin by 6-11B-1 antibody **(F)**. White arrow: olfactory placode.

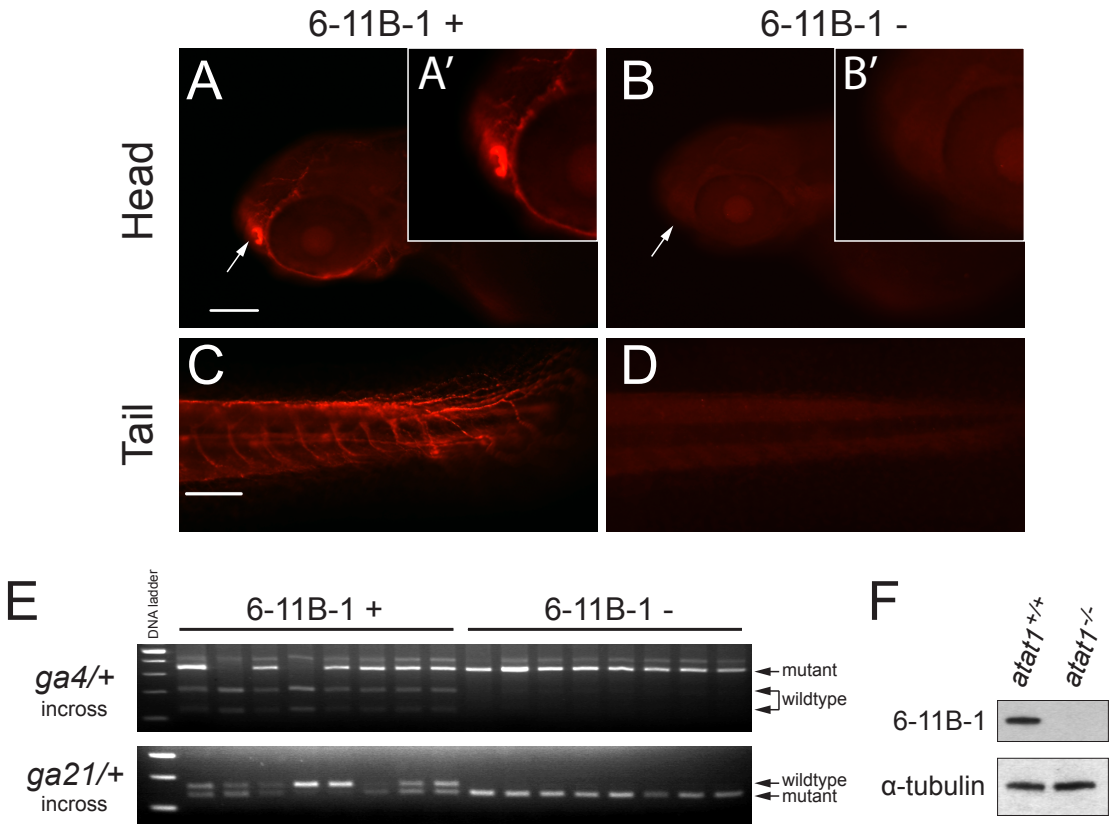
6-11B-1 +
6-11B-1 -
A
A′
B
B′
Head
C
D
Tail
E
DNA ladder
6-11B-1 +
6-11B-1 -
ga4/+
incross
mutant
wildtype
ga21/+
incross
wildtype
mutant
F
atat1+/+
atat1-/-
6-11B-1
α-tubulin

Figure 4.3. Lack of acetylated α-tubulin phenotype in *atat1*$^{-/-}$ embryos can be rescued by injecting *atat1* mRNA. The distribution of acetylated α-tubulin in72hpf embryos in head **(A-E)**, olfactory placode **(A'-E')**, tail **(F-J)**, and trunk **(K-O)** is shown. In *atat1*$^{-/-}$ embryos, acetylated α-tubulin is restored when embryos are injected with zebrafish *atat1* mRNA (*Zatat1*) and mouse *atat1-eyfp* mRNA (*Matat1-eyfp*). *atat1*$^{-/-}$ embryos injected with either *βgal* mRNA or mouse *atat1-GGL-eyfp* mRNA (*Matat1-GGL-eyfp*) do not restore acetylated α-tubulin. Scale bar=100μm.

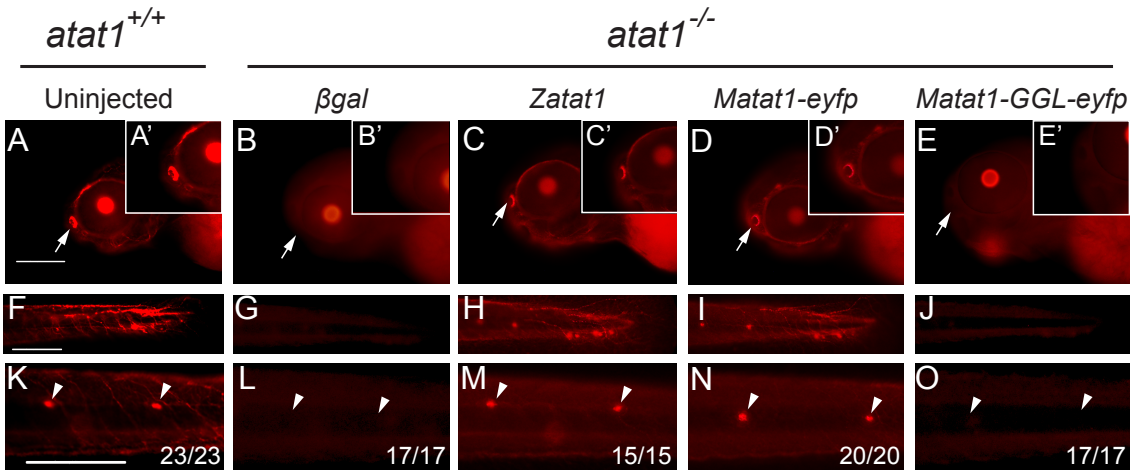
atat1+/+
atat1-/-
Uninjected
βgal
Zatat1
Matat1-eyfp
Matat1-GGL-eyfp
A
A'
B
B'
C
C'
D
D'
E
E'
F
G
H
I
J
K
L
M
N
O
23/23
17/17
15/15
20/20
17/17

Figure 4.4. Acoustic response of *atat1* mutants. Startle response bias of 120hpf larvae responding to acoustic stimuli (*atat1*$^{+/-}$: N=49; *atat1*$^{-/-}$: N=31) **(A)**. Short-term startle habituation of 120hpf larvae responding to acoustic stimuli (*atat1*$^{+/-}$: N=47; *atat1*$^{-/-}$: N=28) **(B)**. Hypersensitivity (*atat1*$^{+/-}$: N=47; *atat1*$^{-/-}$: N=28) and pre-pulse inhibition (*atat1*$^{+/-}$: N=14; *atat1*$^{-/-}$: N=18) responding to acoustic stimuli **(C)**. All data is presented as mean±SEM, all $p>0.05$, Student's t-test.

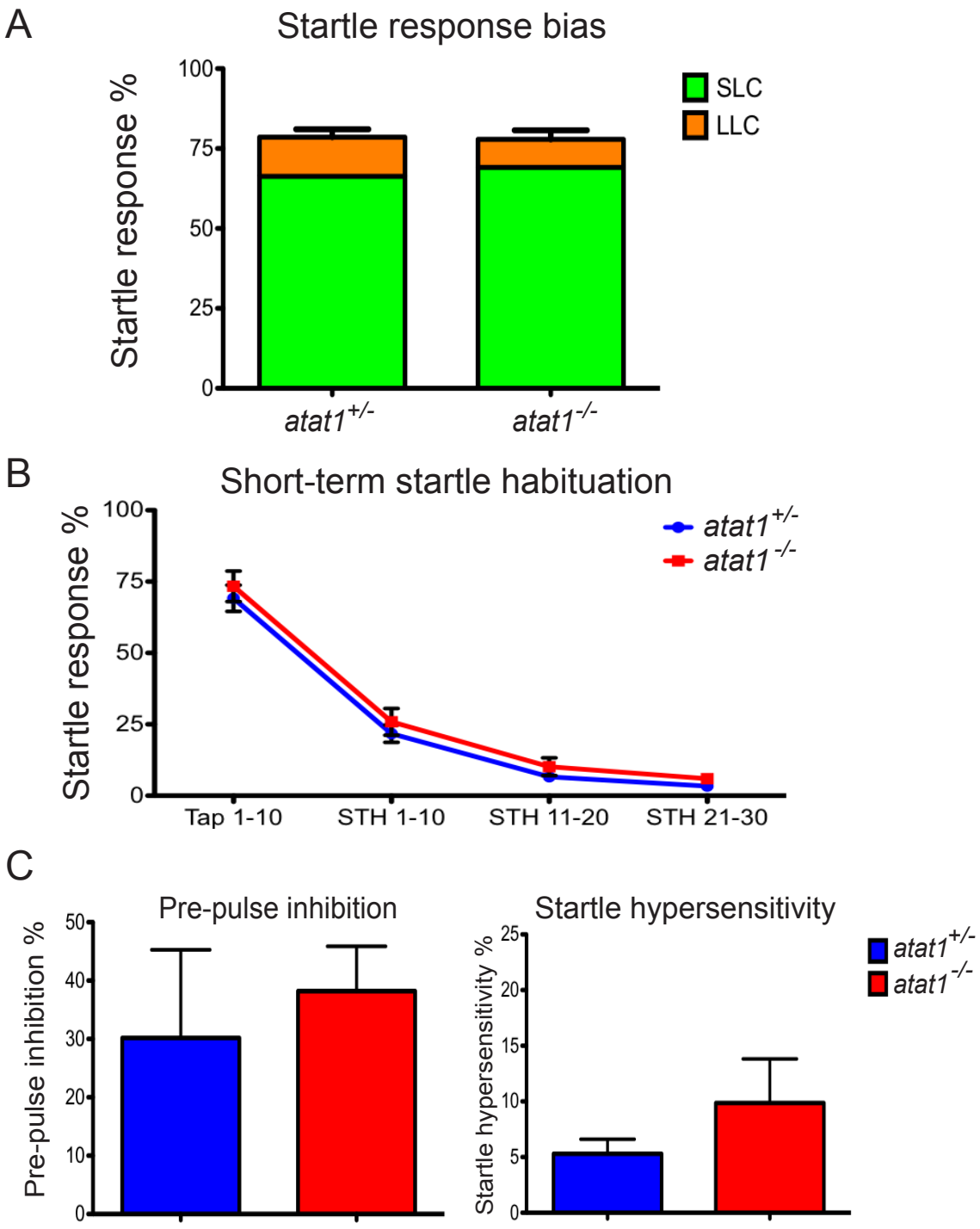
A
Startle response bias
Startle response %
100
75
50
25
0
SLC
LLC
atat1+/-
atat1-/-
B
Short-term startle habituation
Startle response %
100
75
50
25
0
atat1+/-
atat1-/-
Tap 1-10
STH 1-10
STH 11-20
STH 21-30
C
Pre-pulse inhibition
Pre-pulse inhibition %
50
40
30
20
10
0
Startle hypersensitivity
Startle hypersensitivity %
25
20
15
10
5
0
atat1+/-
atat1-/-

Figure 4.5. Visual response of *atat1*$^{-/-}$ larvae. O-bend responsiveness of 120hpf larvae (*atat1*$^{+/-}$: N=44; *atat1*$^{-/-}$: N=34) responding to dark flash visual stimuli. All data is presented as mean±SEM, $p>0.05$, Student's t-test.

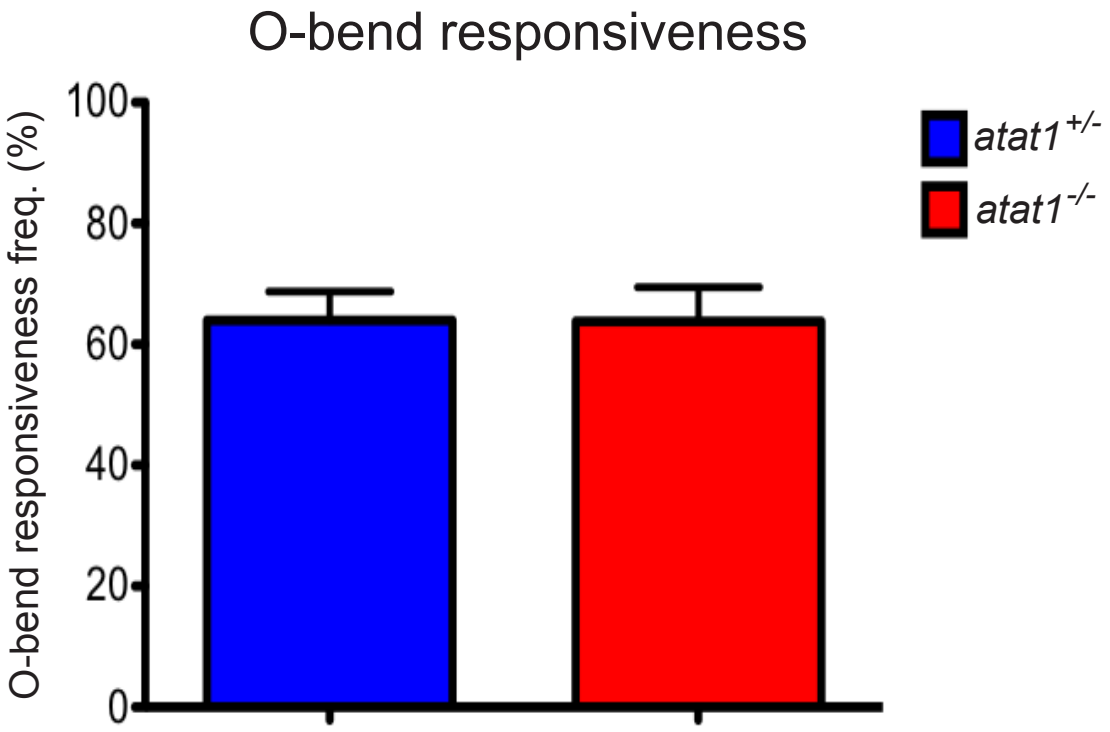
O-bend responsiveness
O-bend responsiveness freq. (%)
100
80
60
40
20
0
atat1+/-
atat1-/-

Figure 4.6. Spontaneous movement of *atat1*$^{-/-}$ larvae. Total distance traveled of 120hpf spontaneously moving larvae (*atat1*$^{+/-}$: N=44; *atat1*$^{-/-}$: N=36) **(A)**. Spontaneous movement frequency of 120hpf larvae (*atat1*$^{+/-}$: N=44; *atat1*$^{-/-}$: N=36) **(B)**. All data is presented as mean±SEM, all $p>0.05$, Student's t-test.

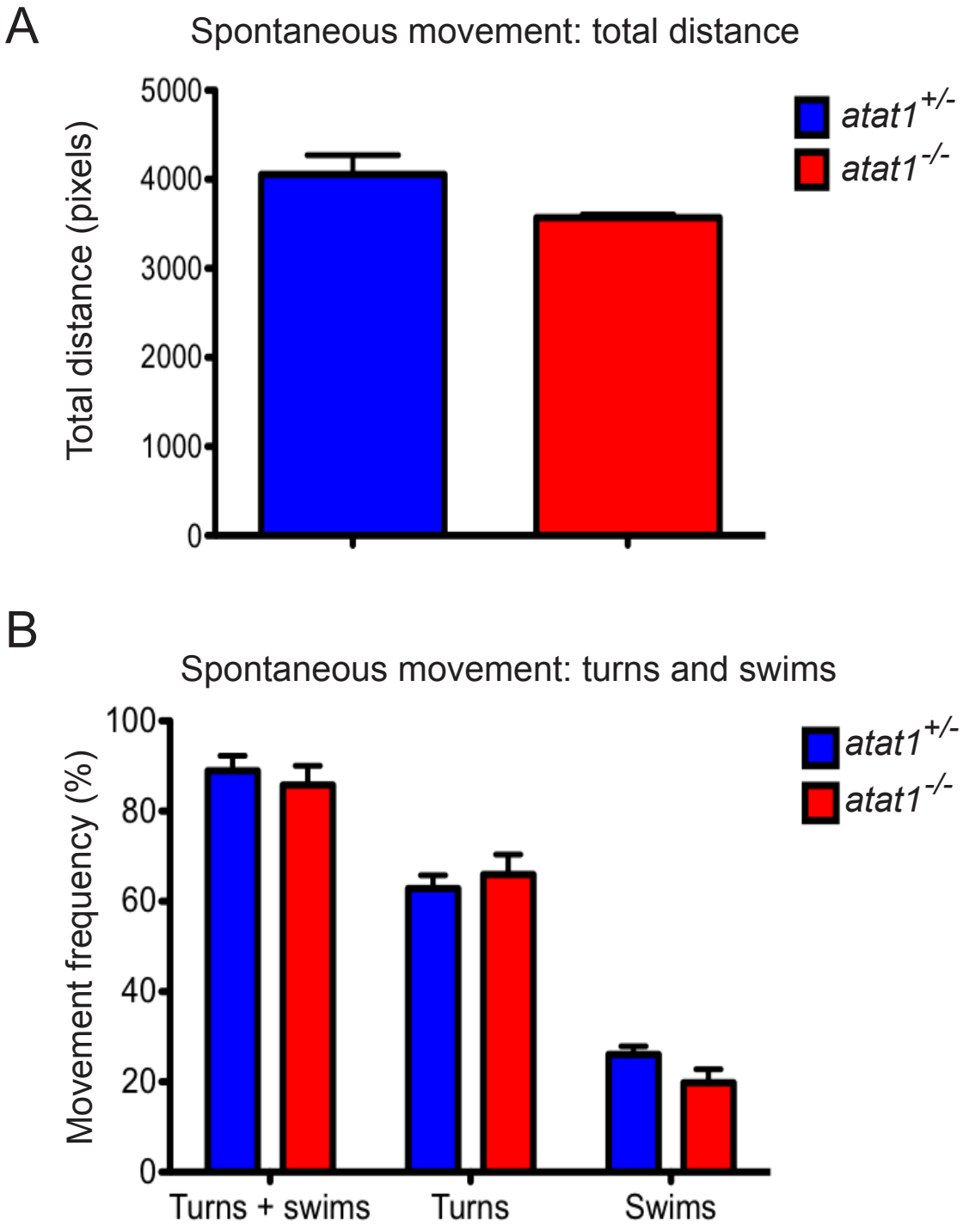
A
Spontaneous movement: total distance
Total distance (pixels)
5000
4000
3000
2000
1000
0
atat1+/-
atat1-/-
B
Spontaneous movement: turns and swims
Movement frequency (%)
100
80
60
40
20
0
Turns + swims
Turns
Swims
atat1+/-
atat1-/-

Figure 4.7. Paclitaxel delays the epiboly movement in *atat1*$^{-/-}$ embryos. 2-somite stage embryos treated with DMSO **(A and B)** or 100μM Paclitaxel **(C and D)** are shown. Note that the epiboly movement is delayed in Paclitaxel-treated embryos **(C and D)**. 24hpf embryos treated with DMSO **(E and F)** or 100μM Paclitaxel **(G and H)** are shown. Some Paclitaxel-treated *atat1*$^{-/-}$ embryos exhibit "openback" phenotype at 24hpf. Arrowhead: the leading edge of epiboly.

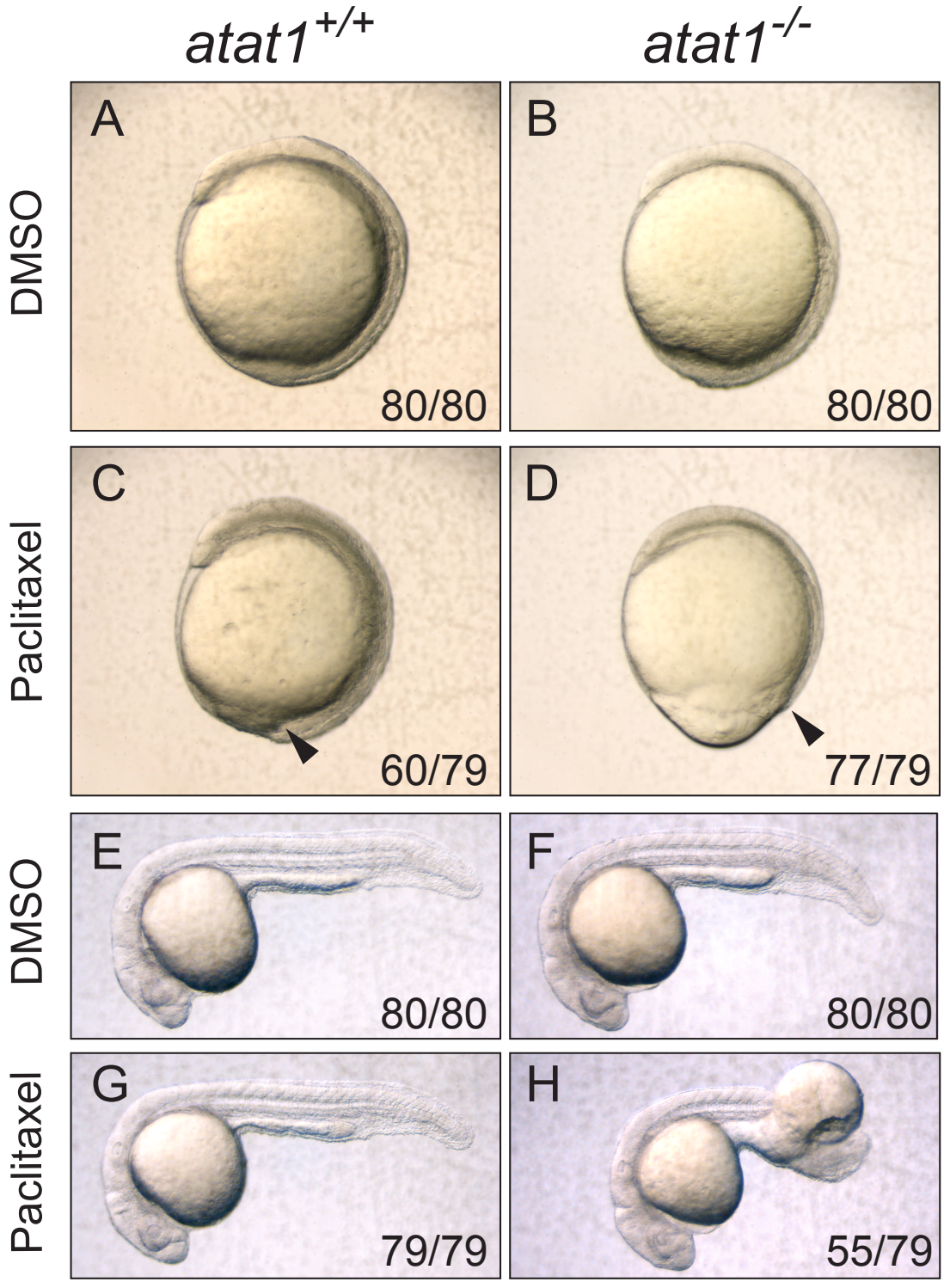
atat1+/+
atat1-/-
DMSO
Paclitaxel
DMSO
Paclitaxel
A
B
C
D
E
F
G
H
80/80
80/80
60/79
77/79
80/80
80/80
79/79
55/79

Figure 4.8. Tubulin PTMs in zebrafish testes. Western blot of monoglycylated, polyglycylated, glutamylated, polyglutamylated, and acetylated tubulin in both *atat1*$^{+/+}$ and *atat1*$^{-/-}$ zebrafish testes. Note that monoglycylated tubulin is greatly elevated, whereas polyglycylated tubulin is reduced in *atat1*$^{-/-}$ embryos.

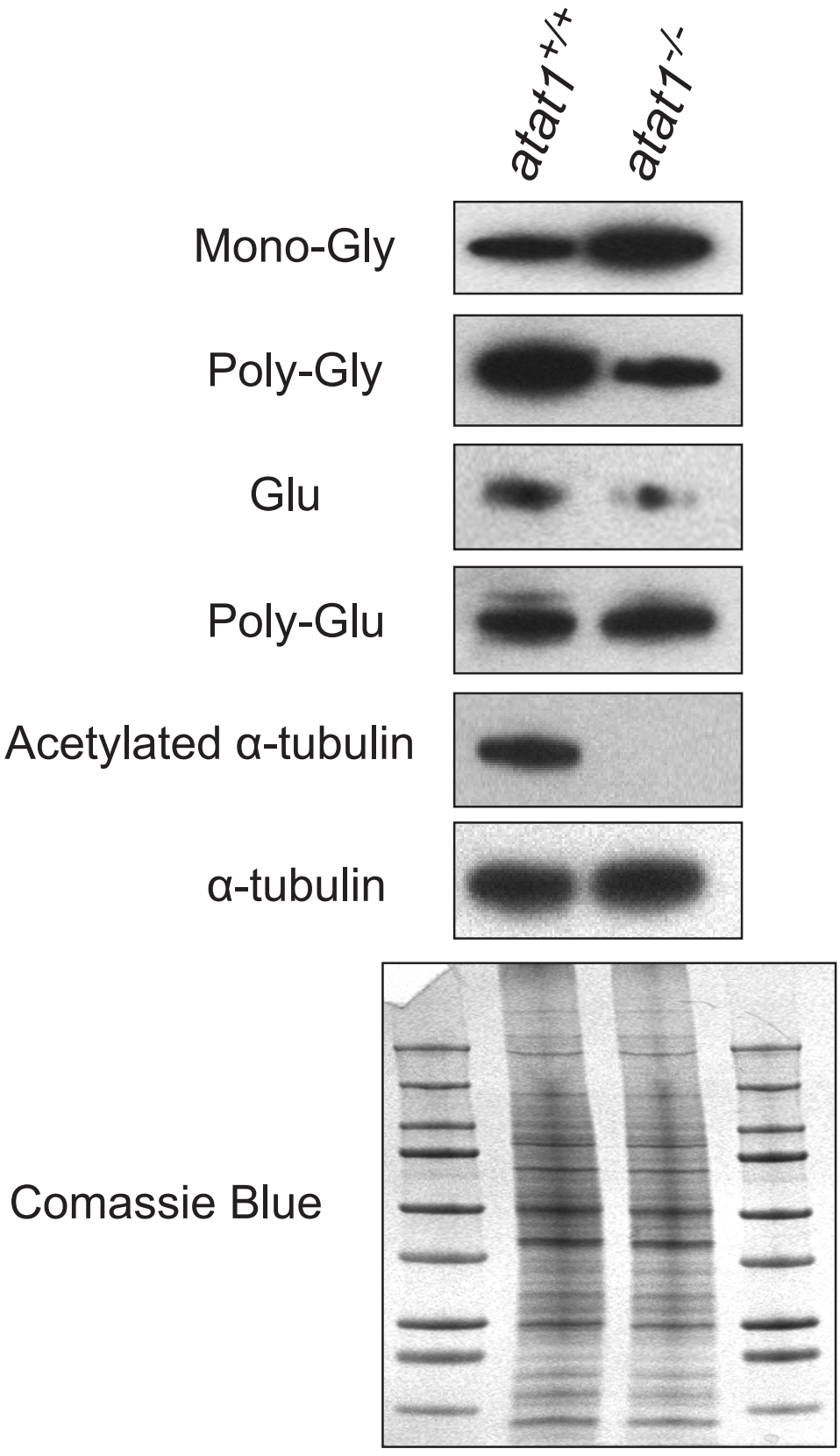
atat1+/+
atat1-/-
Mono-Gly
Poly-Gly
Glu
Poly-Glu
Acetylated α-tubulin
α-tubulin
Comassie Blue

Figure 4.9. Cilia-related defects in *ttll3* morphants. 48hpf *atat1*$^{+/+}$ and *atat1*$^{-/-}$ embryos injected with either *ttll3*MisMO or *ttll3*MO are shown **(A-D)**. Curved body axis phenotype is occasionally found in *atat1*$^{+/+}$ embryos injected with *ttll3*MO, but it is more frequently observed in *atat1*$^{-/-}$ embryos injected with *ttll3*MO **(C and D)**. Frequency of curved body axis phenotype is significantly increased in *atat1*$^{-/-}$ injected with *ttll3*MO, *: Statistically significant, $p<0.05$, Student's t-test **(E)**. Monoglycylated tubulin in the pronephros of 48hpf *atat1*$^{+/+}$ and *atat1*$^{-/-}$ embryos injected with either *ttll3*MisMO or *ttll3*MO are shown. Note that the signal of monoglycylated tubulin is slightly stronger in *atat1*$^{-/-}$ embryos **(F-I)**. Monoglycylated tubulin is depleted in the pronephros of embryos injected with *ttll3*MO **(H and I)**. Scale bar=100μm. The frequency of curved body axis phenotype is slightly reduced in *atat1*$^{-/-}$ embryos injected with *ttll3*MO and *atat1* mRNA. *: Statistically significant, $p<0.05$, Student's t-test **(J)**. Arrow: pronephros.

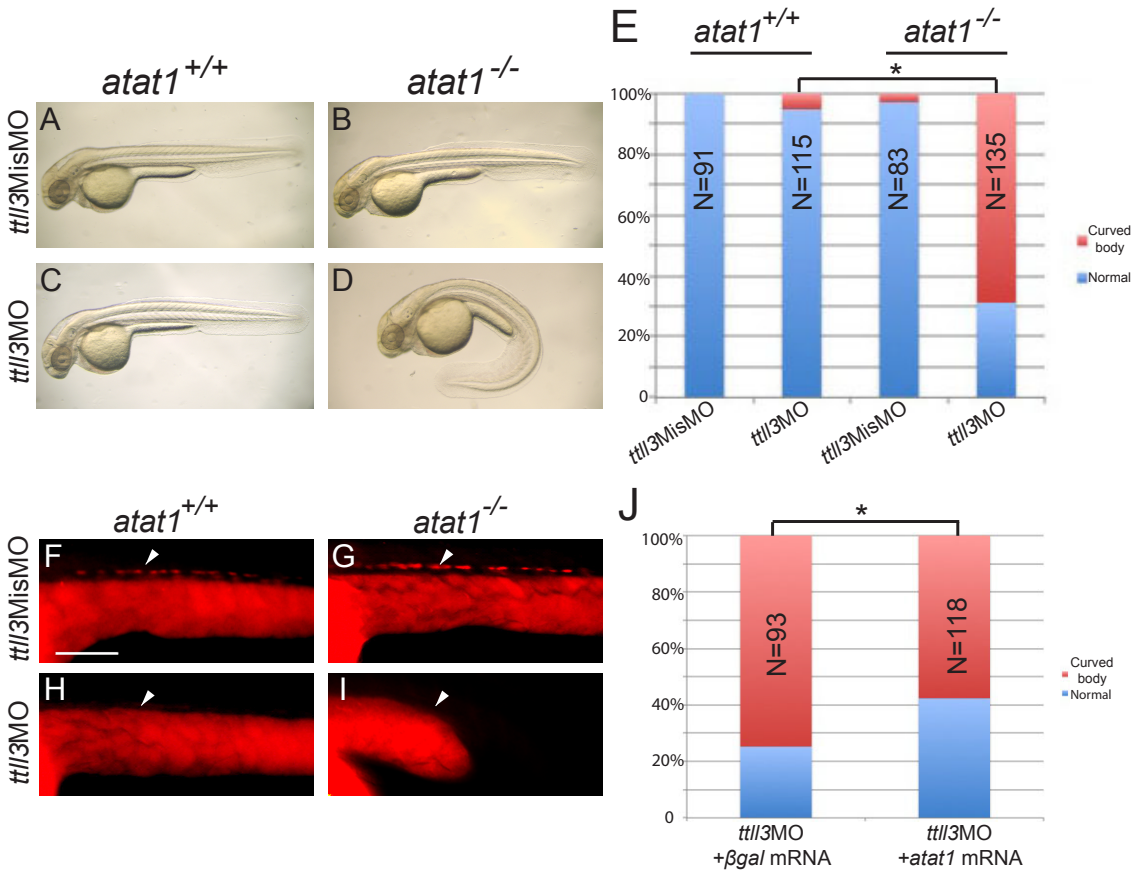
atat1+/+
atat1-/-
ttll3MisMO
ttll3MO
A
B
C
D
E
N=91
N=115
N=83
N=135
100%
80%
60%
40%
20%
0
*
Curved body
Normal
F
G
H
I
J
N=93
N=118
ttll3MO +βgal mRNA
ttll3MO +atat1 mRNA

SUPPLEMENTARY FIGURES AND FIGURE LEGENDS

Figure S4.1. Cyclopia phenotype is observed in a subset of *atat1*$^{-/-}$ embryos.

Phenotypes of 28hpf embryos obtained from *atat1*$^{+/-}$ (allele *ga4*) incrosses **(A-F)**. The result of genotyping is shown in **(G)**. All genotyped cyclopic embryos are *atat1*$^{-/-}$. However, only very few *atat1*$^{-/-}$ embryos exhibit cyclopia phenotype.

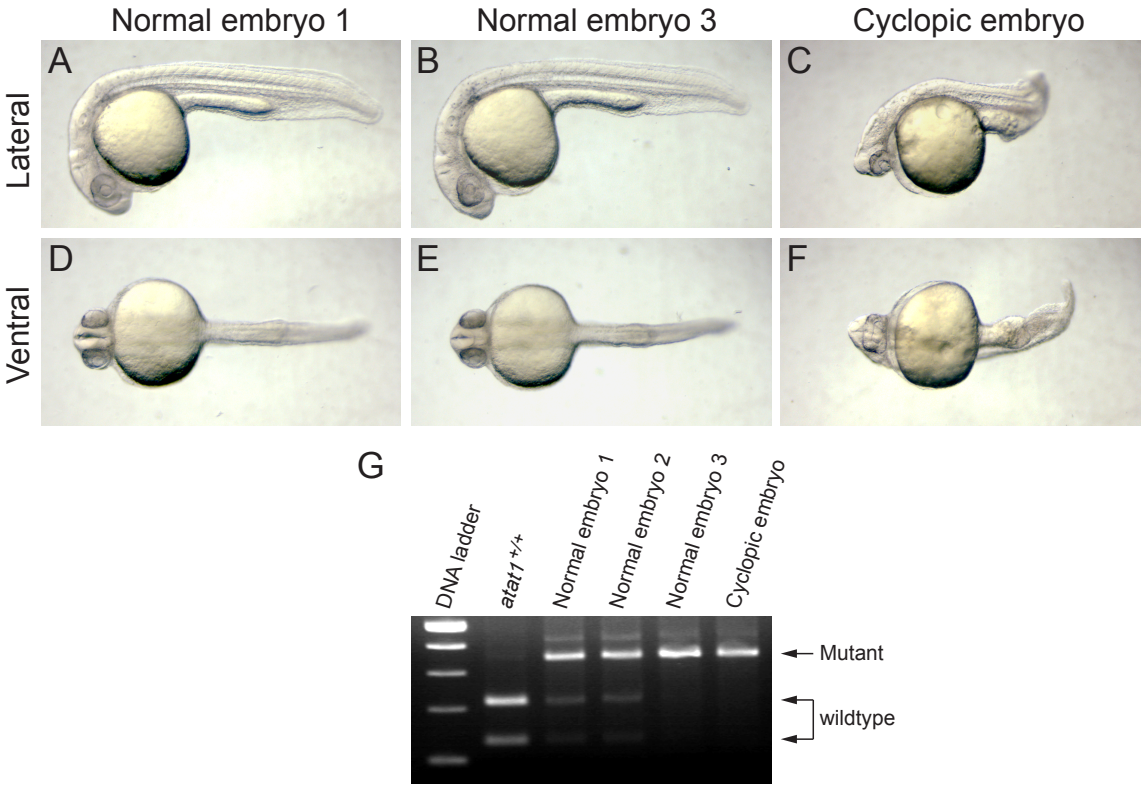
Normal embryo 1
Normal embryo 3
Cyclopic embryo
Lateral
Ventral
A
B
C
D
E
F
G
DNA ladder
atat1+/+
Normal embryo 1
Normal embryo 2
Normal embryo 3
Cyclopic embryo
Mutant
wildtype

Figure S4.2. *atat1* mRNA expression in zebrafish embryos. The expression of *atat1* mRNA in *atat1*$^{+/+}$ **(A)** and *atat1*$^{-/-}$ **(B)** from 8-cell to 72hpf stage is detected by RT-PCR.

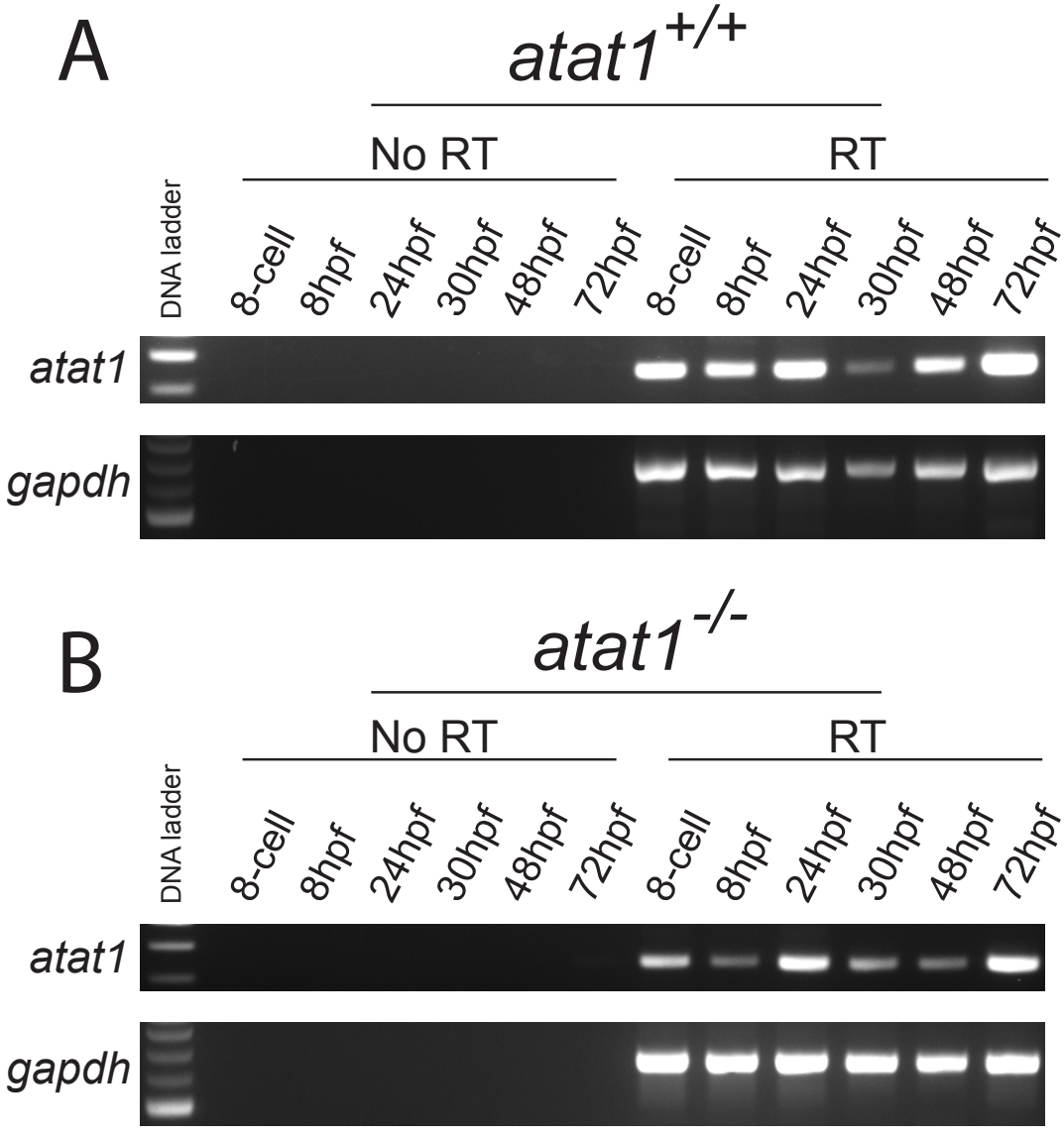
A
atat1+/+
No RT
RT
DNA ladder
8-cell
8hpf
24hpf
30hpf
48hpf
72hpf
8-cell
8hpf
24hpf
30hpf
48hpf
72hpf
atat1
gapdh
B
atat1-/-
No RT
RT
DNA ladder
8-cell
8hpf
24hpf
30hpf
48hpf
72hpf
8-cell
8hpf
24hpf
30hpf
48hpf
72hpf
atat1
gapdh

Figure S4.3. The acetyltransferase activity is required for maintaining the stability of ATAT1. *atat1*$^{+/+}$ embryos overexpress mouse ATAT1-EYFP (MATAT1-EYFP) at 6hpf **(A and B)**, 11hpf **(C and D)**, and 22hpf **(E and F)**. *atat1*$^{-/-}$ embryos overexpress mouse MATAT1-EYFP (MATAT1-EYFP) at 6hpf **(G and H)**, 11hpf **(I and J)**, and 22hpf **(K and L)**. *atat1*$^{+/+}$ embryos overexpress mouse enzyme-dead ATAT1-GGL-EYFP (MATAT1-GGL-EYFP) at 6hpf **(M and N)**, 11hpf **(O and P)**, 22hpf **(Q and R)**. *atat1*$^{-/-}$ embryos overexpress mouse enzyme-dead ATAT1-GGL-EYFP (MATAT1-GGL-EYFP) at 6hpf **(S and T)**, 11hpf **(U and V)**, 22hpf **(W and X)**. All images are taken under the same exposure. Note that the decrease of EYFP intensity starting from 11hpf in both *atat1*$^{+/+}$ and *atat1*$^{-/-}$ embryos that overexpress MATAT1-GGL-EYFP (O, Q, U, and W).

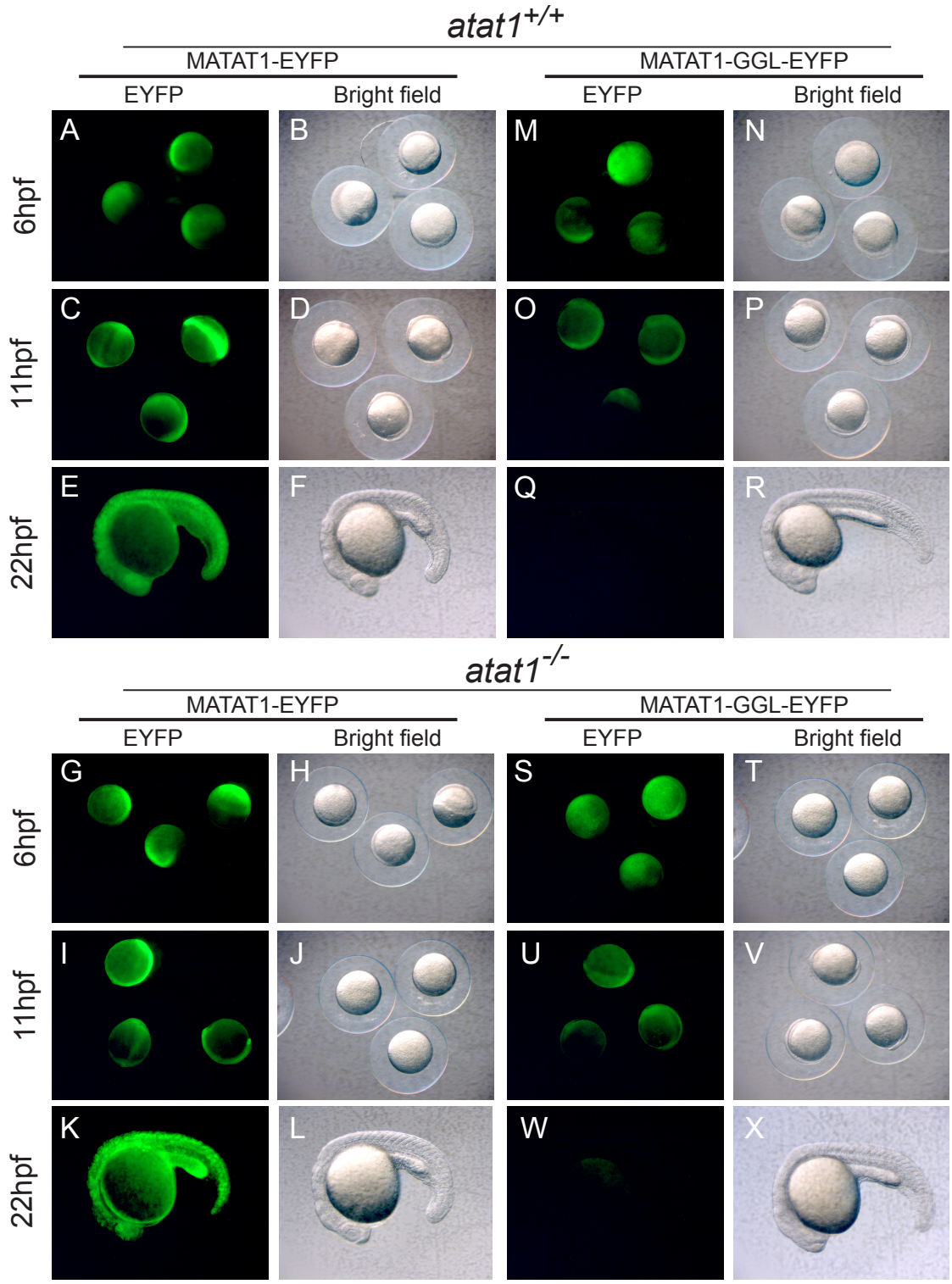
atat1+/+
MATAT1-EYFP
MATAT1-GGL-EYFP
EYFP
Bright field
EYFP
Bright field
6hpf
11hpf
22hpf
A
B
M
N
C
D
O
P
E
F
Q
R
atat1-/-
MATAT1-EYFP
MATAT1-GGL-EYFP
EYFP
Bright field
EYFP
Bright field
6hpf
11hpf
22hpf
G
H
S
T
I
J
U
V
K
L
W
X

Figure S4.4. Injecting *atat1*MO results in non-ATAT1-specific defects. 48hpf embryos injected with *atat1*MO with or without *p53*MO are shown **(A-C)**. Chart shows the frequency of each phenotype in *atat1*$^{+/+}$ injected with different MOs (*atat1*MisMO: N=55, *atat1*MO: N=67, *atat1*MisMO+*p53*MO: N=47, *atat1*MO+*p53*MO: N=96) and *atat1*$^{-/-}$ injected with different MOs (*atat1*MisMO: N=58, *atat1*MO: N=81, *atat1*MisMO+*p53*MO: N=74, *atat1*MO+*p53*MO: N=78) Note that the severity of phenotypes (normal, moderate, and severe) shifts toward the milder end when embryos are co-injected with *p53*MO **(D)**. All data is presented as mean ± SEM.

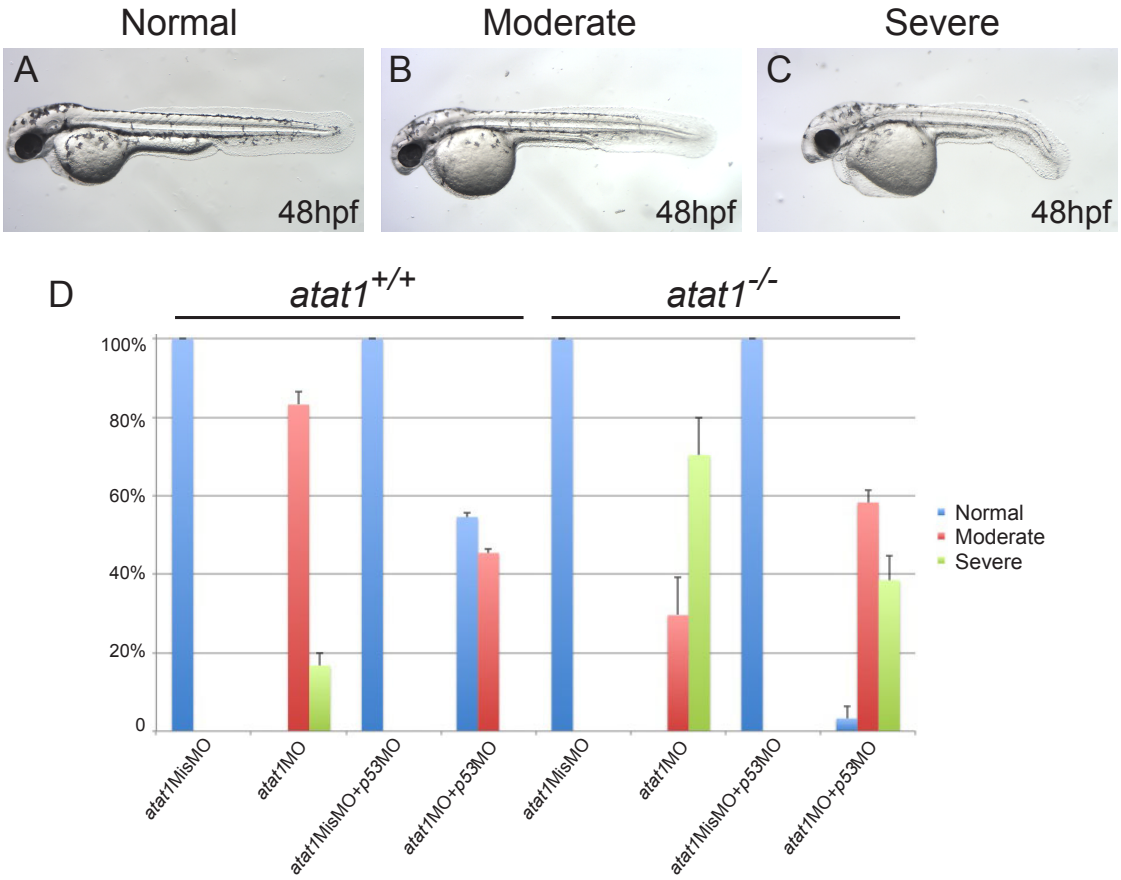
Normal
Moderate
Severe
A
48hpf
B
48hpf
C
48hpf
D
atat1+/+
atat1-/-
100%
80%
60%
40%
20%
0
atat1MisMO
atat1MO
atat1MisMO+p53MO
atat1MO+p53MO
atat1MisMO
atat1MO
atat1MisMO+p53MO
atat1MO+p53MO
Normal
Moderate
Severe

Figure S4.5. Injecting *acvr1l*MO results in the lost-a-fin phenotype in both *atat1*$^{+/+}$ and *atat1*$^{-/-}$ embryos. Both uninjected *atat1*$^{+/+}$ and *atat1*$^{-/-}$ embryos develop normal ventral tail fins at 24hpf **(A and B)**. Both *acvr1l*MO-injected *atat1*$^{+/+}$ and *atat1*$^{-/-}$ embryos exhibit the lack of ventral tail fin (lost-a-fin, C1) phenotype at 24hpf **(C and D)**. Occasional stronger dorsalized phenotype (C2) is also observed in both *acvr1l*MO-injected *atat1*$^{+/+}$ and *atat1*$^{-/-}$ embryos **(E and F)**. Chart shows that the frequency of each class of dorsalization phenotypes (C1 and C2) in both *acvr1l*MO-injected *atat1*$^{+/+}$ (N=86) and *atat1*-/- (N=81) embryos **(G)**. All data is presented as mean ± SEM, $p>0.05$, Student's t-test. Arrowhead: ventral tail fin.

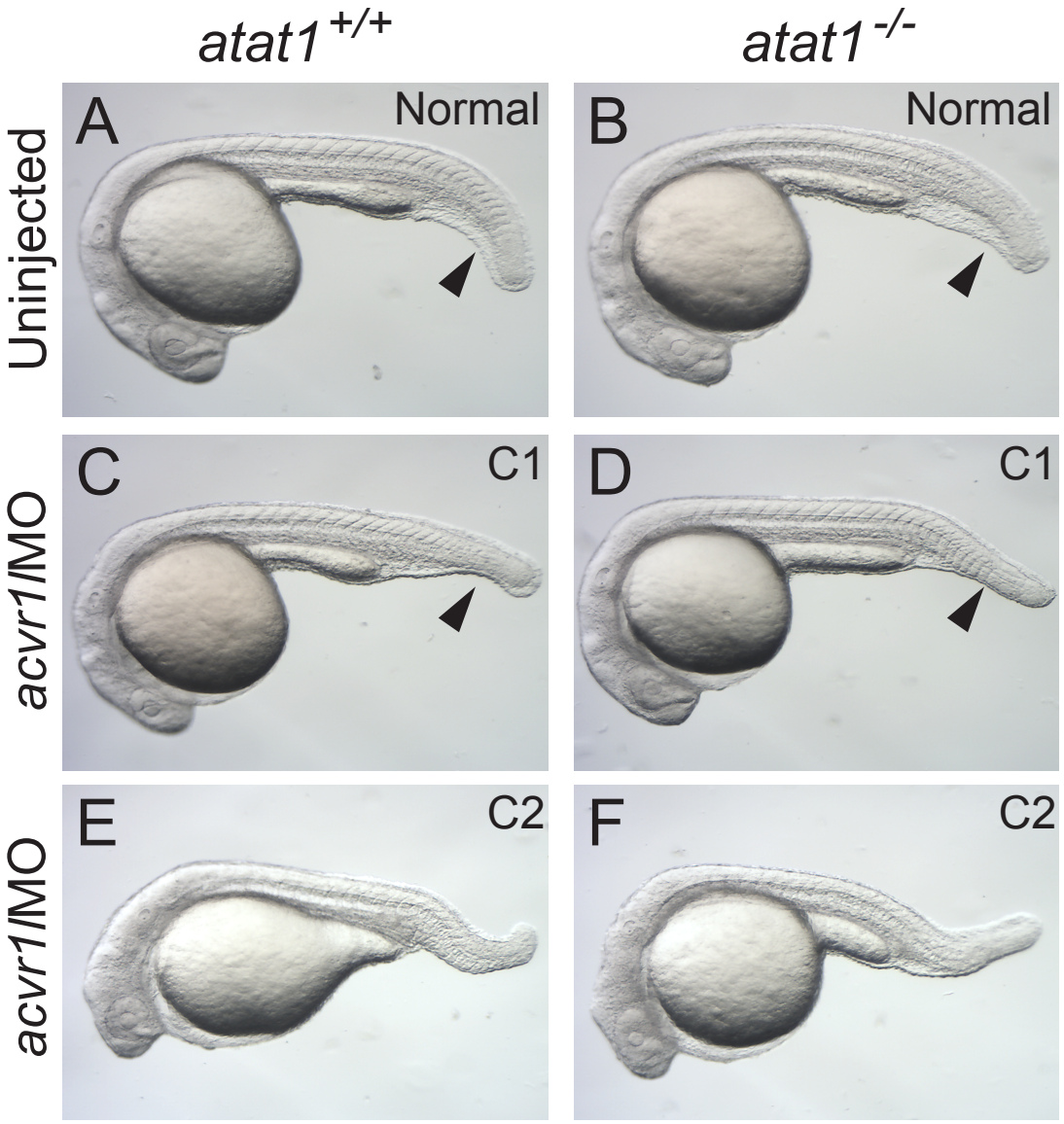
atat1+/+
atat1-/-
Uninjected
acvr1/MO
acvr1/MO
A
Normal
B
Normal
C
C1
D
C1
E
C2
F
C2

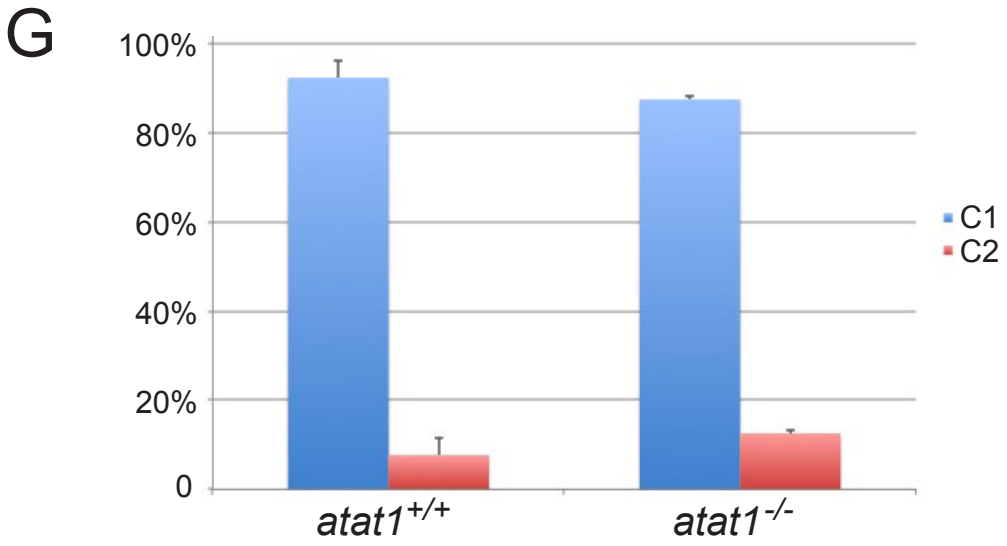
G
100%
80%
60%
40%
20%
0
C1
C2
atat1+/+
atat1-/-

CHAPTER 5

CONCLUSIONS AND FUTURE DIRECTIONS

DISCUSSION

Mga is a regulator of neural crest development in zebrafish

When the expression of Mga is suppressed by antisense morpholino oligonucleotides (MO) in zebrafish embryos, the development of most cell lineages derived from neural crest (NC) is affected. This phenotype has been mentioned in a previous study [1], and is analyzed in depth in our study. In this study, we injected lower dose of MOs into each zebrafish embryo comparing to those used in previous studies [1, 2]. Therefore, it is possible the reason why Mga is suppressed but not completely depleted in our *mga* morphants. The MO combination we used in our study has been proven to efficiently eliminate the full-length Mga isoform, but is less effective against the shorter isoform [2] in zebrafish embryos. Besides, Mga is known to be expressed both maternally and zygotically in zebrafish embryos, making it more difficult to completely eliminate the expression of Mga by injecting MOs into embryos [1, 2]. Although MO has been shown to be able to induce non-specific effect and possible p53-mediated cell death in zebrafish [3, 4], our result is unlikely to be the case because we included *p53*MO in our injection to inhibit the MO-induced p53-dependent cell death. In addition, we were also able to rescue the NC defects by injecting mouse full-length *mga* mRNA. Therefore, Mga is T-

box/bHLHzip domains containing transcription factor that participate in the regulation of NC development in zebrafish. More clues might be gathered using *mga* potentially null mutants that we generated.

Interestingly, since the NC phenotype we observed in our study could be a result of *mga* partially knockdown, moderate reduction of Mga in zebrafish embryos might be the cause of NC phenotype. A previous study using higher dose of *mga*MOs exclusively in the YSL shows the significant reduction of BMP signaling during the gastrulation[2]. However, we did only observe the mild reduction of BMP signaling in our study. Additionally, genetic ablation of *mga* in mice leads to an early embryonic lethal phenotype, suggesting that the complete loss of *mga* might lead to severe or even lethal developmental defects [5]. Hence, the predicted phenotype of maternal-zygotic *mga* null zebrafish mutants might be too severe to recapitulate the NC phenotype discovered in *mga* morphants since Mga would be completely depleted in null mutants. Zygotic *mga* null mutants might be more likely to exhibit the NC defects. Nevertheless, the maternal contribution of *mga* in *mga* zygotic mutants might be the key to determine whether NC development would be affected since we found that Mga might act early during the gastrulation to regulate NC formation. Thus, how much maternal Mga left in *mga* zygotic mutants at this stage might determine the phenotype. If the level of Mga is high enough, zygotic mutants might be able to undergo normal NC formation during early development. If the level of Mga is lower just like what we observed in *mga* morphants, it is possible that these mutants develop the NC formation defect. To sum up, the participation of Mga in NC development might be difficult to be recapitulated due to the

complexity of Mga level exists in *mga* zygotic zebrafish mutants. Embryos injected with MOs might still be the best model to study the correlation between Mga and NC development.

Mechanisms of how Mga affects NC development

Mga was first discovered as a binding partner of Max, suggesting the possibility that it plays a role to regulate Myc activity [6]. It has also been shown to regulate the transcription of *bmp2b* in zebrafish YSL when it binds to Max and Smad4 [2]. Thus, we hypothesize that Mga regulates NC development via either antagonizing Myc activity or fine tuning the level of BMP signaling in zebrafish embryos. Intermediate level of BMP signaling during the gastrulation has been shown to be required for normal NC development in zebrafish [7, 8]. The strength of BMP signaling is mildly reduced in *mga* morphants during the gastrulation, suggesting that this could be the reason why NC formation is altered. Due to the complexity of signaling network in zebrafish embryos, overexpression of BMP in *mga* morphants might not be able to rescue NC defects because BMP is required during the gastrulation but has to be turned off by the end of gastrulation in the NC domain [7-9]. Ectopic expression of BMP might lead to the misregulation of NC formation at different time point. Additionally, BMP signaling is known to participate in a variety of biological processes such as dorsoventral patterning, which also occurs during the gastrulation [10]. Thus, a better way to rescue the NC defects in *mga* morphants might be injecting mRNA of transcription factors that particularly regulate BMP expression or are downstream targets of BMP signaling required for NC formation during the gastrulation. Cvl2 is a transcription factor known to

regulate Bmp2b/4/7a expression during the gastrulation but not the neurulation [7]. Thus, it might be able to rescue the NC defects in *mga* morphants by injecting and fine tuning the mRNA level of *cvl2*. In addition, a transcription factor Tfap2a required for NC formation has been reported to participate in either upstream or downstream of BMP signaling during the gastrulation [8, 11]. Therefore, Tfap2a might be another candidate that could be used to test whether it can rescue the NC defects in *mga* morphants.

Another possible mechanism that Mga utilizes to regulate NC development might be antagonizing Myc activity. Zebrafish Mych has been shown to be required for NC cell survival during the gastrulation [12, 13]. Suppression of Mga expression might disrupt the balance between Mga, Max, and Myc because the formation of heterodimers with Max is required for the activity of both Mga and Myc. Hence, it is possible that *mga* morphants exhibit NC defects that are the result of elevated Myc activity. To test this hypothesis, examining the Myc activity in *mga* morphants using an E-Box enhancer binding activity reporter construct might be able to reveal whether Myc activity is increased [14]. In addition, it is reported that Mych activation leads to the cell survival during the gastrulation in zebrafish [12]. If Myc activity is elevated, presumptive NC cells might over-proliferate and not acquire appropriate cues for normal NC development. These cells might undergo apoptosis as we observed in *mga* morphants later in the embryonic development. A novel small molecule Mycro3 has been shown to be an inhibitor of Myc-Max dimerization [15], suggesting a possibility of utilizing this compound to reduce Myc activity in *mga* morphants. If we fine tune the dose of Myc inhibitor and apply it to *mga* morphants for only a limited period of time during the

gastrulation, we might be able to rescue the NC defects. Taken together, further examination is needed in order to explore how Mga contributes to NC formation.

Functions of Mga in zebrafish

Mga has been shown to participate in a variety of biological processes, including regulating *bmp2b* expression in zebrafish YSL, controlling the development of heart, gut, and brain, survival of the inner cell mass, and lymphoma [1, 2, 5, 16]. In our study, we also discover that Mga is a novel regulator of NC development in zebrafish. However, it is possible that Mga also plays roles in other biological processes. During zebrafish embryonic development, Nodal signals from YSL are required to initiate the expression of Nodal-related gene in blastomeres for patterning the formation of mesendoderm [17]. Nevertheless, it is not clear whether the expression of Nodal-related gene is also controlled by other transcription factors. One clue is that the promoter region of Nodal-related gene *sqt* contains a conserved T-box binding site. Thus, it is possible that the expression of *sqt* is regulated by the binding of T-box domain containing transcription factors. It has been shown that the maternal T-box domain containing transcription factor Eomesa regulates zygotic expression of *nodal* for mesendoderm induction in zebrafish embryos [18]. In zebrafish, Mga is antother known T-box domain containing transcription factors that are expressed maternally, suggesting the possibility that Mga plays a role in regulating the expression of *nodal* either by itself or by working together with Eomesa in zebrafish embryos. Besides, we found that suppressing the expression of Mga also resulted in the defective pectoral fin development in zebrafish embryos. Another T-box transcription Tbx5 has been shown to be essential for the formation of

pectoral fin bud in zebrafish [19]. Therefore, Mga might participate in the formation of pectoral fin via its T-box domain. To investigate the role of Mga in pectoral fin development, it is crucial to know more about the targets of Mga. Additionally, mutations of *mga* in humans have been reported to be associated with Richter's Syndrome, an aggressive form of lymphoma, which occurs in some patients with chronic lymphocytic leukemia (CLL) [16]. Further investigation is required to study the correlation between Mga and cancers. Therefore, the generation of zebrafish *mga* null mutants and possibly conditional null mutants would be greatly useful in terms of exploring the functions and mechanisms that Mga is involved in.

ATAT1 is the major α-tubulin acetyltransferase in zebrafish

Although ATAT1 has been reported as the major α-tubulin acetyltransferase in ciliates, worms and mice [20-23], it is still not clear whether ATAT1 plays the same role in zebrafish because *atat1* knockdown in zebrafish only leads to partially reduced tubulin acetylation [23]. Here we generate two zebrafish *atat1* null mutants by TALENs-mediated gene targeting and show that both *atat1* mutants have no detectable acetylated α-tubulin. In zebrafish embryos, tubulin acetylation is highly enriched in the nervous system and ciliated tissues, including olfactory placode, nerve fibers, neuromasts, and pronephros. Genetic ablation of *atat1* results in the absence of tubulin acetylation in zebrafish, suggesting that other acetyltransferases such as Nat10 and Nat15 are not capable to acetylate α-tubulin. However, another acetyltransferase αTAT-2 has been shown to perform the function as the α-tubulin acetyltransferase in *C. elegans* [24]. Furthermore, it has been identified that acetyltransferase San acetylates lysine 252

(K252) of β-tubulin. This β-tubulin acetylation, though only occurs on soluble α/β-tubulin heterodimers but not on polymerized microtubules, might be involved in regulating the assembly/disassembly of microtubules [25]. Although we have shown that ATAT1 is the major α-tubulin acetyltransferase in zebrafish, we still cannot rule out the possibility that some other acetylatransferases might act to acetylate α-tubulin under certain conditions.

Functions of tubulin acetylation

α-tubulin K40 acetylation is the only known tubulin PTM that occurs on the luminal surface of microtubules [23, 26, 27]. The presence of α-tubulin K40 acetylation usually associates with stable microtubules such as axonemes of cilia and flagella. Hence, it was thought to be involved in stabilizing microtubules. However, *in vitro* study has shown that the acetylation of α-tubulin K40 residue has no effect on the ultrastructure of microtubules, suggesting that it might not directly participate in maintaining the stability of microtubules [28]. Instead, it might affect the function of microtubules by interacting with other microtubule binding proteins and motors [29]. For example, tubulin acetylation has been reported to increase the binding of Kinesin-1 [30]. Although tubulin acetylation does not affect the structure of microtubules directly, its biological importance is significant, especially under abnormal conditions. When cells are under the stress such as starvation, cells may respond to the stress by activating autophagy. Tubulin acetylation is elevated and required in cells for stress-induced autophagy [31, 32]. It is also reported that tubulin acetylation is up-regulated in metastatic and basal-like breast

cancer cells and possibly involved in invasive cell migration [33]. Therefore, functions of tubulin acetylation might be more evident when cells encounter abnormal conditions.

Non-enzymatic functions of ATAT1

Although ATAT1/MEC-17 has been shown to play an essential role in mechanosensory function of *C. elegans*, its acetyltransferase function is not required for maintaining normal mechanosensation [20]. In *C. elegans*, the enzymatic activity of ATAT1/MEC-17 allows the production of 15-protofilament (15-p) microtubules in touch receptor neurons (TRNs), whereas most other cells contain 13-p microtubules. Loss of the enzymatic activity also changes the number and organization of microtubule in TRNs. However, enzymatically inactive ATAT1/MEC-17 is sufficient for touch sensitivity and normal axonal outgrowth without correcting the microtubule defects in *C. elegans* [34]. This result suggests that ATAT1/MEC-17 might perform its non-enzymatic activity to maintain normal mechanosensation in *C. elegans*. Additionally, ATAT1 has also been reported to destabilize microtubules via its non-enzymatic activity. Embryonic fibroblasts from *atat1* knockout mice exhibit strong resistance to nocodazole-induced microtubule depolymerization [21]. A previous study using cell culture system also shows that the microtubule-destabilizing function of ATAT1 is independent of its enzymatic function [35]. In our study, the epiboly is significantly delayed in *atat1*$^{-/-}$ embryos treated with Paclitaxel, suggesting that yolk microtubules in *atat1*$^{-/-}$ zebrafish are possibly more sensitive to the treatment of Paclitaxel. Paclitaxel is a microtubule-stabilizing agent that can be used to slow down the epiboly movement in zebrafish embryos [36]. Our result indicates that yolk microtubules in *atat1*$^{-/-}$ embryos are more stable after the Paclitaxel

treatment comparing to those in *atat1*$^{+/+}$ embryos, whereas the epiboly progression shows no difference between *atat1*$^{+/+}$ and $^{-/-}$ embryos under the normal condition. Since yolk microtubules are very dynamic during the epiboly, it is unlikely that the slower epiboly movement we observed is due to the tubulin acetylation. Therefore, our result also supports the idea that ATAT1 might destabilize microtubules. Nevertheless, Taxol binds to β-tubulin on the luminal surface of microtubules [37]. Since ATAT1 also acetylates α-tubulin on the luminal surface of microtubules, it is possible that Paclitaxel binds to β-tubulin more efficiently when ATAT1 or tubulin acetylation is depleted. Hence, the slower epiboly movement we observed could possibly be the result of more efficient Paclitaxel binding on microtubules but not due to the loss of ATAT1 microtubule destabilizing function. Although ATAT1 has been shown to perform its non-enzymatic activity in regulating microtubule dynamics and stability, its enzymatic activity is essential to maintain its stability [38]. Here we also show that enzyme-dead mouse ATAT1 degrades faster than normal ATAT1, suggesting a possible ATAT1 self-regulation mechanism that utilizes the enzymatic activity of ATAT1 to control its own half-life in cells.

ATAT1 and tubulin PTMs

While ATAT1 mediates the only known tubulin PTM that occurs on the luminal surface of microtubules, enzymes such as TTLL3 and TTLL6 are responsible for catalyzing other tubulin PTMs on the outer surface of microtubules [29]. The relationship between tubulin acetylation and other tubulin PTMs is poorly understood because of their structurally separate modification sites on microtubules. However, Δ2 modification, a type of tubulin

PTMs, accumulates in long-lived microtubules of differentiated neurons and axonemes of cilia and flagella [39]. Tubulin acetylation is also found to be concentrated in cells with more stable microtubules [26]. Therefore, tubulin PTMs on the outer surface of microtubules might be able to coordinate with tubulin acetylation on the inside. In our study, tubulin monoglycylation is up-regulated in *atat1*$^{-/-}$ testes and pronephros, suggesting that a possible mechanism that compensates the absence of tubulin acetylation. Tubulin monoglycylation occurs on the CTT domains of α- and β-tubulin in axonemal microtubules and is primarily mediated by an tubulin monoglycylase TTLL3 [40]. Although TTLL3 is the major tubulin glycylase, suppressing the expression of TTLL3 alone does not result in severe defects in zebrafish embryos. Nevertheless, zebrafish embryos exhibit significant cilia-related defects when the expression of both TTLL3 and tubulin glutamylase TTLL6 are suppressed [41]. Hence, the combination of different tubulin PTMs might form a unique "tubulin code" for microtubule-interacting proteins to read. Some different combinations of tubulin PTMs might be translated into the same message as no significant change of microtubules is identified in *atat1*$^{-/-}$ zebrafish even though several tubulin PTMs are altered. This result suggests that cells exhibit some degrees of flexibility to accommodate the change of tubulin PTMs in order to maintain the homeostasis within cells. *atat1*$^{-/-}$ embryos show significant cilia-related defects such as curved body axis when the expression of TTLL3 is suppressed, indicating that both tubulin acetylation and glycylation are required for maintaining normal functions of cilia. Zebrafish maternal-zygotic *oval/ift88* mutant embryos lack all cilia and also exhibit curved body axis that is possibly due to the dampened but expanded Hedgehog signaling [42]. However, it is not clear how TTLL3 "reads" the change of

tubulin acetylation from the lumen of microtubules. *in vitro* study has shown that ATAT1 can bind to the outer surface of microtubules and interact with CTT domains of tubulin [38]. Hence, the activity of TTLL3 might be increased because of the lack of ATAT1 that interacts with CTT domains in *atat1*$^{-/-}$ zebrafish. The elevation of tubulin monoglycylation might be utilized to compensate the loss of tubulin acetylation, and therefore generate the "tubulin code" that can still be translated into the message required for maintaining structural and functional integrity of microtubules. To understand how the absence of both tubulin acetylation and monoglycylation affects microtubules, further investigation is required to examine if either the structure of microtubules or the binding of microtubule-interacting proteins is altered.

REFERENCES

1. Amir Rikin, T.E. (2010). The tbx/bHLH transcription factor mga regulates gata4 and organogenesis. Developmental Dynamics *239*, 535-547.
2. Yuhua Sun, W.-C.T., Xiang Fan, Rebecca Ball, Scott T. Dougan (2014). Extraembryonic Signals under the Control of MGA, Max, and Smad4 Are Required for Dorsoventral Patterning. Developmental Cell *28*, 322-334.
3. Didier Y.R. Stainier, Z.K., Andrea Rossi (2015). Making Sense of Anti-Sense Data. Developmental Cell *32*, 7-8.
4. Mara E Robu, J.D.L., Soraya Beiraghi, Charles Brenner, Steven A Farber, Stephen C Ekker (2007). p53 Activation by Knockdown Technologies. PLoS Genetics *3*, e78.

5. Andrew J. Washkowitz, C.S., Kun Zhang, Wolfgang Wurst, Thomas Floss, Jesse Mager, Virginia E. Papaioannou (2015). Mga is essential for the survival of pluripotent cells during peri-implantation development. Development *142*, 31-40.

6. Peter J. Hurlin, E.S., Neal G. Copeland, Nancy A. Jenkins, Robert N. Eisenman (1999). Mga, a dual-specificity transcription factor that interacts with Max and contains a T-domain DNA-binding motif. EMBO Journal *18*, 7019-7028.

7. Sabine Reichert, R.A.R., Caroline S. Hill (2013). A BMP regulatory network controls ectodermal cell fate decisions at the neural plate border. Development *140*, 4435-4444.

8. Wen-Der Wang, D.B.M., Mercedes Montero-Balaguer, Antonis K. Hatzopoulos, Ela W. Knapik (2011). Tfap2a and Foxd3 regulate early steps in the development of the neural crest progenitor population. Developmental Biology *360*, 173-185.

9. Jennifer A. Schumacher , M.H., Vu H. Nguyen, Mary C. Mullins (2011). An Intermediate Level of BMP Signaling Directly Specifies Cranial Neural Crest Progenitor Cells in Zebrafish. PLoS ONE *6*, e27403.

10. Yvette G Landon, M.C.M. (2011). Maternal and zygotic control of zebrafish dorsoventral axial patterning. Annual Review of Genetics *45*, 357-377.

11. Neha Bhat, H.-J.K., Bruce B. Riley (2013). A gene network that coordinates preplacodal competence and neural crest specification in zebrafish. Developmental Biology *373*, 107-117.

12. Kay Kotkamp, E.K., Björn Wendik, Bożena K. Polok, Shifra Ben-Dor, Daria Onichtchouk, Wolfgang Driever (2014). Pou5f1/Oct4 Promotes Cell Survival via

Direct Activation of mych Expression during Zebrafish Gastrulation. PLoS ONE *9*, e92356.

13. Sung-Kook Hong, M.T., Igor B. Dawid (2008). The Mych Gene Is Required for Neural Crest Survival during Zebrafish Development. PLoS ONE *3*, e2029.

14. Meltem Weger, B.D.W., Nicolas Diotel, Sepand Rastegar, Tsuyoshi Hirota, Steve A. Kay, Uwe Strählea, Thomas Dickmeis (2013). Real-time in vivo monitoring of circadian E-box enhancer activity: A robust and sensitive zebrafish reporter line for developmental, chemical and neural biology of the circadian clock. Developmental Biology *380*, 259-273.

15. Iok In Christine Chio, G.Y., David Tuveson (2014). MAX-ing Out MYC: A Novel Small Molecule Inhibitor Against MYC-Dependent Tumors. Journal of the National Cancer Institute *106*, dju365

16. Lorenzo De Paoli, M.C., Sara Monti, Silvia Rasi, Valeria Spina, Alessio Bruscaggin, Mariangela Greco, Carmela Ciardullo, Rosella Famà, Stefania Cresta, Rossana Maffei, Marco Ladetto, Maurizio Martini, Luca Laurenti, Francesco Forconi, Roberto Marasca, Luigi M. Larocca, Francesco Bertoni, Gianluca Gaidano, Davide Rossi (2013). MGA, a suppressor of MYC, is recurrently inactivated in high risk chronic lymphocytic leukemia. Leukemia & Lymphoma *54*, 1087-1090.

17. Xiang Fan, E.G.H., , Bo Xu, Christina Sias, Koichi Kawakami, Rebecca D. Burdine, Scott T. Dougan (2007). Nodal signals mediate interactions between the extra-embryonic and embryonic tissues in zebrafish. Developmental Biology *310*, 363-378.

18. Pengfei Xu, G.Z., Yixia Wang, Jiawei Sun, Xingfeng Liu, Ye-Guang Chen, Anming Meng (2014). Maternal Eomesodermin regulates zygotic nodal gene expression for mesendoderm induction in zebrafish embryos Journal of Molecular Cell Biology *6*, 272-285.

19. Dae-gwon Ahn, M.J.K., Laurel A. Rohde, Lee M. Silver, Robert K. Ho (2002). T-box gene tbx5 is essential for formation of the pectoral limb bud. Nature *417*.

20. Brent Neumann, M.A.H. (2014). Loss of MEC-17 Leads to Microtubule Instability and Axonal Degeneration. Cell Report *6*, 93-103.

21. Nereo Kalebic, S.S., Emerald Perlas, Giulia Bolasco, Concepcion Martinez, Paul A. Heppenstall (2013). αTAT1 is the major α-tubulin acetyltransferase in mice. Nature Communications *4*, 1962.

22. Guillaume Montagnac, V.M.-Y., Marie Irondelle, Antonio Castro-Castro, Michel Franco, Toshinobu Shida, Maxence V. Nachury, Alexandre Benmerah, Jean-Christophe Olivo-Marin, Philippe Chavrier (2013). αTAT1 catalyses microtubule acetylation at clathrin-coated pits. Nature *502*, 567-570.

23. Jyothi S. Akella, D.W., Jihyun Kim, Natalia G. Starostina, Sally Lyons-Abbott, Naomi S. Morrissette, Scott T. Dougan, Edward T. Kipreos, Jacek Gaertig (2010). MEC-17 is an α-tubulin acetyltransferase. Nature *467*, 218-222.

24. Toshinobu Shida, J.G.C., Zhenjie Xu, Miriam B. Goodman, Maxence V. Nachury (2010). The major α-tubulin K40 acetyltransferase αTAT1 promotes rapid ciliogenesis and efficient mechanosensation. Proceedings of the National Academy of Sciences USA *107*, 21517-21522.

25. Chih-Wen Chua, F.H., Junmei Zhangb, Lilian Phuc, Alex V. Loktevd, Donald S. Kirkpatrickc, Peter K. Jacksond, Yingming Zhaoe, Hui Zou (2011). A novel acetylation of β-tubulin by San modulates microtubule polymerization via down-regulating tubulin incorporation. Molecular Biology of the Cell *22*.

26. Dorota Wloga, J.G. (2010). Post-translational modifications of microtubules. Journal of Cell Science *123*, 3447-3455.

27. Eva Nogales, S.G.W., Kenneth H. Downing (1998). Structure of the alpha beta tubulin dimer by electron crystallography. Nature *391*, 199-203.

28. Stuart C. Howesa, G.M.A., Toshinobu Shidac, Maxence V. Nachuryc, Eva Nogales (2014). Effects of tubulin acetylation and tubulin acetyltransferase binding on microtubule structure. Molecular Biology of the Cell *25*, 257-266.

29. Janke, C. (2014). The tubulin code: Molecular components, readout mechanisms, and functions. Journal of Cell Biology *206*, 461-472.

30. Nathan A. Reed, D.C.T.L.B., Gloria T. Jih, Edgar Meyhofer, Jacek Gaertig, Kristen J. Verhey (2006). Microtubule Acetylation Promotes Kinesin-1 Binding and Transport. Current Biology *16*, 2166-2172.

31. Rafah Mackeh, S.L., Ameetha Ratier, Najet Mejdoubi-Charef, Anita Baillet, Arnaud Bruneel, Ahmed Hamaï, Patrice Codogno, Christian Poüs, Daniel Perdiz (2014). Reactive Oxygen Species, AMP-activated Protein Kinase, and the Transcription Cofactor p300 Regulate α-Tubulin Acetyltransferase-1 (αTAT-1/MEC-17)-dependent Microtubule Hyperacetylation during Cell Stress. The Journal of Biological Chemistry *289*, 11816-11828.

32. Camille Geeraert, A.R., Simon G. Pfisterer, Daniel Perdiz, Isabelle Cantaloube, Audrey Rouault, Sophie Pattingre, Tassula Proikas-Cezanne, Patrice Codogno, Christian Poüs (2010). Starvation-induced hyperacetylation of tubulin is required for the stimulation of autophagy by nutrient deprivation. The Journal of Biological Chemistry *285*, 24184-24194.

33. Amanda E. Boggs, M.I.V., Rebecca A. Whipple, Monica S. Charpentier, Olga G. Goloubeva, Olga B. Ioffe, Kimberly C. Tuttle, Jana Slovic, Yiling Lu, Gordon B. Mills, Stuart S. Martin (2015). α-Tubulin Acetylation Elevated in Metastatic and Basal-like Breast Cancer Cells Promotes Microtentacle Formation, Adhesion, and Invasive Migration Cancer Research *75*, 203-215.

34. Irini Topalidou, C.K., Nereo Kalebic, Ken C.Q. Nguyen, Hannah Somhegyi, Kristin A. Politi, Paul Heppenstall, David H. Hall, Martin Chalfie (2012). Genetically Separable Functions of the MEC-17 Tubulin Acetyltransferase Affect Microtubule Organization. Current Biology *22*, 1057-1065.

35. Nereo Kalebic, C.M., Emerald Perlasa, Philip Hublitza, Daniel Bilbao-Cortesa, Karol Fiedorczuka, Annapaola Andolfob, Paul A. Heppenstall (2013). Tubulin Acetyltransferase αTAT1 Destabilizes Microtubules Independently of Its Acetylation Activity. Molecular and Celluler Biology *33*, 1114-1123.

36. Lilianna Solnica-Krezel, W.D. (1994). Microtubule arrays of the zebrafish yolk cell: organization and function during epiboly. Development *120*, 2443-2455.

37. Linda A Amos, J.L. (1999). How Taxol stabilises microtubule structure Chemistry & Biology *6*, 65-69.

38. Satoru Yuzawa, S.K., Junya Hayase and Hideki Sumimoto (2015). Structural basis of cofactor-mediated stabilization and substrate recognition of the α-tubulin acetyltransferase αTAT1. Biochemical Journal.

39. Laurence Paturle-Lafanechère, M.M., Nathalie Trigault, Fabienne Pirollet, Honoré Mazarguil, Didier Job (1994). Accumulation of delta 2-tubulin, a major tubulin variant that cannot be tyrosinated, in neuronal tissues and in stable microtubule assemblies. Journal of Cell Science *107*, 1529-1543.

40. Dorota Wloga, D.M.W., Krzysztof Rogowski, Marie-Hélène Bré, Nicolette Levilliers, Maria Jerka-Dziadosz, Carsten Janke, Scott T. Dougan, Jacek Gaertig (2009). TTLL3 Is a Tubulin Glycine Ligase that Regulates the Assembly of Cilia. Developmental Cell *16*, 867-876.

41. Narendra Pathak, C.A.A., Iain A. Drummond (2011). Tubulin Tyrosine Ligase-like Genes ttll3 and ttll6 Maintain Zebrafish Cilia Structure and Motility. The Journal of Biological Chemistry *286*, 11685-11695.

42. Peng Huang, A.F.S. (2009). Dampened Hedgehog signaling but normal Wnt signaling in zebrafish without cilia. Development *136*, 3089-3098.